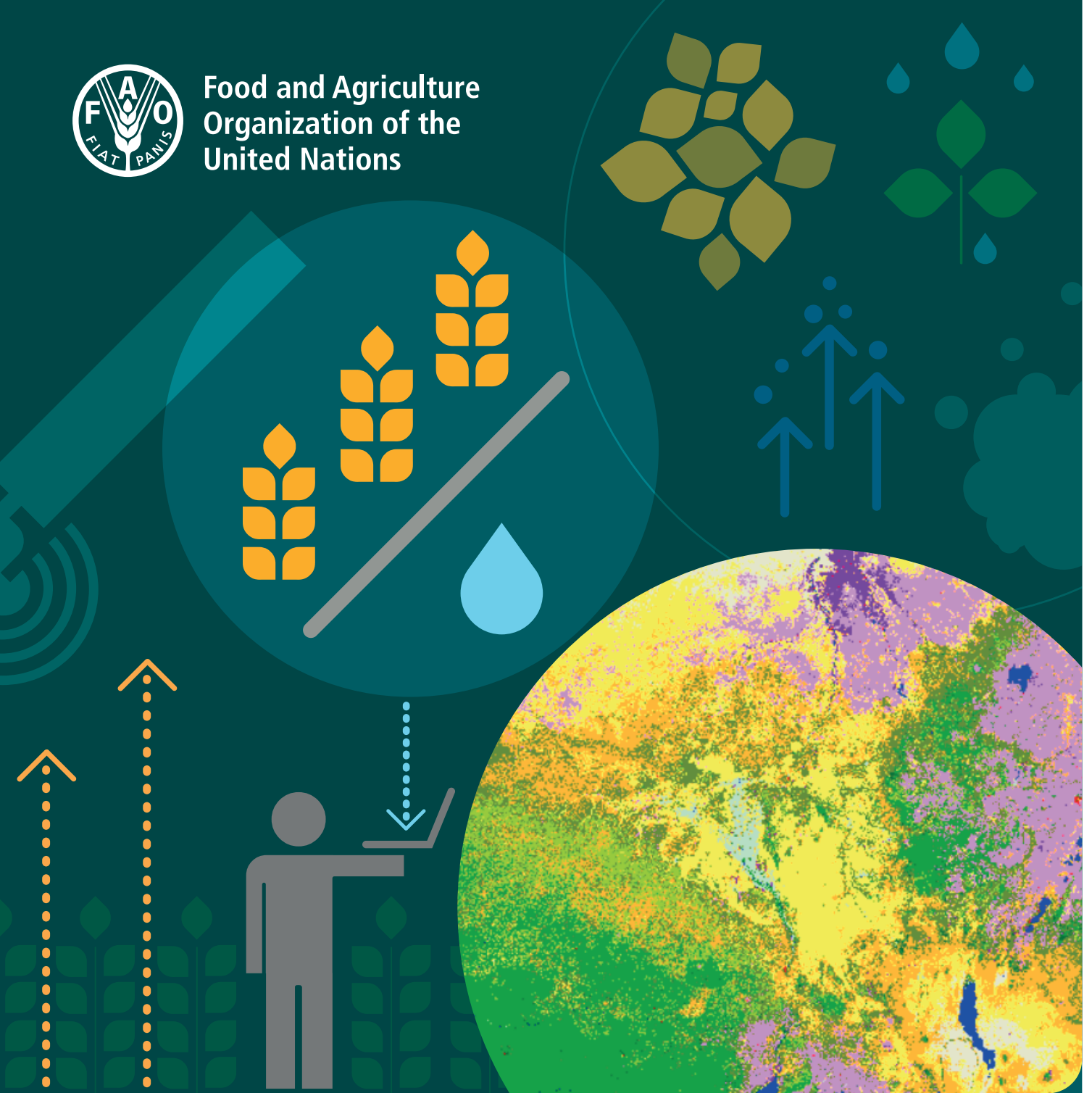**Food and Agriculture Organization of the United Nations**

WaPOR V2 quality assessment

Technical report on the data quality
of the WaPOR FAO database version 2

WaPOR quality assessment

Technical report on the data quality of the WaPOR FAO database version 2

Contents

Appendixes

Figures

Tables

Preface

"Achieving Food Security in the future while using water resources in a sustainable manner will be a major challenge for current and future generations. Increasing population, economic growth and climate change all add to increasing pressure on available resources. Agriculture is a key water user and careful monitoring of water productivity in agriculture and exploring opportunities to increase it is required. Improving water productivity often represents the most important avenue to cope with increased water demand in agriculture. Systematic monitoring of water productivity using Remote Sensing can help to identify water productivity gaps and evaluate appropriate solutions to close these gaps." (FAO, 2017).

The FAO Water Productivity web portal (WaPOR) provides open access to 10 years (2009 to present) of continuous remote sensing-based observations on agricultural water productivity over Africa and the Near East. The portal contains various spatial data layers related to land and water use for agricultural production and allows for direct data queries, time series analyses, area statistics and download of key data variables to estimate water and land productivity gaps in irrigated and rain fed agriculture.

WaPOR Version 2.1 became available from June 2019 onwards. This report provides a quality evaluation of the WaPOR V2 evapotranspiration, biomass and water productivity data across Africa and the Near East, currently distributed through the FAO - WaPOR portal. The FRAME consortium[1] consists of eLEAF, VITO, ITC-UTwente and the Waterwatch Foundation.

The report is an output of the project "Using remote sensing in support of solutions to reduce agricultural water productivity gaps" (http://www.fao.org/in-action/remote-sensing-for-water-productivity/en/), implemented by FAO and funded by the Government of The Netherlands.

---

1. For more information regarding FRAME, pls. contact eLEAF (http://www.eleaf.com/). Contact persons are FRAME project manager: Annemerie Klaasse (Annemarie.klaasse@eleaf.com) a/o Managing Director: Steven Wonink (steven.wonink@eleaf.com).

Acknowledgements

---

1. Currently Post-doctoral fellow at the University of Göttingen, Germany

Abbreviations and acronyms

AGBP	Above Ground Biomass Production
DMP	Dry Matter Productivity
CV	Coefficient of Variation
E	Soil Evaporation
EC	Eddy Covariance (flux tower)
EOS	End of Season
ET_a	Actual Evapotranspiration
ETI_a	Actual Evapotranspiration and Interception
ET_a-EC	ETa from eddy covariance flux tower measurements
ET_a-Fu	ETI_a estimated from Fu
ET_a-MOD16	ETI_a and interception obtained from MOD16 dataset
ET_a-MSG	ETI_a obtained from geostationary Meteosat dekadal GPP product from the EUMETSAT LandSAF (LSASAF)
ET_a-WB	ETI_a obtained from the physical water balance
ETI_a-WPR	ETI_a obtained from WaPOR database and methodology
fAPAR	Fraction of Absorbed Photosynthetically Active Radiation
GPP	Gross Primary Productivity
HI	Harvest Index
I	Interception of rainfall
L1	Level 1 (250m resolution)
L2	Level 2 (100m resolution)
L3	Level 3 (30m resolution)
LAI	Leaf Area Index
LCC	Land Cover Classification
LE	Latent Energy (latent heat of evaporation)
LST	Land Surface Temperature
LUE	Light Use Efficiency
METE	Metehara
MODIS	Moderate Resolution Imaging Spectroradiometer
NDVI	Normalised Difference Vegetation Index
NPP	Net Primary Productivity
NPP-MOD17	NPP obtained from MOD17 dataset
NPP-MSG	NPP obtained from geostationary Meteosat dekadal GPP product from the EUMETSAT LandSAF (LSASAF)
NPP-WPR	NPP obtained from WaPOR database
ODN	Office du Niger
PCP	Precipitation
PHE	Phenology (crop)
PSN	Net Photosynthesis
Q	Surface run-off
QAQC	Quality assurance/quality control
r	Correlation Coefficient

R^2	Coefficient of Determination
RET	Reference Evapotranspiration (FAO-56 definition)
RET-EC	RET from eddy covariance flux tower meteorological data
RET-WPR	RET from WaPOR database (GEOS-5 model meteorological data)
RMSE	Root Mean Square Error
SMC	Relative Soil Moisture Content (wetness indicator)
SOS	Start of Season
SR	Solar Radiation
T	Transpiration (by vegetation)
TBP	Total Biomass Production
V1	WaPOR version 1.1
V2	WaPOR version 2.1
WaPOR	The FAO portal to monitor WAter Productivity through Open access of Remotely sensed derived data
WON	Wonji
WP	Water Productivity
ZAN	Zankalon
ß	WaPOR beta version
ε_a	Autotrophic (plant) Respiration (fraction)

Executive Summary

This document presents the results of a validation of the version-2 of the WaPOR database, produced by the FRAME consortium partners, eLEAF and VITO. The report summarises the work done by the validation partner (ITC-UTwente) to assess the quality of the new V2 core data components, currently used to estimate and derive agricultural water productivity for Africa and the Near East.

WaPOR represents a comprehensive open access data portal that provides information on biomass productivity (with focus on food and agriculture production) and evapotranspiration (evaporative losses and water use) for Africa and the Near East in near real time covering the period from 1 January 2009 to date. WaPOR offers continuous data on a 10-day average basis across Africa and the Near East at three spatial resolutions. The continental level-1 data (250m) cover entire Africa and the Near East (L1). The national level-2 (100m) data cover 21 countries and four river basins (L2). The third level-3 data (30m) cover eight irrigation areas (L3). The quality assessment focused on the core data of the WaPOR database i.e., the evaporative loss components: plant transpiration (T), soil evaporation (E) and interception (I) combined in ETI, the net primary productivity – NPP, the total (TBP) and above ground biomass productivity (AGBP) and reference evapotranspiration – RET.

To quantify the accuracies and uncertainties of the WaPOR V2 data components, we used a number of validation methods, further described in this document. We checked the physical mass balance consistency of evaporative losses, water use and consumption against water supply by rainfall and availability including an evaluation of the long-term water balance of 22 major African river basins. We crosschecked the biomass production (in the form of net primary productivity) and evapotranspiration against other recognized reference datasets. We verified continental spatial and temporal trends and internal data consistency of evapotranspiration and biomass productivity for the major climatic zones in Africa and the Near East. We directly validated WaPOR evapotranspiration and biomass estimates against in-situ data of eddy covariance (EC) flux tower stations, and respectively used i.e. 14, 5 and 8 in-situ locations for verification of evapotranspiration, net primary productivity and reference ET. Finally, we checked the data consistency among the three different spatial resolutions, analysed the changes between the WaPOR versions-1 (V1) and version-2 (V2), and confirmed the WaPOR portal numerical information retrieval with an independent computation. We give detailed results on the application of the five different validation techniques in Chapter 3. We summarized our conclusions in Chapter 4.

1. Introduction and description of the validation data

The WaPOR database is a comprehensive database that provides information on biomass (for food production) and evapotranspiration (for water consumption) for Africa and the Near East in near real-time covering the period from 01-January-2009 to present (FAO, 2020a). The WaPOR offers continuous data at a 10-day average time step for Africa and the Near East at three spatial resolutions. The continental-level data (250m) covers continental Africa and large parts of the Near East (L1). The national-level data (100m) covers 21 countries and four river basins (L2). The third level (30m) covers eight irrigation areas (L3). This document describes both the quality assessment methodology and the validation results of the main water productivity data components, evapotranspiration (ETI_a), biomass (net primary productivity – NPP), including the resulting water productivity (WP), as distributed through the WaPOR portal.

Data components soil evaporation – E, plant transpiration – T, rainfall interception – I, reference evapotranspiration – RET, NPP, precipitation – PCP, the normalised difference vegetation index (NDVI) quality layer and land surface temperature (LST) quality layer, are all available for download from the WaPOR portal (FAO 2020a). Intermediate data components refer to datasets that were created during pre-processing and are used as input in the final processing of the evapotranspiration and biomass data components. These include solar radiation – SR, relative soil moisture content – SMC and the normalised difference vegetation index – NDVI, amongst others. Intermediate data components are not available from the portal.

The datasets used in the validation, along with the intermediate components used in the quality checks are described in Table 1-1. The evaporation and transpiration component could not be validated separately (due to lack of unique data on plant transpiration and soil evaporation).

Table 1-1. WaPOR data components and validation methods used in the quality assessment. The spatial levels used in the assessment are denoted as L1, L2 and L3.

Data Component	Physical mass balance	Cross or Inter-product validation	Internal or Intra-product validation	Direct validation to in-situ	Level consistency
Main data components and focus of the data quality evaluation					
ETI_a (T, E, I)	L1	L1	L1	L1, L2, L3	L1, L2, L3
NPP	-	L1	L1	L1, L2, L3	L1, L2, L3
RET	-	-	L1	L1	-
Products and intermediate data components used in the data quality evaluation					
T, E	-	-	L1	L1	L1, L2, L3
PCP	L1	-	-	L1	-
SMC	-	-	L1	L1	-
NDVI	-	-	L1	L1	-
SR	-	-	L1	-	-
NDVI quality later	-	-	-	L1	-
LST quality layer	-	-	-	L1	-

1.1. Short description of main WaPOR data components

The primary analysis datasets are the ETI_a (ETI_a-WPR) and NPP (NPP-WPR) version 2 (V2) products available on the WaPOR portal. This section provides a brief description of the conceptual approach to estimating the ETI_a-WPR and NPP-WPR components.

The ETI$_a$-WPR is based on a modified version of the ETLook model (Bastiaanssen *et al.*, 2012; Pelgrum *et al.*, 2012), hereafter referred to as ETLook-WaPOR. The ETLook-WaPOR model uses a remote sensing data-based Penman-Monteith (PM) model to estimate ET$_a$, which is also the ET approach commonly used by FAO, and described in the FAO-56 Irrigation & Drainage series paper (Allen, Pereira, Raes & Smith, 1998). The ETI$_a$ - WPR estimates soil evaporation and plant transpiration separately using Equations 1 and 2. The interception is evaluated as a function of the vegetation cover, leaf area index (LAI) and precipitation (PCP). The ETI-WPR is calculated as the sum of evaporation, transpiration and interception.

$$(1) \quad \lambda E = \frac{\Delta(R_{n,soil} - G) + \dfrac{\rho_{air} C_p (e_{sat} - e_a)}{r_{a,soil}}}{\Delta + \gamma \left(1 + \dfrac{r_{s,soil}}{r_{a,soil}} \right)}$$

$$(2) \quad \lambda T = \frac{\Delta(R_{n,canopy}) + \dfrac{\rho_{air} C_p (e_{sat} - e_a)}{r_{a,canopy}}}{\Delta + \gamma \left(1 + \dfrac{r_{s,canopy}}{r_{a,canopy}} \right)}$$

Where E and T (kg.m^{-2}.s^{-1}) are the evaporation and transpiration, respectively, and λ is the latent heat of vaporisation (J.kg^{-1}). R$_n$ (MJ/m^2/day) of the soil ($R_{n,soil}$) and canopy ($R_{n,canopy}$) is the net radiation and G (MJ/m^2/day) is the ground heat flux. ρ_{air} (kg/m^3) is the density of air, C$_P$ (MJ/kg/°C) is the specific heat of air, (e_{sat} $- e_a$) (kPa) is the vapour pressure deficit (VPD), r$_a$ (s/m) is the aerodynamic resistance, r$_s$ (s/m) is the soil resistance, or canopy resistance when using the PM-model to estimate evaporation or transpiration respectively. $\Delta = d(e_{sat})/dT$ (kPa/°C) is the slope of the curve relating saturated water vapour pressure to the air temperature, and γ is the psychometric constant (kPa/°C). This approach partitions the ETI$_a$-WPR to evaporation and transpiration using the modified versions of PM, which differentiate the net available radiation and resistance formulas based on the vegetation cover according to the ETLook model (Bastiaanssen *et al.*, 2012). A major difference between the ETLook-WaPOR model and the ETLook model is the source of remote sensing data for the soil moisture. In the original ETLook model, soil moisture was derived from passive microwave, and in the WAPOR approach, soil moisture is derived using a Land Surface Temperature (LST) – vegetation index model (Wang, 2011). The normalised difference vegetation index (NDVI) is used to determine the partitioning of the R_n into $R_{n,soil}$ and $R_{n,canopy}$, along with the interception, ground heat flux, and the minimum stomatal resistance.

Interception (I) is the process where the leaves intercept rainfall. Interceted rainfall evaporates directly from the leaves and requires energy that is not available for transpiration. Interception [mm/day] is a function of the vegetation cover, leaf area index (LAI) and PCP, expressed as:

$$(3) \quad I = 0.2 \, Ilai \left(1 - \frac{1}{1 + \dfrac{c_{vegPCP}}{0.2 \, I_{lai}}} \right)$$

Net Primary Production (NPP) is a fundamental characteristic of an ecosystem, expressing the conversion of carbon dioxide into biomass driven by photosynthesis. NPP is the GPP minus autotrophic respiration, the losses caused by the conversion of basic products (glucose) to higher-level photosynthesis (starch, cellulose, fats, proteins) and the respiration needed for the maintenance of the standing biomass. The NPP-WPR, as defined in WaPOR, is expressed as:

(4) $\quad NPP = S_c * R_s * \varepsilon_p * fAPAR * S_M * \varepsilon_{lue} * \varepsilon_T * \varepsilon_{CO2} * \varepsilon_{AR} \, [\, \varepsilon_{RES} \,]$

Where S_c [-] is the scaling factor from dry matter productivity (DMP) to NPP, R_s (MJT/ha/day) is the total shortwave incoming radiation, ε_p is the fraction of photosynthetically absorbed radiation (PAR) (0.4–0.7gm) in total shortwave with a value of 0.48 ($J_{Par}/J_{Total-sw}$). $fAPAR$ [-] is the PAR-fraction absorbed by green vegetation. S_M [-] is the soil moisture stress reduction factor. ε_{lue} (-) is the Light use efficiency (LUE) (DM=Dry Matter) at optimum ($kgDM/GJ_{PA}$), ε_T (-) is the normalized temperature effect, ε_{CO2} (-) is the normalized CO_2 fertilization effect, the ε_{AR} (-) is the fraction kept after autotrophic respiration and ε_{RES} (-) is the fraction kept after residual effects (including soil moisture stress).

When Total (TBP) or Above Ground Biomass Productivity (AGBP) is derived from the continental NPP data (without prior information on crop type), the following conversions are used:

(5) $\quad TBP \left(\dfrac{kg\ DM}{ha.day} \right) = 22.22 * NPP$

(6) $\quad AGBP \left(\dfrac{kg\ DM}{ha.day} \right) = 0.65 * 22.22 * NPP$

Where 0.65 is the conversion fraction from total to above ground biomass and 22.22 is the conversion from gC/m^2/day NPP to DMP (above and below ground dry biomass) in kg/ha/day, assuming a carbon fraction of 0.45 in organic matter.

Different Agricultural Water Productivity estimators are available in the WaPOR portal, pending the WaPOR version used. In version-1, the annual Gross or AGBP WP was estimated as:

(7) $\quad AGBP\ WP \left(\dfrac{kg}{m^3} \right) = \dfrac{\Sigma\ AGBP\ (kg)}{ETI_a\ (mm) * 10}$

Due to the uncertainty, introduced by the Total to Above-Ground Biomass conversion factor, the ABGP-WP was replaced in WaPOR version-2 by the Total Biomass WP, and estimated as:

(8) $\quad TBP\ WP \left(\dfrac{kg}{m^3} \right) = \dfrac{\Sigma\ TBP\ (kg)}{ETI_a\ (mm) * 10}$

We also distinguish Net Water Productivity estimators, only accounting for water use and transpiration by the vegetation or agricultural crops, and neglecting soil evaporation and interception losses. In version-2, Net WP is estimated as:

(9) $\quad Net\ WP \left(\dfrac{kg}{m^3} \right) = \dfrac{\Sigma\ TBP\ (kg)}{T_a\ (mm) * 10}$

The WaPOR database provides ETIa-WPR and NPP-WPR in three spatial resolutions dependent on the location and extent (Table 1-2). The ETIa and NPP is produced using the same processing chain at all resolution levels. NDVI, surface albedo and LST components are derived from satellite data. Other data input sources are described in Table 1-3.

Table 1-2. Description of the WaPOR V2 ETI$_a$-WPR and NPP - WPR data products, available on the WaPOR portal.

	Spatial resolution	Temporal resolution *	Spatial extent (in Africa)	Satellite (spatial resolution | return period)
Level I (L1)	250m	Dekadal	Continental Africa and Near East	MODIS (250m|1-day)
Level II (L2)	100m	Dekadal	Morocco, Tunisia, Egypt, Ghana, Kenya, Niger, Sudan, South Sudan, Mali, Benin, Ethiopia, Rwanda, Burundi, Mozambique, Uganda, Lebanon, Palestine, Jordan, Syria, Iraq, Yemen. **River basins:** Awash, Jordan, Litani. Niger, Nile.	** MODIS (250m|1-day) ** PROBA-V (100m|2-day)
Level III (L3)	30m	Dekadal	Awash, Ethiopia; Koga, Ethiopia; Office du Niger (ODN), Mali; Zankalon, Egypt; Bekaa Valley, Lebanon; Lamego, Mozambique; Busia, Kenya and Gezira, Sudan	Landsat (30m|16-day)

* Dekadal is approximately 10 days. It splits the month into three parts, where the first and second dekads are 10 days and the third dekad covers the remaining days in the month.
** MODIS is resampled to 100m up to 2013 and PROBA-V is used from March 2014.

Datasets (including intermediate datasets) used in the validation of ETI$_a$-WPR and NPP - WPR are described in Table 1-3. The SMC and NDVI layers were provided by the producer for the purpose of validation only. All other layers are available on the WaPOR portal. The NDVI quality layer and the LST quality layer are indicators of the quality of the input satellite data. The NDVI quality layer provides the gap, in days, since the last valid observation for that variable (though currently the NDVI quality layer, used in this evaluation, are giving the length of the gap). The LST quality layer provides the number of the days between the date of the data file and the previous remote sensing observation on which the data is based.

WaPOR further relies on input from weather data, air temperature, relative humidity wind speed, which are obtained from MERRA up to the start of 21-02-2014 and the GEOS-5 model after 21-02-2014 (Rienecker *et al.*, 2011). The weather data is resampled using a bilinear interpolation method to the 250m resolution. Air temperature is also resampled using SRTM digital elevation data and an adiabatic atmospheric lapse rate (FAO, 2020).

Table 1-3. Description of the intermediate and product datasets used for the validation of ETI$_a$-WPR and NPP-WPR (FAO, 2020) and the validation procedure they are used in. All datasets are available for the L1 data extent.

Dataset	Spatial | Temporal resolutions	Data sources	Sensors
NDVI		MOD09GQ, MOD09GQ, PROBA-V, Landsat 5,7,8	MODIS, PROBA-V, Landsat
SMC	Available for L1, L2 and L3 (per Table 1-2)	MOD11A1, MYD11A1, Landsat 5,7,8	MODIS, PROBA-V, Landsat
SR		SRTM, DEM	MSG
LST quality layer	As for L1; Table 1-2	MOD11A1, MYD11A1	MODIS
NDVI quality later	As for L1; Table 1-2	MOD09GQ, MOD09GQ, PROBA-V, Landsat 5,7,8	MODIS, PROBA-V, Landsat
PCP*	5km|daily	CHIRPS v2, CHIRP	TRMM, GPM,
RET	25km|daily	SRTM	MSG, MERRA/GEOS-5

The description of each L3 irrigated area used in the evaluation are given in Table 1-4. The L3 areas vary in major crop types and average plot sizes. Three irrigation schemes were the focus of field data collection; two in the Awash (the Wonji and the Metehara), which are located at either end of the L3 area, and the Bekaa Valley in Lebanon. The other three L3 locations, Lamego, Busia and Gezira, are not included in this validation report. Validation activities are currently underway in Gezira and will be published later in the year.

Table 1-4. Description of L3 irrigated scheme areas used in the product evaluation.

	Bekaa	Awash (Wonji and Metehara)	Koga	Zankalon	ODN
Average plot size of irrigated area (ha)	1.8	10.40	0.24	0.21	5.93
SD plot area (ha)	-	6.24	0.12	0.13	0.46
Major crops in irrigated area	Wheat, barley, legumes, potato, mixed vegetable, maize, grapes, fruit trees	Major: sugarcane. Minor: maize, fruit trees, haricot, crotalaria	Wheat, maize, potato, onion, cabbage, barley	Wheat, rice, maize, cotton, sugar beet, berseem, fava bean, tomato, potato	Rice, sugarcane
Vegetation in non-irrigated area	Sparse arid	Rainfed agriculture, bare/natural vegetation	Rainfed agriculture, bare/natural vegetation	NA	Sparse arid

A full description of the data products is given in the WaPOR methodology and user manual documents. The current available methodology documents detail the version-1 (V1) methodology for L1 (FAO, 2018a), L2 (FAO, 2018b) and L3 (FAO, 2018c). The recent version, version-2 (V2) includes changes to the SMC and RET components. In the previous version Globcover was used to provide estimates on certain land surface characteristics, in the current version the WaPOR land use classification has been used (which is now based on the EU Copernicus land cover classification). The details of these changes are available in the version 2 methodology (FAO, 2020b).

2. Validation methodology

2.1. WaPOR database validation process and analysis approach

The Committee on Earth Observing Satellites (CEOS) working group for calibration & validation (WGCV) defines validation as the process of assessing, by independent means, the quality of the data products derived from satellite observations. This is called product validation. The product validation ensures that the quality of the products is properly assessed, through quantification of the uncertainties in both the data itself and the measurement system deployed for generating the data. It includes a quantitative understanding and characterization of the measurement system and its bias in time and space. In this context, validation can be considered a process that encompasses the entire system, from sensor to product, and this corresponds to the Quality Assurance/Quality Control (QAQC) methods proposed for the WaPOR database (Zeng et al, 2015).

For the WaPOR data, the validation process consisted of several analyss and work procedures, carried out by the validator team (ITC), with feedback to the data producers (eLEAF and VITO), until a release version was obtained (Figure 2-1). The validation team operated on an independent basis from the data producers. These work processes and procedures have led so far to the β-version (2017), V1 (2018) and V2 (2019) of the WaPOR database.
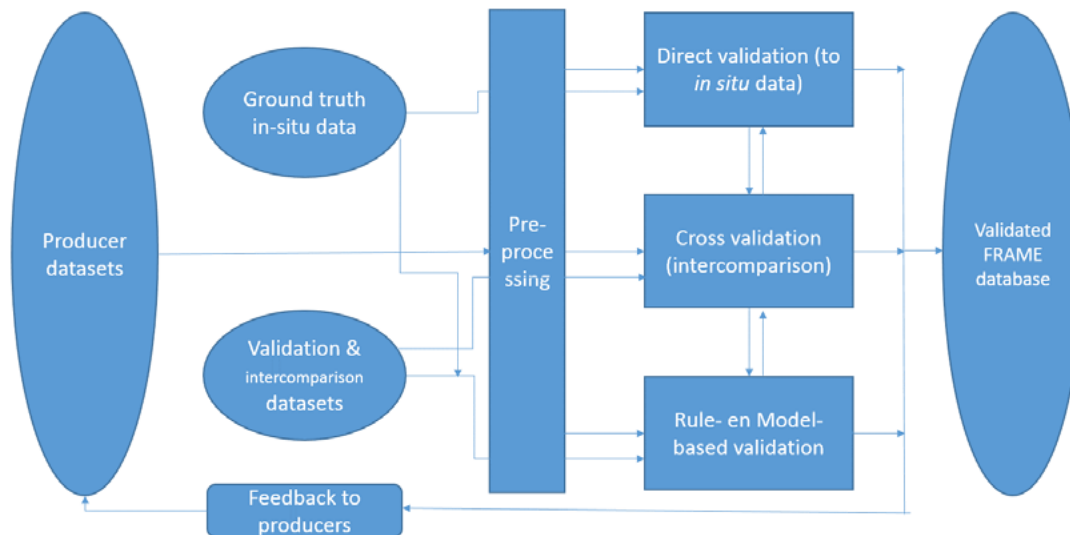
Figure 2-1. WaPOR database validation process and procedures (ref. FRAME Methodology reports).

Most large geospatial datasets cannot be fully quality-controlled against independent (e.g. in-situ) measurements and observations. This is especially the case for WaPOR, presenting Remote Sensing-based data components for Africa and the Near East and regions with (still) lesser density of *in-situ* observation infrastructure, compared to e.g. European, Asian and American regions and/or countries. Therefore, additional physical data consistency and plausibility considerations needed to be included in order to get better insight in the product quality and performance. Here, cross validation or inter comparisons to other available reference (peer-reviewed) datasets and/or comparisons to model simulations come into play, as well as physical rule- or model based data consistency evaluations, such as mass balance appraisals.

These major considerations on validation led to the selection and application of a number of recognized Earth Observation data validation techniques:

- Rule- or model-based physical consistency evaluation (e.g., mass balance appraisal)

- Cross validation using inter-product comparison to reference datasets

- Internal validation of spatial and temporal consistency (e.g. of time series)

- Direct validation against measured *in-situ* data and observations

- Consistency of data components among the three spatial resolution levels

Because the WaPOR database represents time series of data on the same water productivity variables at three spatial resolutions, the evaluation and validation of spatial and temporal data consistency among the three different spatial resolution layers (250m, 100m, and 30m) was also considered important.

The data analysis and validation approach and the workflows on the data are schematically illustrated in Figure 2-2. The different validation components and methods can also be recognized. We can mention cross- and internal validation for inter- and intra-product physical data consistency appraisal, direct validation to in-situ ground data and the evaluation of the spatial resolution level data consistency. The product physical validation and direct validation were undertaken on the L1 product for the period 2009-2018. The physical validation includes inter- and intra-product physical consistency. The inter-product physical comparison includes an assessment of the water balance and water availability (ETI_a), comparison to other global products (ETI_a and NPP) and literature (cross-validation) (ETI_a) for basins in Africa. The water balance utilises other existing continental datasets to complete the water balance and is therefore also considered cross-validation. The intra-product physical consistency check is undertaken by observing the spatial and temporal consistency between WaPOR products for Africa and the Near East. The spatial and temporal consistency checks if spatial and temporal patterns are being captured by not only the ETI_a and NPP, but the SMC, NDVI and SR and also considers how they inter relate. We therefore consider this an intra-product spatial and temporal consistency check. The direct validation involves comparison to ET_a, NPP and RET to estimations from in-situ EC stations and to farmer reported yields (NPP only). The level consistency checks for the consistency between levels and therefore indicates if the quality of the L1 product is representative of the L2 and L3 products. Additionally, a comparison between V1 and V2 ETI_a and NPP products was undertaken. The metrics used in the validation are summarized in Annex A.
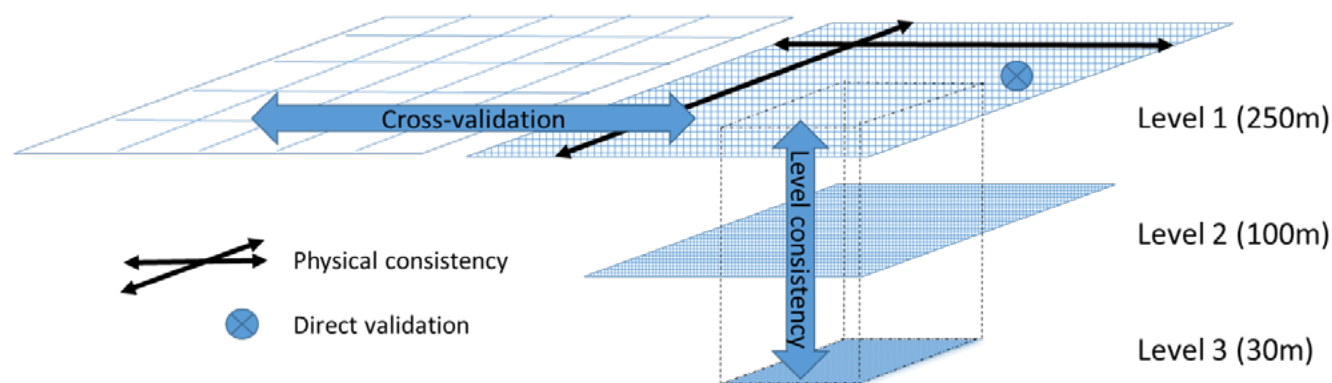
Figure 2-2. Approach used for the validation of the ETI_a and NPP WaPOR products in Africa and the Near East.

2.2. Rule- and model-based validation for physical consistency

2.2.1. Water availability and mass balance appraisal

The basin-scale performance of ETI_a-WPR was analysed for the 22 major hydrological river basins of Africa (Lehner & Grill, 2013) (Figure 2-3). First, the ETI_a-WPR was compared to the PCP on an annual basis to compare the water used by evaporative processes or ETI_a-WPR to the water available from precipitation or PCP. Second, the basin-scale water balance approach compared the long term ETI_a-WPR product to the long term

ET_a derived from (i) the water balance (ET_a-WB), (ii) the Budyko (1974) approach (ET_a-Fu), (iii) MODIS ET_a (ET_a-MOD16) and against available literature. In many studies the long term water balance (>1 year) for large basins assumes a negligible change in storage (Hobbins, Ramírez, & Brown, 2001; Wang & Alimohammadi, 2012; Zhang *et al.*, 2012)suggesting that positive trends in evaporation may occur in 'wet' regions where energy supply limits evaporation. However, decadal trends in evaporation estimated from water balances of 110 wet catchments do not match trends in evaporation estimated using three alternative methods: 1. The long-term water balance, taken from 2009-2018 in this case, was therefore defined using equation 5.

$$(10) \quad ET_a \text{ - WB (mm/yr)} = PCP \text{ (mm/yr)} - Q \text{ (mm/yr)}$$

Where PCP is the long-term precipitation and Q is the long-term surface run-off and the ET_a-WB is the long term ET_a derived from the water balance. The PCP product found in the WaPOR portal was obtained from the Climate Hazards group Infrared Precipitation with Stations (CHIRPS) dataset. CHIRPS uses the Tropical Rainfall Measuring Mission Multi-satellite Precipitation Analysis version 7 (TMPA 3B42 v7) to calibrate the global Cold Cloud Duration (CCD) rainfall estimates as well as a 'smart' interpolation of gauge data from the World Meteorological Organization's Global Telecommunication System (GTS) (Funk *et al.*, 2015). The long term Q is obtained from the Global Streamflow Characteristics Dataset (GSCD) from Beck, De Roo and Van Dijk (2015)including mean annual Q, baseflow index, and a number of flow percentiles. Testing coefficients of determination for the estimation of the Q characteristics ranged from 0.55 for the baseflow recession constant to 0.93 for the Q timing. Overall, climate indices dominated among the predictors. Predictors related to soils and geology were relatively unimportant, perhaps due to their data quality. The trained neural network ensembles were subsequently applied spatially over the entire ice-free land surface, resulting in global maps of the Q characteristics (0.125° resolution). The GSCD consists of global streamflow maps, including percentile and mean Q, providing information about runoff behaviour for the entire continental land surfaces including ungauged regions.
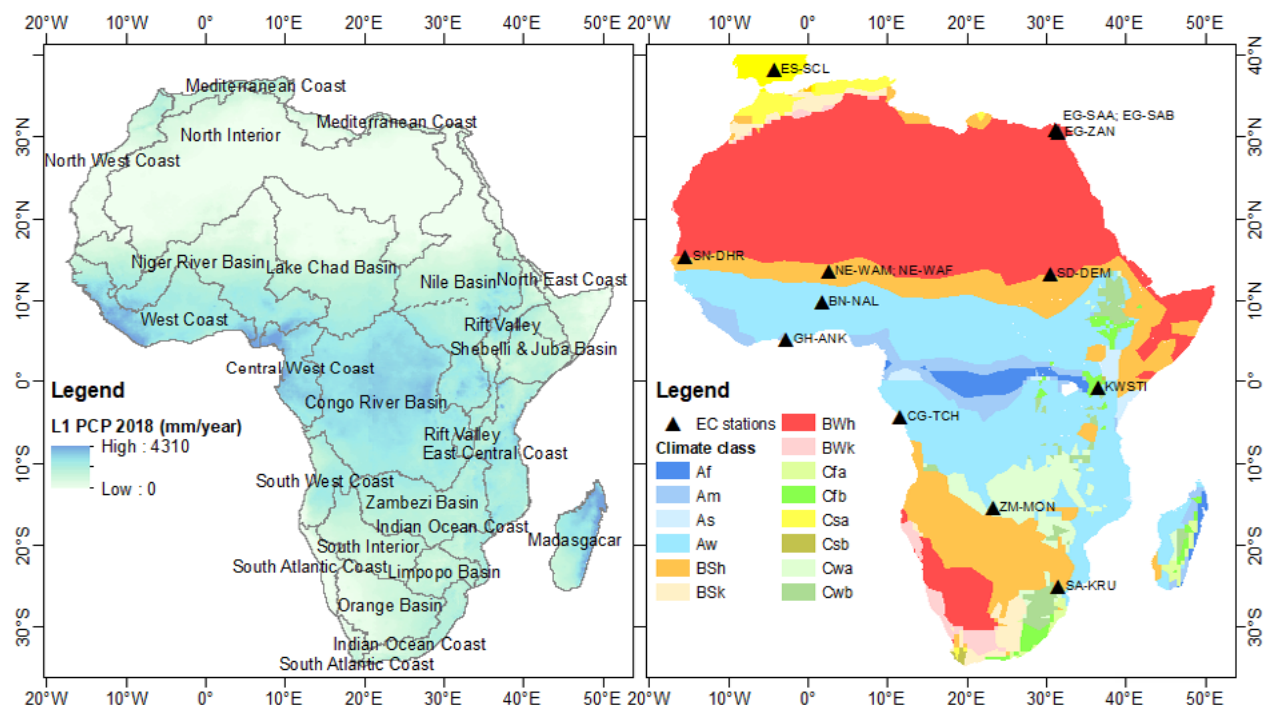
Figure 2-3. The 22 major hydrological basins of Africa with annual rainfall (L1 1 PCP-2018 as example) used in the water balance approach (left) and right – Koppen-Geiger climate classification and locations of eddy covariance stations (right). Climate class legend: Af – tropical rainforest, Am – tropical monsoon, As – tropical dry savanna, Aw – tropical wet savanna, BSh – arid hot steppe, BSk, arid steppe cold, BWh – arid hot desert, BWk – arid cold steppe, Cfa – temperate without dry season hot summer, Cfb – temperate without dry season warm summer, Csa – temperate dry summer hot summer, Csb – temperate dry summer warm summer, Cwa – temperate dry winter hot summer, Cwb – temperate dry winter warm summer.
Source: FAO 2020a, with authors' additional inputs

Studies show that long term average ET_a shows a good relationship with long term precipitation at catchment scale (Zhang *et al.*, 2004). Budyko (1974) postulated that the long-term mean ET_a at catchment scale was governed by water availability (PPT) and atmospheric demand (Rn). With the advent of long-term datasets of ET_a, precipitation and Rn can be assessed and compared at catchment scale (Zhang *et al.*, 2008). Lu Zhang *et al.*, (2008) estimated the ET_a based on Fu (1981) and Budyko (1974). The ET_a at the basin scales becomes:

$$(11) \qquad \frac{ET_a - Fu}{PCP} = 1 + \frac{RET}{PCP} - \left[1 + \left(\frac{RET}{PCP} \right)^w \right]^{\frac{1}{w}}$$

Where w is the plant-water availability factor. This factor was taken to be 2.78. This relationship is similar to Budyko (1958) in assuming that equilibrium water balance is controlled by water availability and atmospheric demand. L. Zhang *et al.* (2004) argued that Fu's (1981) approach has a better "physical basis and is a better model for estimating mean annual ET_a compared with other similar empirical equations".

The ET_a values from WaPOR, from the water balance and from Budyko were compared to the ET_a from the MODIS Global Evapotranspiration Project (ET_a-MOD16) for the period 2000-2013 (Mu, Heinsch, Zhao, & Running, 2007; Mu, Zhao, & Running, 2013)and the second was the Penman-Monteith (P-M and to values from literature for basins where data is available. The ET_a-MOD16 product is also based on the PM equation and considers the surface energy partitioning process and environmental constraints on ET_a. Like, ETI_a-WPR, ET_a-MOD16 is considered the sum of soil evaporation, plant transpiration and rainfall interception by vegetation. The algorithm uses ground-based meteorological observations and remote sensing observations from MODIS.

2.3.   Cross validation using comparison to reference data

The L1 NPP-WPR and L1 ETI_a-WPR were compared (cross-validation) on an annual scale to the annual NPP from the MODIS/Terra 8-day L4 Global 500m Net Primary Productivity (GPP-MOD17) (Mu *et al.*, 2011) and the MODIS Global Evapotranspiration Project 8-day L4 Global 500m (ET_a-MOD16) (Running *et al.*, 2017). The spatial consistency between products was also considered (i.e. a visual comparison and the average values per LCC and climate class – Table 2-1 and Figure 2-3). A sample size (the same described for the next section - section 2.4) was used. The products were aggregated to an annual scale for comparison. The GPP-MOD17 was multiplied by 0.5 to obtain NPP-MOD17 (same factor as applied in WaPOR).

The next inter comparison of L1 NPP-WPR and ETI_a-WPR data was with the geostationary Meteosat dekadal 10-day GPP (GPP-MSG) and 1-day ET_a (ET_a-MSG) product from the EUMETSAT LandSAF (LSASAF) (www.landsaf.ipma.pt). We refer to these webpages for more information on this data. The LSASAF has since April 2018 released the GPP data for the MSG dish covering Africa, Europe and part of the Middle-east. This EO product is derived from the high frequency (15-minute) geostationary (3 km resolution and 1 km HRV) MSG current Meteosat-10 observations on radiation, land surface variables and uses also the Monteith (1977, 1972) PAR-LUE efficiency modelling approach (for ref. see webpages). The ET_a-MSG is based on the Tiled ECMWF Surface Scheme for Exchange Processes over Land (TESSEL) and the Soil-Vegetation- Atmosphere Transfer (SVAT) scheme used by ECMWF (Pieroux *et al.*, 2001). The product is daily, therefore the daily values are aggregated to agree with the temporal resolution of the ETI_a-WPR product.

We used this data comparison to verify the spatial and temporal pattern at a continental, dekadal scale, and to briefly analyze differences observed. To be able to compare both data values, we used the same plant autotrophic respiration or Ra adjustment used in L1 NPP-WPR data set, to convert the GPP-MSG to NPP values (NPP-MSG = GPP-MSG x 0.5). The L1 NPP-WPR and ETI_a-WPR values were resampled to the coarser 3km MSG resolution for pixel-based comparison purposes. A 25km grid was created to extract points to plot a linear regression for cross-comparison. The data are displayed in a MSG geostationary projection, but can also be resampled to more conventional equirectangular (e.g. LEAE Plate Carrée) or EPSG:32636 – WGS84 / UTM Zones (Universal Transverse Mercator projection) for more close inspections. Four dekads, representing each

season, were selected for comparison: 1801 (ETI$_a$ only), 1810, 1820, 1830, 1901 (NPP only).

The L1 and L3 ETI$_a$-WPR were compared to literature values in the Bekaa Valley, Lebanon (L3 area). Seasonal and annual basin mean values were compared to other remote sensing based ET approaches, including pySEBAL, METRIC and MODIS.

Table 2-1. Land Cover Classification and corresponding class numbers as used in the L1 WaPOR Land Cover dataset.

LCC	Class #
Shrubland	20
Grassland	30
Cropland/rainfed	41
Cropland/irrigated	42
Built-up	50
Bare / sparse vegetation	60
Shrub or herbaceous cover, flooded	90
Tree cover: closed, evergreen broadleaved	112
Tree cover: closed, deciduous broadleaved	114
Tree cover: closed, unknown type	116
Tree cover: open, evergreen broadleaved	122
Tree cover: open, deciduous broadleaved	124
Tree cover: open, unknown type	126

2.4.   Internal validation of spatial and temporal consistency

The temporal and spatial trends were observed over the African continent in space and time by observing mean ETI$_a$-WPR, NPP - WPR, SMC, SR and NDVI for all climate zones during the study period on a 10-day average time series basis. The Köppen-Geiger climate classification (Figure 2-3) was used to consider the mean 10-day values for the main climatic zones in Africa (Kottek, Grieser, Beck, Rudolf, & Rubel, 2006). A sample size of 30,000 stratified random pixels was used to represent the continent. This corresponds to <0.01% of the total image data, however, was considered a suitable sample size to represent the seasonal trends for the major climate zones (Blatchford *et al.*, 2019 – under review). Africa is dominated by only a few climate classes, i.e., the arid or desert class -B (57.2%), followed by the tropical class - A (31%) and then warm temperate - C (11.8%). The largest sample count corresponds to the largest climate zones, with a linear 1:1 line representing area to count. The data was further disaggregated based on the northern and southern hemispheres to account for opposite seasonal patterns. Further, the water productivity trend on an annual scale was analysed for each climate zone to observe if trends aligned with expected trends. The AGBP water productivity (AGBP WP) was assessed for each climate zone on an annual scale to verify water productivity trends based on climate.

2.5.   Direct validation to *in-situ* ground observations

2.5.1.   Comparison to Eddy Covariance flux tower data

Eddy Covariance (EC) flux measurements permit to determine sensible heat fluxes and also H2O and CO2 gas exchanges between the land surface - vegetation complex and the lower atmosphere. The eddy covariance technique samples upward and downward moving air (vertical turbulent motions) to determine the net difference of heat or gas exchange moving across the canopy-atmosphere interface (Baldocchi, 2003). Eddy covariance

is one of the most reliable and accurate methods available or quantifying exchanges of carbon dioxide, water vapour and energy exchange. The range of error associated with EC measurements, when carried out by an expert, can be as high as 10-15% (Allen *et al.*, 2011). Others have reported EC to underestimate latent heat fluxes by up to 20%(Glenn *et al.*, 2011).

The ETI_a-WPR, NPP-WPR and RET-WPR was compared to the in-situ ET_a (ET_a-EC), NPP (NPP-EC) and RET-EC from EC flux tower measurements at a 10-day (dekad) and monthly scale at 14 locations (Figure 2-3). The country, station code, vegetation, climate zones and available data for comparison – for both WaPOR and the local sites, are shown in Table 2-2. Each of the major climates classes are represented by at least one station, four sites are located in the equatorial class, four are located in the warm temperate class and nine are located in the semi-arid to arid classes.

The SA-SKU, SN-DHR, GH-ANK, SD-DEM, CG-TCH, ZM-MON and ES-SCL EC sites were sourced from the global Fluxes Database Cluster Dataset (FLUXNET). The FLUXNET 2015 (https://fluxnet.fluxdata.org/) dataset consist of open-source high-quality data collected from multiple regional networks. The NE-WAM, NE-WAF and BN-NAL sites were under the African Monsoon Multidisciplinary Analysis—Coupling the Tropical Atmosphere and the Hydrological Cycle (AMMA-CATCH) project, aiming at establishing long term observations on climate and the environment over Western Africa. The KWSTI in Kenya site is operated by the Faculty for Geo-Information Science and Earth Observation of the University of Twente (ITC-UTWENTE) in partnership with the Water Resources Management Authority (WRMA), the Kenya Wildlife Services (KWS) and Egerton University. The EG-ZAN, EG-SAA and EG-SAB sites are operated through the University of Tsukuba, in partnership with Cairo University, National Water Research Center, Delta Barrage, Qalubia, Egypt and the Agriculture Research Center, Giza, Egypt in the Nile Delta. These irrigated sites in the Nile Delta, are under rotation with three major summer crops – rice, maize and cotton – and four major winter crops – wheat, berseem (*Trifolium alexandrinum*), fava beans and sugar beet.

The ETI_a-WPR and NPP-WPR for L1 (250m) was spatially averaged over a 3x3 pixel window covering the EC station, based on the assumption that the window represents the measurement footprint of the EC flux tower station. The ETI_a-WPR for the in-situ comparison was taken as the sum of soil evaporation, plant transpiration and interception. The ET_a-EC data were derived from the latent heat flux (LE) measurements and aggregated temporally to dekadal averages to match the temporal resolution of the WaPOR ETI_a products. The NPP-EC was derived by assuming the NPP at the EC station is equal to GPPx0.5 (which is also assumed in the WaPOR database). This is the same NPP to GPP fraction as used by WaPOR. The RET-EC was compared directly to the pixel due to the lower spatial resolution of the RET-WPR. The RET-EC was estimated using the same method adopted by WaPOR (FAO 2018), which is based on FAO-56 (1996), and was derived from in-situ meteorological data:

(12) $$RET = \frac{\Delta(R_n - G) + p * c_p * \frac{(e_{sat} - e_a)}{r_a}}{\Delta + \gamma \left(1 + 0.34 * \frac{r_s}{r_a}\right)}$$

Where p is air density (kg/m3), c_p is the specific heat (J/°C), r_a is the aerodynamic resistance (s/m), r_s is the bulk surface resistance (s/m), Δ is the slope vapour pressure curve [kPa/°C] and γ psychrometric constant [kPa/°C]. The Reference ET estimation, r_s is taken as 70 s/m and the r_a is taken as 208/uobs. uobs is the observed wind speed (m/s) at 10m.

Intermediate products, including WaPOR NDVI, SMC, SR and the NDVI and LST quality layers were analysed along with the ET_a trends to identify possible sources of error. When the 30-min data was available the LE flux data was aggregated to daily and dekadal timesteps by taking into account for no data (NaN flag), non-removed spikes, early morning (dawn) and evening (day-night inversion issues), dew spiking, etc, which are not necessarily all removed by the standard Eddy Covariance pre-processing software's (converting the high frequency sonic 2 to 30-second and gas analyser measurements to 30-minute interval fluxes). Some data was pre-processed and only available on a daily timestep.

Table 2-2. EC flux tower site descriptions and available data for direct '*in-situ*' validation.

Site	Product	Country	Ecosystem	Climate	Data-years used	Reference Paper
SA-SKU	ET_a	South Africa	Savannas wooded grassland	BSh	2009; 2011	Majozi *et al.*, (2017a)
SN-DHR	ET_a, NPP, RET	Senegal	Savannas	BWh	2010 - 2013	Tagesson *et al.*, (2015)
SD-DEM	ET_a, NPP, RET	Sudan	Savannas	BWh	2009	Ardö, Mölder, El-Tahir, & Elkhidir (2008)
NE-WAM	ET_a	Niger	Crops (millet, bare soil, tiger bush)	BSh	2009 - 2012	Boulain, Cappelaere, Séguis, Favreau, & Gignoux (2009); Ramier *et al.*, (2009)
NE-WAF	ET_a	Niger	Crops (fallow; shrubs)	BSh	2010 - 2011	
ES-SCL	ET_a	Spain	Pasture and Scatter oak trees	Csa	2016 - 2017	Personal Communication with Maria P Gonzalez
GH-ANK	ET_a, NPP, RET	Ghana	Evergreen broadleaf forests	Am	2011 - 2014	Chiti, Certini, Grieco, & Valentini (2010)
BN-NAL	ET_a	Benin	Guinean savanna vegetation	Aw	2009	Mamadou *et al.*, (2014)
KWSTI	ET_a	Kenya	Open shrubland	Cfb	2012 - 2014	Odongo *et al.*, (2016)Ltd.
CG-TCH	ET_a, NPP, RET	Republic of Congo	Savanna grassland	Aw	2009	Merbold *et al.*, (2009)
ZM-MON	ET_a, NPP, RET	Zambia	Deciduous broadleaf forest	Cwa	2009	
EG-ZAN	ET_a, RET	Egypt	Irrigated agriculture	BWh	2011 - 2013	Sugita, Matsuno, El-Kilani, Abdel-Fattah & Mahmoud (2017)
EG-SAA	ET_a, RET	Egypt	Irrigated agriculture	BWh	2011 - 2013	
EG-SAB	ET_a, RET	Egypt	Irrigated agriculture	BWh	2011 - 2013	

2.5.2.   Comparison with field survey and farmer reported *in-situ* data

The field validation approach in this report focused on two L3 areas of the WaPOR portal: the Litani Basin (Bekaa valley) in Lebanon and the upper Awash river Basin in Ethiopia (Figure 2-4). Field data, focusing on crop rotations, soil and irrigation management and crop yields, were collected by UT-ITC in the 2016-2018 period.
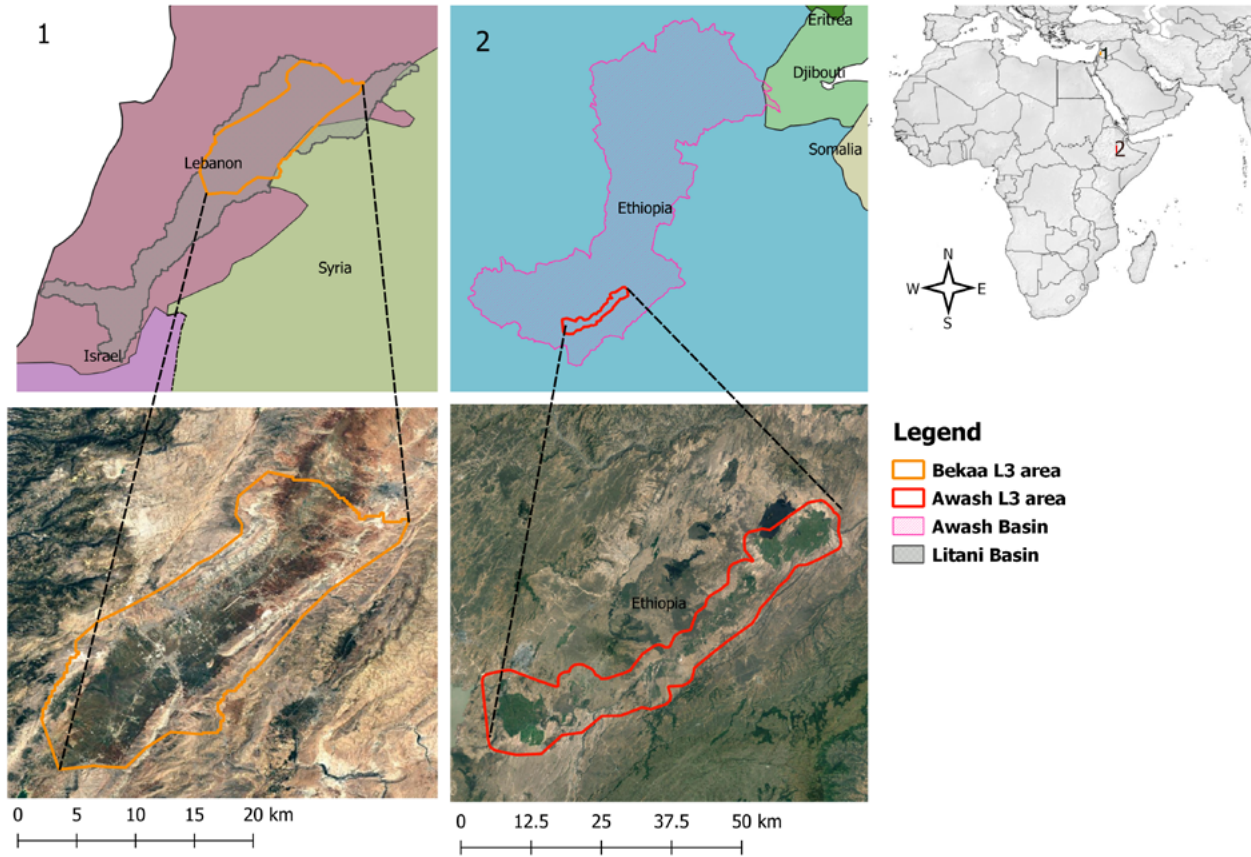
Figure 2-4. Location of the Bekaa Valley and Awash areas visited for the field validation.
Source: FAO 2020a, with authors' additional inputs

Bekaa Valley, Lebanon

A field survey campaign was carried out in July 2017 (by H.Nouri from UT-CTW and M.Blatchford from UT-ITC). The area represents a mixed cropping system with frequent crop rotation. The visit was done during the potato and wheat harvests, therefore these crops were the focus of the field survey. In total 19 potato and 15 wheat surveys were used in the validation of the WaPOR NPP in the Bekaa Valley. The locations of the field surveys were selected on ease of access and security. The WaPOR yields for the field plots was estimated by extracting the mean NPP from each delineated plot for each dekad over the season and aggregating the mean values. The NPP was then converted to yield using the following equation (9):

$$(13) \quad Yield\ (ton * ha^{-1}) = \frac{HI * LUE\ \text{cor}\ \Sigma_{SOS}^{EOS} NPP\ (gC * m^{-2} * day)}{a * AGBF\ (1 - \theta)}$$

The start of season (SOS) and end of season (EOS) were recording during the interviews with farmers. The varying number of days per dekad are into account (between 8-11 days per dekad) by multiplying the average dekadal NPP by the number of days in the dekad. All dekads within the crop season (SOS and EOS) period are than aggregated (summed). The conversion factors and constants are shown in Table 2-3, which were based on literature and information from the WaPOR data producers. These correction factors are based on the plots

being classified as either LCC=41 and LCC=42 in the L2 Land Cover Classification (L2-LCC) map in the portal. The LUE associated with these LCC in WaPOR is 2.7 gDM/MJ or 1.215 gC/MJ. This corresponds to values found in literature, which report the LUE for C3 crops, such as potato and wheat to be 1.17 gC/MJ (Kooman and Rabbinge, 1996) and 1.13 gC/MJ (Lobell *et al.*, 2002), All other parameters for wheat and potato were taken from the parameters suggested by the producer. A LUE correction can be used in case one wants to use a specific crop LUE, which differs from the currently C3 average standard (2.7 gDM/MJ or 2.7 kgDM/GJPA) used by WaPOR.

Table 2-3. Parameters used to derive potato tuber yield, wheat yield and sugarcane AGBP from NPP-WPR.

Acronym	Factor	Wheat (grain+straw)	Potato tuber	Sugarcane AGBP
LUE cor	LUE correction (LUE actual/LUE WaPOR)	0.93	0.96	2.15*
AGBF	Above Ground Biomass Fraction	0.86	0.20	0.80
HI	Harvest Index	0.37	0.80	0.95
θ	Moisture content	0.15	0.80	0.65
a	NPP (gC/m^2/day) <-> DMP (tonDM/ha/day)	All crops = 0.045 x 10^6		

(*) Sugarcane C4 crop LUE correction for current WaPOR LUE standard (based on an average C3 vegetation LUE)

Awash river basin, Ethiopia

The Wonji and Metehara irrigated sugarcane plantations (further denoted as Wonji and Metehara) were the focus of the second L3 field visit, in September-October 2018. The Wonji and Metehara are located in the L3 area located in the Awash Basin, Ethiopia (Figure 2-4). The Wonji is at the Southern end of the L3 area and the Metehara is located at the Northern end of the L3 area. The focus crop in the plantations is sugarcane has a general growing season of 10-24 months in that region. After the first season (the plantation season), there are up to eleven ratoon seasons. Between the final ratoon season and the following plantation season, the field is left either fallow or planted with legumes (primarily haricot) for the length of a legume growing season. The harvest date is selected based on the crop growth stage and logistics associated with harvest. The Wonji has some smaller expansion areas, some of which are located within the L3 spatial extent. However, due to safety and security reasons, some of these small areas could not be included in the 2017 field visit.

The available sugarcane harvest, the soil class and the management practices and above ground biomass (AGBP) were provided by the Wonji Estate manager. This included 66 plots within the area with usable yield data within the WaPOR data timeframe and within the L3 spatial extent. Similar field data were collected for the Metehara irrigated sugarcane plantation, which lies in the L3 WaPOR spatial extent, with over 1000 plots, distributed over space and time. The reported AGBP (with planting and harvest dates) were used for a direct NPP comparison.

The average dekad value for each NPP-WPR pixel falling within the field was aggregated over the growing season for each plot, and the yield was derived using the conversion factors in Table 2-3, following Equation 9. The yield was taken as the estate or farmer reported above ground biomass production (AGBP). All parameters used in the conversion of NPP-WPR to sugarcane AGBP, with the exception of the harvest index or HI, were taken from the WaPOR land cover classification and crop type tables with their associated parameters. As fresh AGBP was compared rather than yield, the HI was taken as 0.95 (allowing 5% for losses).

Current values of WaPOR NPP are underestimated for C4 crops, such as maize and sugarcane. A LUE correction factor of 2.15 was therefore used for the C4 crop sugarcane, which converts the default WaPOR LUE value (C3 crop average) to the LUE for sugarcane, which is 5.8 gDM/MJ and equivalent to 2.6 gC/MJ. The default value for the above ground biomass fraction (AGBF) was used. The HI of 0.95 was used as the sugarcane is cut as close to the ground as possible. The reported yield is fresh matter and not dry matter, a conversion for moisture content was also required.

2.6. Validation of consistency among the three spatial resolution levels

L3 and L2 ETI_a-WPR and NPP-WPR were compared to the L1 data for the period of 2009-2018 on a 10-day aggregated time step basis. A bilinear resampling method was used to spatially aggregate the high-resolution L3 and L2 layers to the coarse L1 layer resolution. A stratified random sample of 30,000 points over the entire L2 extent was used for the comparison of the L1 and L2. The L1 and L3 comparison was done over the entire L3 extent of the Awash, Zankalon, ODN and Koga L3 irrigation areas for all pixels.

The root mean square error (RMSE), bias, correlation (r) and coefficient of determination (R^2) were estimated for all dekads to determine if disagreement between levels was systematic or random. Since the EC station at Zankalon (Nile delta, Egypt) is located in a L3 area, all three levels were also compared to the ET_a-EC at this station as part of the level consistency. The method described in section 2.5 was used to extract the L2 and L3 ETI_a-WPR at the station.

The implications of level consistency of water productivity were than assessed for three irrigation schemes – the Wonji (in the Awash), the ODN and the Koga. The water productivity was taken as the crop water productivity in the Wonji (as the crop is known – sugarcane) and as AGBP WP in the ODN and Koga. The values were taken as annual values. Annual WP for all years between 2009-2018 at plot and at scheme level were compared.

2.7. Comparison between WaPOR version updates

Two most recent WaPOR versions (v.1 and v.2) were compared as follows:

- comparison of annual basin level (as per section 2.2.1) NPP and ETI_a

- NPP, ETI_a, plant transpiration (T) and soil evaporation (E), at the WaPOR time step (daily values aggregated over approx. 10-day (3 dekads per month) periods), (as per section 2.4)

- 10-day time step (dekadal), at pixel scale (3x3 L1 window) at the 14 Eddy Covariance flux tower locations (as per section 2.5) for ETI_a and NPP data components

The V1 data were extracted using the same procedures as described in sections 2.2.1, 2.4 and 2.5 and compared directly to version V2 data. The statistical metrics used for comparison are described in the Appendix A.

3. Validation Results

The numerical accuracy of the retrieval of water productivity estimates from the FAO-WaPOR web portal was also verified by a fully independent estimation of AGBP-WP and TBP-WP for a specific location in Africa (Level-1 250m pixel). For this test, a one-year sample (36-dekads of 2018) of core L1 ETI_a and L1 NPP time series data directly received from the WaPOR database developer eLEAF was used. The results of this quality control exercise are documented in Annex E. No difference was detected (four decimals precision) between the two independent WP estimates for the location, confirming the data downloads and pre-processing routines (e.g. time series generation) for direct analysis on the WaPOR portal, are fully consistent with the data from the developer.

3.1. Rule- and model-based validation of physical consistency

3.1.1. Water mass balance and Budyko curve (Fu-model variant) appraisal

The annual basin ETI_a-WPR divided by the annual basin PCP (ETI_a/PCP) during 2009-2018 for Africa is shown in Figure 3-1. The annual ETI_a-WPR exceeds the annual PCP (ETI_a/PCP >1) on 55% occasions for all basins over the 10 years study period. The highest number of exceedances occur in 2014 and 2016 (64%) and the lowest number of exceedances occur in 2018 (27%). The majority of these exceedances, 66%, are however less than 10%. The average ETI_a-WPR to PCP ratio for the continent of Africa is 0.93. The lowest ratio is in 2010, 0.87, and the highest is in 2015, 0.97. These ratios are significantly higher than the suggested average, 0.65, of evapotranspiration to precipitation ratio over the global terrestrial surfaces (McDonald, 1961). This ratio is expected to be lower in dry continents. Except for Lake Chad Basin, basins in the Central, North and West of Africa have ETI_a-WPR less than PCP. Most of the exceedances (ETI_a > PCP) occurs in the Southern part of Africa and in the Eastern Horn of Africa.

The basins have the highest ETI_a-WPR/PCP ratio in 2015, particularly in Southern Africa. All basins south of Zambezi Basin show a significant decrease in PCP from 2014 to 2015, including a 246, 98 and 238 mm/year drop respectively in Limpopo, Orange and the South Interior. In the same timeframe, the largest ETI_a-WPR change is observed in Limpopo, with a 17 mm/year increase, followed by the South Atlantic Coast with a 35mm/year decrease. The decrease in PCP is attributed to the drought in this region during this period as a result of the El Nino climatic event (USAID, 2016). However, ETI_a-WPR does not seem to respond appropriately to these extreme drops in PCP, which is likely because the SMC does not show any significant response to reduced PCP in this period. The PCP drop in 2015 in drought affected basins ranged from 16.8-39.1% of the 2009-2018 average while the SMC drop only ranged from 2.2-6.0%. Therefore the ETI_a-WPR is not being properly limited by reduced water availability in the soil.

The average (av.), minimum (min) and maximum (max) annual ETI_a-WPR and PCP values for the 2009-2018 period are shown in Table 3-1. Where literature is available, annual estimates of ETI_a-WPR and PCP are compared with historical estimates on annual ET_a and PCP, with ET_a-MOD16, ET_a-Fu and with the ET_a-WB. In most cases, the ETI_a-WPR is larger than the ET_a values in literature, from the water balance and from MOD16. The PCP falls within the range of literature for all but 3 basins. The average PCP in the database is higher than that in literature for the Congo. The PCP is less than that found in literature in the Limpopo and Orange Basin, which is also likely due to the drought in this region which occurred after the estimates reported in the literature. It is also important to note that the Congo River Basin, Central West Coast and west coast basins have vast areas of low quality NDVI and LST layers for much of the year. This makes the annual mean ETI_a values derived from optical, infrared and thermal remote sensing less reliable in these basins.
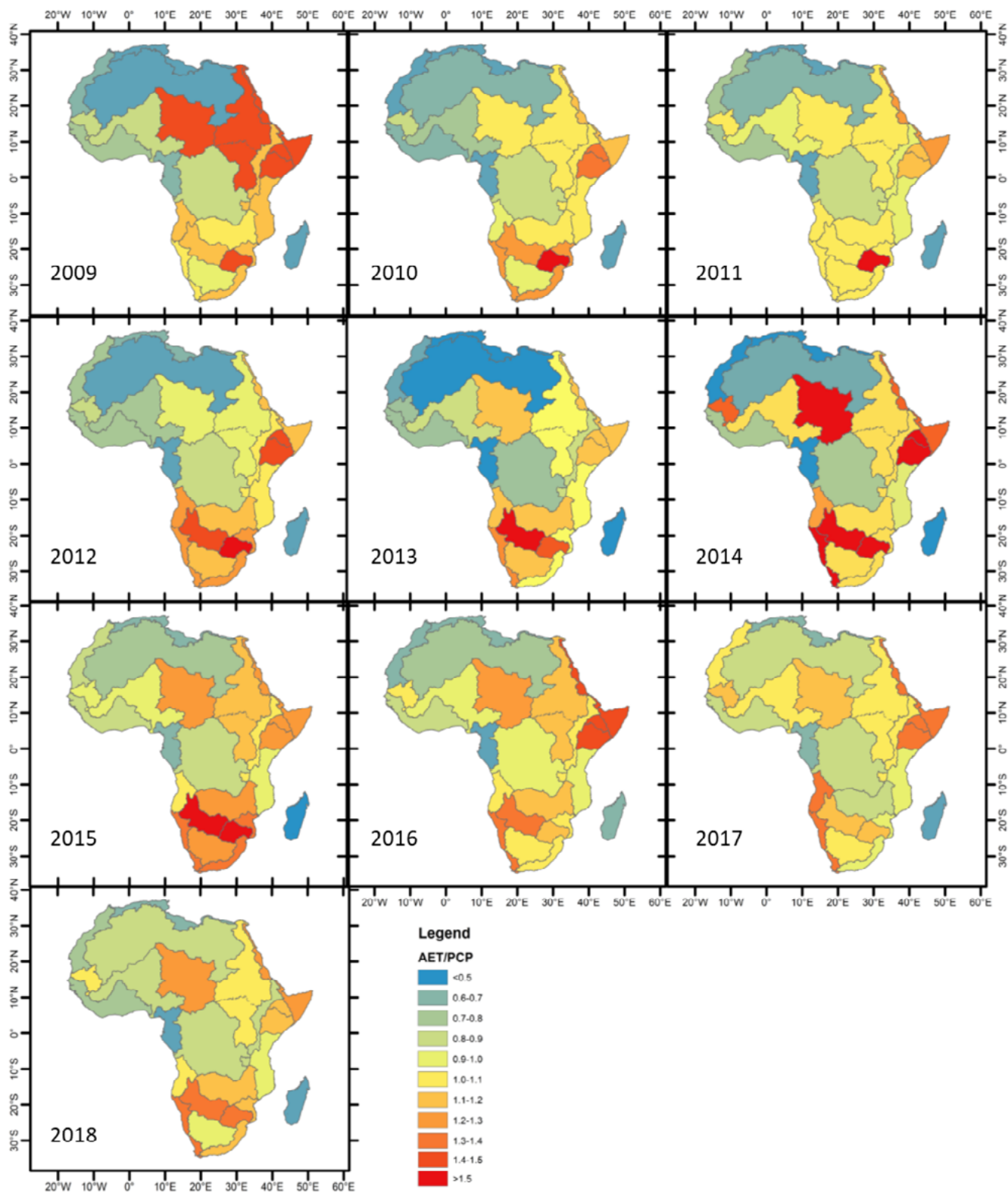
Figure 3-1. Annual basin-averaged ETI$_a$-WPR/PCP ratio's for 22 major river v2basins in Africa for the 10-year period 2009-2018, as derived from Level-1 WaPOR V2.

Source: FAO 2020a, with authors' additional inputs

Table 3-1. Annual PCP and ETI_a (min and max) of major basins derived from the WaPOR database for the period 2009-2018 compared against available values in literature and the ET_a-WB (all values in mm/year).

Basin	PCP-WPR av.* (min|max)	PCP literature	ETI_a-WPR av.* (min|max)	ET_a - MOD16 **	ET_a - Fu	ET_a Literature	ET_a-WB
Lake Chad Basin	374 (322 |442)	236 - 451[1-3]	437 (399 |471)	-	371	216-363[1,3]	346
Nile Basin	649 (538 |706)	512 - 693[1,2,4]	714 (685 |737)	-	628	416-515[1,4]	-
Senegal River Basin	548 (472 |630)	252 - 550[1,2]	529 (475 |589)	-	536	258-323[1]	468
Rift Valley	762 (682 |887)	650[2]	771 (727 |803)	568	715	-	591
Niger River Basin	679 (625 |754)	423 - 740[1-3]	618 (583 |665)	-	656	329-410[1,3]	553
Shebelli & Juba Basin	474 (400 |602)	435 - 518[2,5]	615 (559 |698)	455	465	504	367
Central West Coast	1847 (1598 |1908)	1785[2]	1108 (1046 |1177)	1159	1112	-	959
Congo River Basin	1517 (1452 |1600)	1165 - 1689[1,2]	1318 (1253 |1401)	949	1072	1004-1098[1,6]	-
East Central Coast	966 (876 |1135)	960[2]	970 (928 |1038)	872	1096	-	784
South West Coast	861 (697 |984)	940[2]	968 (886 |1078)	758	864	-	676
Zambezi Basin	928 (772 |1094)	732 - 1016[1,2,7]	1006 (942 |1069)	627	841	637-798[1,7]	-
Limpopo Basin	519 (326 |683)	530 - 648[1,8]	770 (662 |845)	396	503	516-569[1]	474
Orange Basin	303 (213 |368)	325 - 393[1,2]	320 (272 |388)	-	300	306-335[1]	280

[1] Voisin, Wood, & Lettenmaier, (2008) yet outside the developed world in situ networks are so sparse as to make alternative methods of precipitation estimation essential. Several such alternative precipitation products that would be adequate to drive hydrologic prediction models at regional and global scales are evaluated. As a benchmark, a gridded station-based dataset is used, which is compared with the global 40-yr ECMWF Re-Analysis (ERA-40; [2] FAO, (1997); [3] Li, Coe, & Ramankutty, (2005); [4] The Nile Basin Initiative Secretariat, (2014); [5] Sebhat & Wenninger, (2014); [6] Chishugi & Alemaw, (2009); [7] Matondo & Mortensen, (1998) Namibia, Zambia, Botswana, Zimbabwe, Malawi, Tanzania, and Mozambique. The Zambezi river is, therefore, an international river basin. It drains an area of about 1,800,000 square km (Okavango-Chobe system included; [8] LBPTC, (2010)

* av(min\|max) are the yearly average, minimum and maximum for that basin.

** MOD-16 basins are not included where missing values in the averaged product exceed 20%. ET_a-MOD16 values are for 2000-2013.

The ETI_a-WPR, ET_a-MOD16 and ET_a-Fu are plotted against the water balance ET_a-WB in Figure 3-2. The relationship between the ETI_a-WPR, ET_a-MOD16 and ET_a-Fu products show strong linear relationships with ET_a-WB. While the ET_a-WPR product has a better R^2, the ET_a-MOD16 has a lower bias. The ETI_a-WPR shows a slightly positive bias, which is increasing with increasing ET_a-WB. The absolute difference between the ETI_a-WPR and the ET_a-WB is typically increasing with larger ET_a-WB values. The relative differences between ETI_a-WPR and ET_a-WB are lower at high ET_a values. The absolute difference and relative difference between

ETI$_a$-WPR and ET$_a$-MOD16 was greater at lower ET$_a$-MOD16. The ET$_a$-Fu is underestimating ET$_a$ compared to the WB in the basins. The absolute relative difference, between ETI$_a$-WPR and ET$_a$ - WB typically decreases with increasing PCP. The long term ETI$_a$-WPR is larger than the ET$_a$ - WB on 13 out of 22 basins. The Q ranges from 4.4% (South Interior) up to 47.0% (Central West Coast), with a median of 18.6%, of the long term PCP. The Q is larger in basins with higher ETI$_a$-WPR and PCP. In basins where the long term average Q is less than 150 mm/year (18 basins out of 22), the relative difference between ET$_a$ estimates ranges from -20% to +70%. When the long term average Q is greater than 200 mm/year the relative difference ranged from -12% to +20%.
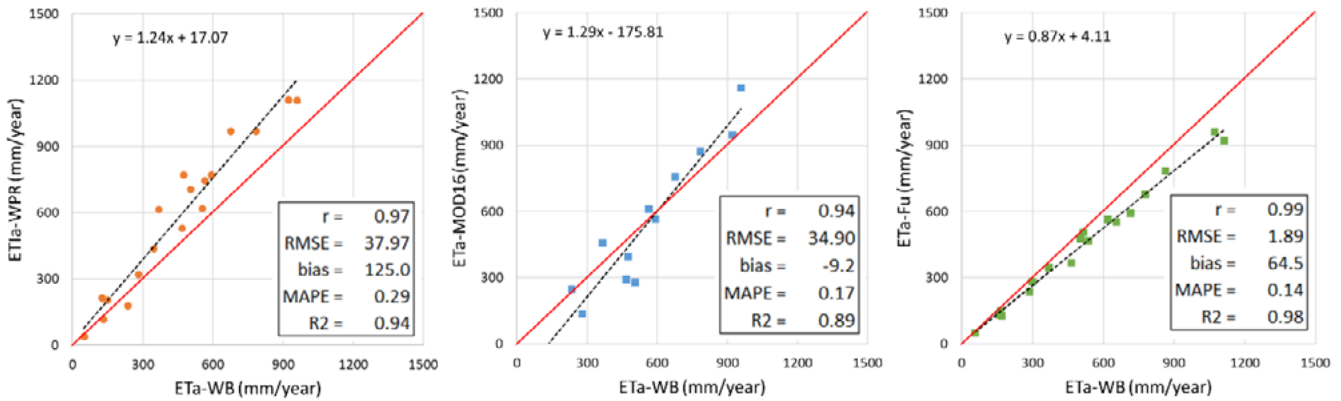
Figure 3-2. The relationship between long-term average annual ETI$_a$-WPR (left), the ET$_a$ - MOD16 (Near) and ET$_a$ - Fu (right) plotted against average annual ET$_a$-WB for major hydrological basins of Africa. The black dotted line is the linear regression and the red line is the 1:1 line.

The long-term (2009-2018) ETI$_a$-WPR for basins in Africa is estimated to be 590.6 mm/year, which is 12.2% larger than the long-term ET$_a$-WB, estimated to be 518.7mm/year. The 2010 ET$_a$ average for the entire WaPOR extent is compared against ETI$_a$-WPR V1 and other models in Figure 5. These values are sourced from the WaPOR V1 validation report (FAO and IHE Delft 2019) and include three remote sensing-based surface energy balance models - Atmosphere-Land Exchange Inverse (ALEXI), Surface Energy Balance System (SEBS), and SSEBop v4, a remote sensing-based Penman-Monteith approach - MOD16, a remote sensing-based artificial neural network product - Water, Energy, and Carbon with Artificial Neural Networks (WECANN), a hybrid remote sensing-based model – ETMonitor, a land surface models with remote sensing data assimilation - Global Land Data Assimilation System (GLDAS), a Priestley-Taylor approach driven by meteoroidal data - GLEAM v3.2, and, an up-scaled FLUXNET product - Multi-Tree Ensemble (MTE). The ALEXI and SSEBop v4, both remote sensing-based surface energy balance models, have a similar performance, 519 and 497 mm/year respectively. All other approaches, including SEBS, MTE, ETMonitor, WECANN, MOD16, GLEAM v3.2 and GLDAS, report a lower average annual ET$_a$ in 2010, ranging from 11% lower (GLDAS) to 38% lower (GLEAM). As compared to the CHIRPS PCP product, ET$_a$ as estimated from these products are consuming 54% (GLEAM) to 78% (GLDAS) of the PCP. Compared to the models with higher ET$_a$ that are consuming 83% (SSEBop) to 87% (ALEXI).
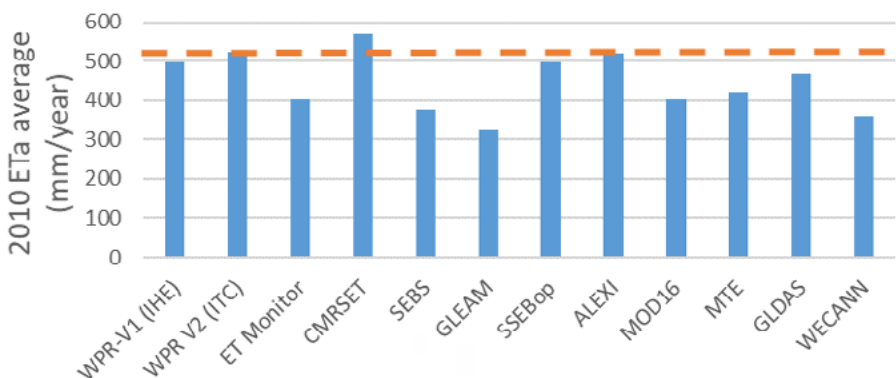
Figure 3-3. Long-term average continental ET$_a$ of various models (values taken from FAO 2019) and ETI$_a$-WPR. The orange dotted line represents the ETI$_a$-WPR and was used for reference to other datasets.

The main source of error in the ET-WB method is the uncertainty in PCP. Studies on the CHIRPS PCP product shows high correlations, at monthly and regional scales, in Eastern Africa (r = 0.70-0.93) (Dinku *et al.*, 2018; Gebrechorkos, Hülsmann, & Bernhofer, 2018) and Burkino Faso (r = 0.95) (Dembélé and Zwart, 2016) with little to no bias. Muthoni *et al.*, (2018) reported that CHIRPS v2 slightly over-estimated low-intensity rainfall below 100 mm and slightly under-estimated high-intensity rainfall above 100 mm compared in Eastern and Southern Africa. On an annual, basin-scale, the CHIRPS PCP product does not show significant bias, except for in largely ungauged tropical basins (e.g. Congo) (Liu *et al.*, 2016)we present a worldwide evaluation of nine ET products (three diagnostic products, three land surface model (LSM. Weergeshi *et al.*, (2019) compared terrestrial water storage by Rodell *et al.*, (2018) and found they represented a maximum of 2.3% of long term basin ET_a for basins in Africa. Therefore the large overestimations of ETI_a-WPR cannot be primarily attributed to the simplified water balance approach.

The Q component also contains uncertainty. The Q component is less than 25% of the PCP in all but three basins used in the comparison, Central West Coast, West Coast and North East Coast (though in the North East Coast ETI_a-WPR > PCP). In basins where Q is a significant component of the water balance its uncertainty is going to have the largest influence on the uncertainty of the ET_a-WB. The R^2 values of modelled GRDC Qmean against streamflow data was >0.9 (Beck *et al.*, 2015). Therefore, the Qmean is expected to be high in gauged basins. Unguaged basins in the analysis, have higher uncertainty and introduce higher uncertainty into ET_a-WB. Basins with no streamflow data include, North Interior, North East Coast, Shebeli & Juba Basin and Limpopo. Of these basins only the North Interior has ETI_a-WPR < PCP. If basins are removed from the analysis with missing streamflow data the regression between ETI_a-WPR and ET_a - WB only marginally improves (R^2 = 0.96 compared to R^2 = 0.94), suggesting the quality of Qmean is appropriate for the water balance check.

3.2.   Cross validation using comparison to reference data

3.2.1.   Comparison of L1 ETI_a-WPR and NPP-WPR data to MODIS products

The mean annual ETI_a-WPR and NPP - PR were compared to ET_a-MOD16 and the NPP-MOD17 and are shown in Figure 3-4. ET_a-MOD16 and NPP-MOD17 do not contain data for large swaths of the Sahara Desert and desert regions in the Near East. Therefore, the comparisons here are taken where data existed for both datasets (i.e. averages) between 2009-2014.

The long-term average annual ETI_a-WPR and ETI_a-MOD16 was 829 mm/year and 568 mm/year (excluding the no-data regions). The long-term average annual NPP - WPR and NPP-MOD17 was 736 gC/m²/year and 605 gC/m²/year. It is important to note that these average values are not the continental averages, but averages of the available data. The MODIS product is showing more variation between years for both ET_a-MOD16 and NPP-MOD17. The lowest ET_a-MOD16 is in 2014, 530 mm/year, and the highest is in 2009, 575 mm/year. However, the lowest NPP-MOD17 is 608 gC/m²/year, in 2009, and the highest is 643 gC/m²/year, in 2014. This is converse to expectations, where one would assume that overall NPP should be higher when ET_a is higher. The WaPOR products are showing less inter-annual variation. The mean annual ETI_a-WPR and NPP - WPR varies between 814-846 mm/year and 735-749 gC/m²/year.

The overall long-term correlation between the ETI_a-WPR and ET_a-MOD16 decreased slightly over time (from 0.76 in 2009 to 0.69 in 2014), conversely the ETI_a-WPR and NPP-WPR improved slightly (from 0.83 in 2009 to 0.86 in 2014). The ET_a and NPP RMSE between the two products, across 2009-2014, is 235 mm/year and 272 gC/m²/year.

ETI_a-WPR and NPP-WPR in the humid tropics and forested areas (e.g. the Congo basin) display much higher values than ETI_a-MOD16 and NPP - MOD17. NPP-MOD17 appears to be smoothing values more, while WaPOR is showing both higher high values (e.g. NPP-WPR is higher than NPP-MOD17 in the central Africa Region) and lower low values (e.g. NPP-WPR is lower in the arid region in Southern Africa). Conversely, ETI_a-WPR appears generally higher than ET_a-MOD16 across the the different regional climates, with the exception of Madagascar. ETI_a-WPR also appears to be capturing the Nile and Nile Delta better. This is not necessarily due to the spatial resolution, as both the NPP-WPR and NPP-MOD17 capture the Nile and Nile Delta.
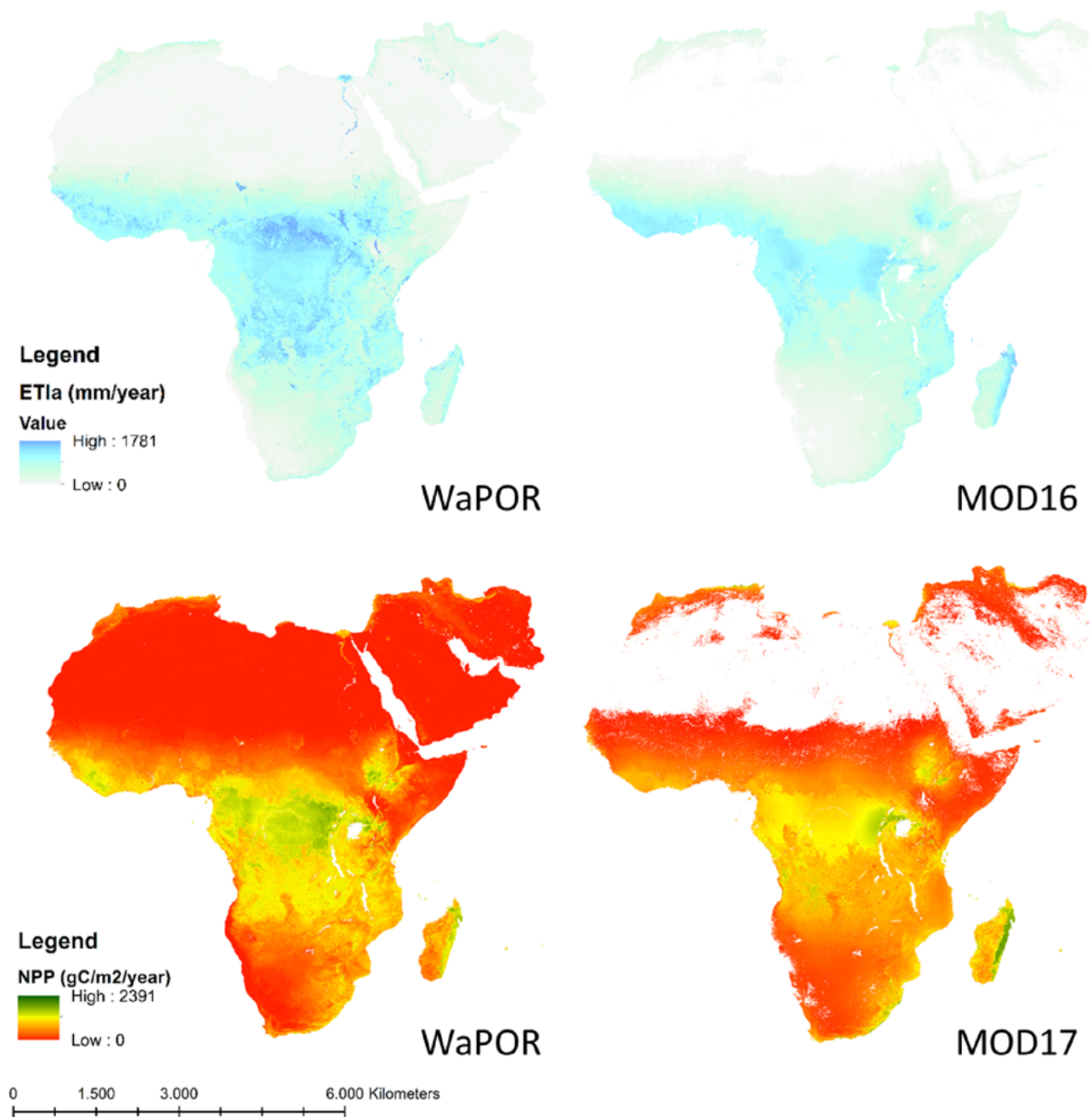
Figure 3-4. Mean annual ETI$_a$ and NPP for WaPOR (2009-2018) and MODIS (2000-2014).

Source: this study

The spatial consistency between the WaPOR and MODIS ET and NPP products varies between land classes and climate zones. The agreement between ETI$_a$-WPR and the NPP-WPR and the ET$_a$-MOD16 and the NPP-MOD17 for each climate class are land class are shown in Figure 3-5 and Figure 3-6 respectively. Please note that comparisons and statistics (including mean values) were derived from values where data existed for both datasets (so excluding the no-data areas in the MODIS products).
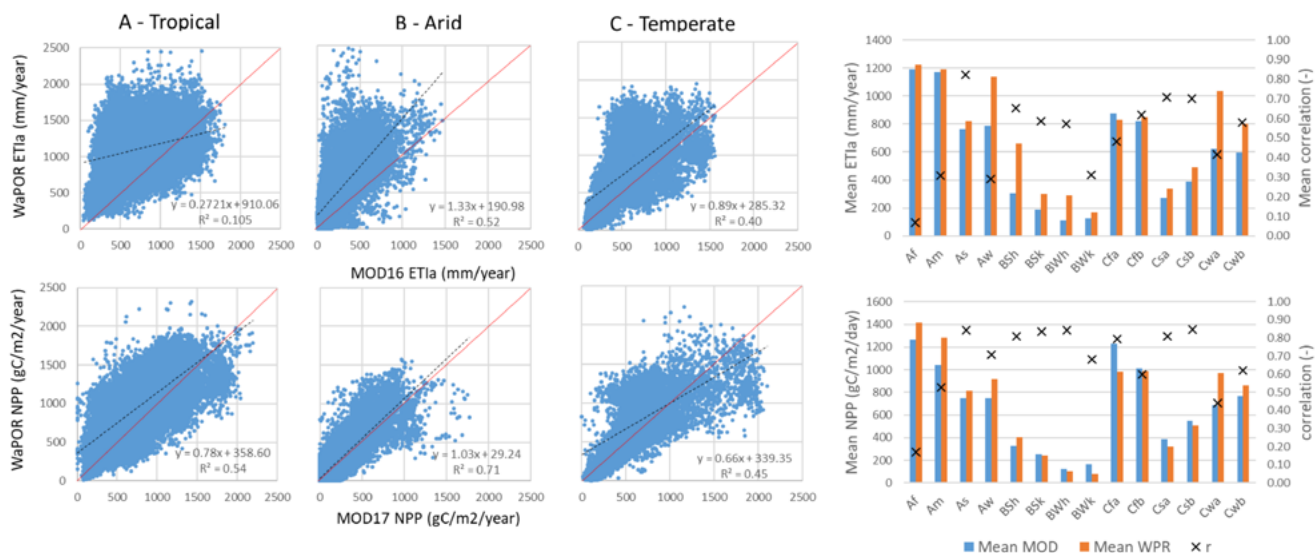
Figure 3-5. WaPOR plotted against MODIS for ETI_a (left - upper) and NPP (left - lower) for years 2009-2014 for major and minor climate classes. Mean annual ETI_a (right – upper) and NPP (left upper) for both WaPOR and MODIS and correlations for each climate class. Black line shows linear regression and red line shows 1:1 line.
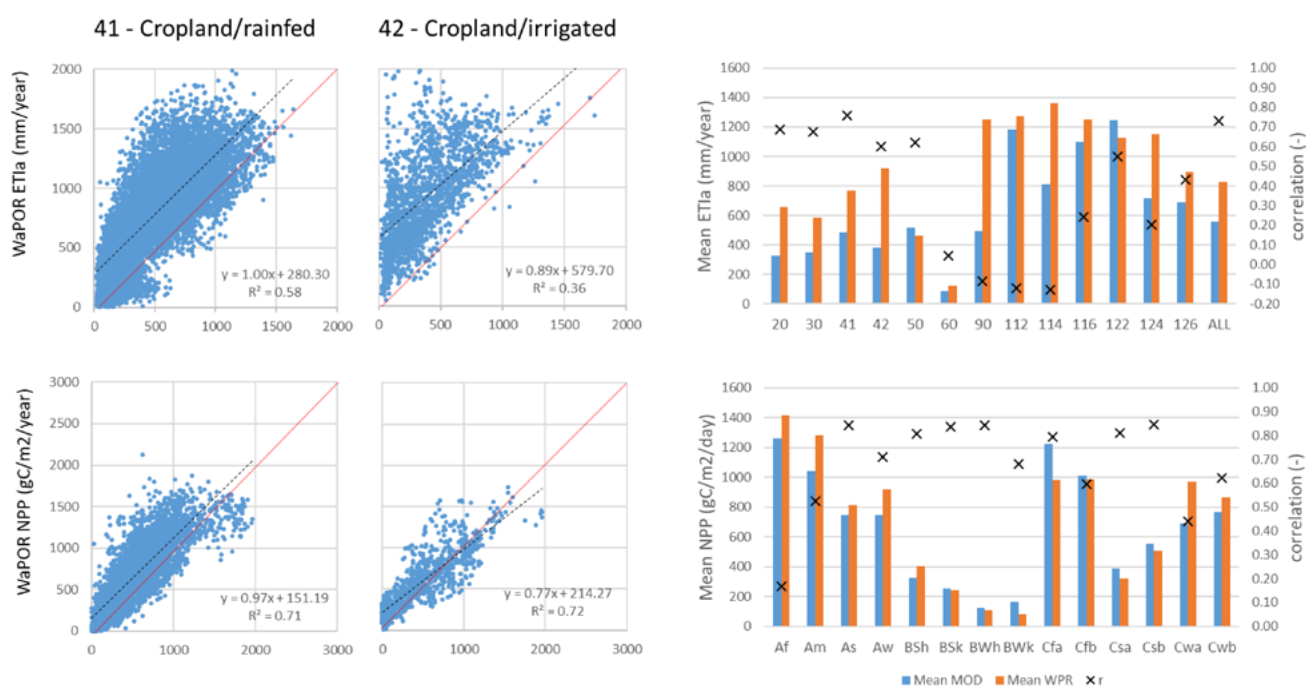
Figure 3-6. WaPOR plotted against MODIS for ETI_a (left - upper) and NPP (left - lower) for years 2009-2014 for crop classes. Mean annual ETI_a (right – upper) and NPP (left – lower) for both WaPOR and MODIS and correlations for each Land Cover Class (FAO-LCCS codes – see Table 2-1). Black line shows linear regression and red line shows 1:1 line.

The NPP-WPR and NPP-MOD17 products generally show a higher agreement than the ETI_a-WPR and ET_a-MOD16 products. The ETI_a-WPR is larger than the ET_a - MOD16 for all climate classes except Cfa, and all land classes except 60 (bare/sparse vegetation). The NPP-WPR is larger than the NPP-MOD17 for all climate classes except BWk, Csa and Csb, and all land classes except 90 (shrub/herbaceous cover). The NPP-WPR and NPP-MOD17 generally showed a higher correlation than the ETI_a-WPR and ET_a-MOD16. The correlation between the ETI_a products is often higher when the correlation between the NPP products is high. This is with the exception of land cover class 90 and land cover class 122 (tree cover open).

Both ETI$_a$ and NPP for WaPOR and MODIS show good agreement in rainfed cropland (class 41), but lower agreement in the irrigated cropland (class 42). This is a good indication as to the performance in the rainfed cropland area. The primary rainfed cropland occurs in the Aw and BSh, which are associated with a higher correlation for NPP-WPR and NPP-MOD17 products. The irrigated cropland is found mainly in Aw, BSh, BSk and BWh climate zones (Figure 3-7). These climates zones all have a high agreement between the NPP-WPR and NPP-MOD17 product. This suggests that the disagreement in the NPP in the irrigated cropland is associated with attributes associated with land cover classification and not climate. Conversely, the agreement between the ETI$_a$-WPR and MOD-16 in irrigated cropland seems to be more influenced by the climate class. The lowest correlation is in the Af and Am zones for both ETI$_a$ and NPP products and the tree cover land classes (except for ETI$_a$ in 122).
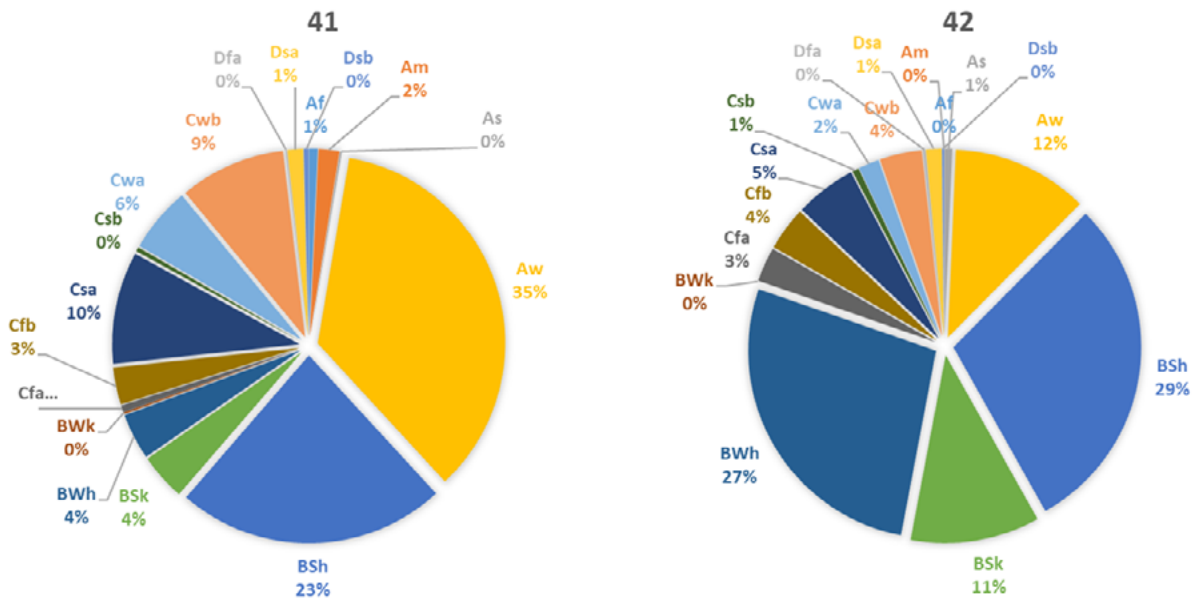
Figure 3-7. Designation (by percent) of cropland by climate class.

The relationship between the annual NPP-WPR and ETI$_a$-WPR products and for the NPP-MOD17 and ET$_a$-MOD16 products is positive, with overall correlations of 0.80 and 0.81 respectively and R^2 of 0.65 and 0.66 respectively. Figure 3-8 shows the annual NPP plotted against the annual ETI$_a$ for the WaPOR and MODIS products and the correlation between the WaPOR and MODIS products for each climate class and LCC. This represents the annual value of all points from the stratified random sample (3.10^4 points) from all years. Although the slope between the NPP - WPR and ETI$_a$-WPR is slightly lower than that compared to the slope between the NPP-MOD17 and ET$_a$-MOD16. This is likely attributed to the higher ETI$_a$-WPR values as compared to the ET$_a$-MOD16. The highest correlations between the NPP and ETI$_a$ are occurring in the shrubland (class 20), grasslands (class (30) and rainfed and irrigated croplands for both MODIS and WaPOR. A low correlation between NPP and ETI$_a$ was found in the tree cover classes for both WaPOR and MODIS. The correlation between NPP and ETI$_a$ for both WaPOR and MODIS was fair for all climate classes except for Af and Am. These climate classes are dominated by tree cover land class 112.
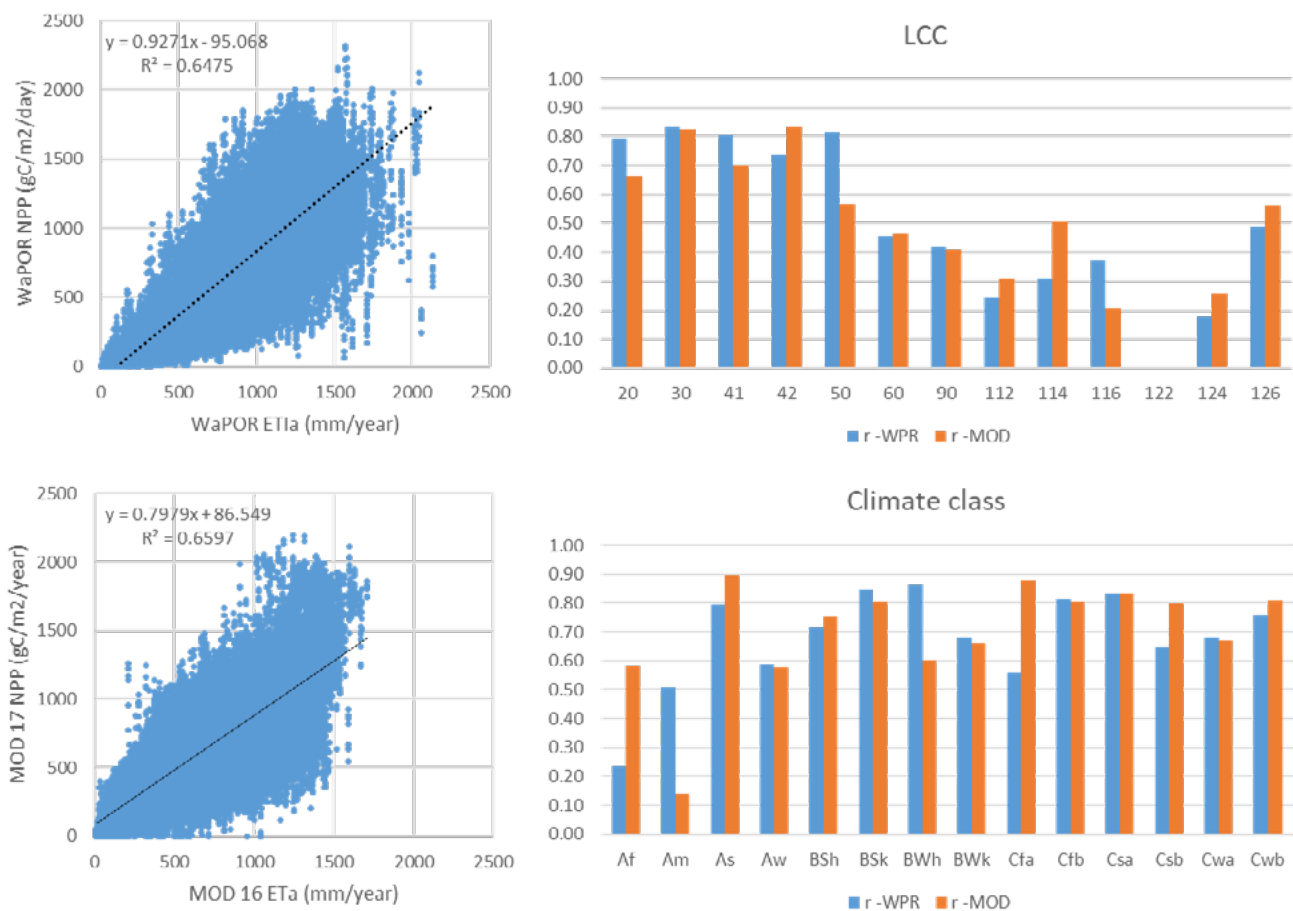
Figure 3-8. Relationship between NPP - WPR and ETI$_a$-WPR (left – upper) and NPP - MOD17 and ET$_a$-MOD16 (left – lower) for years 2009-2014 and the correlations between WaPOR and MODIS products based on land cover class (right - upper) and climate class (right – lower).

The improved MOD16 has been validated against 46 Eddy Covariance (EC) flux tower stations across the globe. The mean absolute bias for ET$_a$-MOD16 was 0.33mm/day (24.6%) driven by tower meteorological data, and 0.31mm/day (24.1%) driven by GMAO data, a global meteorological reanalysis dataset (Mu *et al.*, 2011), with MOD16 overestimating EC data. This dataset showed little averaged bias with EC data. The MOD17 product has been validated across several biomes at 9 in-situ EC locations. Results suggest that the NPP-MOD17 and GPP-MOD17 products are responsive to general trends in the magnitude of NPP and GPP associated with local climate and land use. However, the MOD17 products tend to overestimate at low productivity sites and underestimate at high productivity sites (Turner *et al.*, 2006). A more recent study suggested that GPP-MOD17 products showed a good correlation but consistently underestimated GPP (bias = -5 to -20 gC/m^2/8-day) (Wang *et al.*, 2017). The MOD17 product tends to underestimate GPP or NPP, and therefore suggests that the WaPOR-NPP is in the adequate range at a continental, basin, climate class and land class scale.

3.2.2. Comparison of L1 ETI$_a$-WPR and NPP-WPR with Meteosat MSG products

The spatial ETI$_a$ patterns for MSG-ET$_a$ and ETI$_a$-WPR for dekad 1810 and 1830 can be seen in Figure 3-9. Patterns and map value ranges coincide well, although differences are clearly visible e.g. in the humid tropical (Congo basin). The ET$_a$-MSG product shows more "nodata" pixels as more stringent data quality criteria are used in the production of this data set (and more gap filling through smoothing is used for L1 ETI$_a$-WPR), and aggregation was not undertaken if 1 pixel in the dekad period was missing.
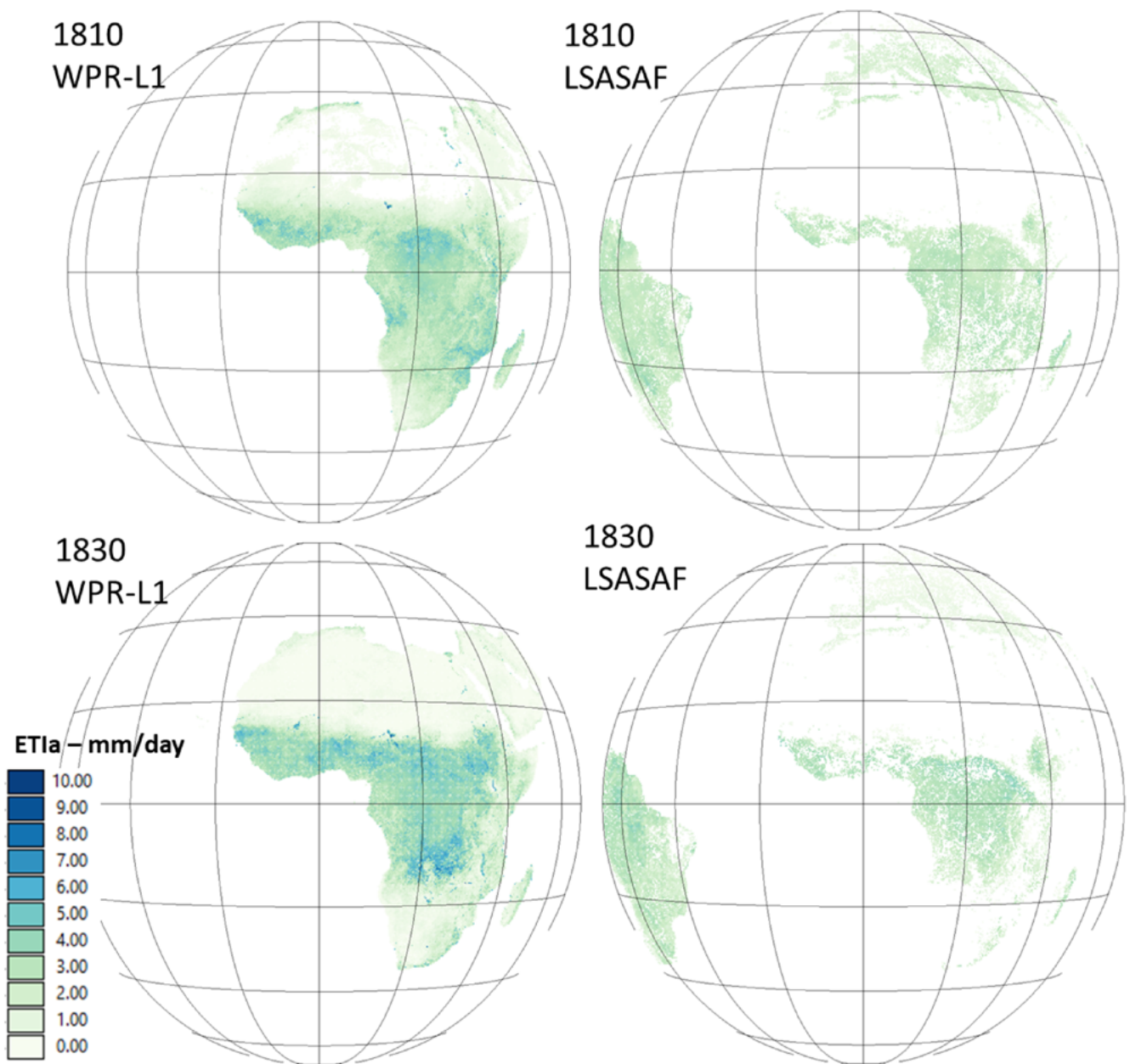
Figure 3-9. Views of ETI$_a$-WPR L1 and ET$_a$-MSG on 01-10 April 2018 (dekad 1810) and 21-31 Oct 2018 (dekad 1830).
Source: this study

Spatial trends are similar between ETI$_a$-WPR and ET$_a$-MSG products, e.g. higher ET$_a$ in the tropics and lower in arid regions. However, the ETI$_a$-WPR is consistently overestimating ETI$_a$ as compared to the ET$_a$-MSG product, particularly in low ET$_a$ regions. A pixel-by-pixel comparison of the resampled ETI$_a$-WPR and ET$_a$-MSG product was performed (crossing) and is shown in Figure 3-10. ETI$_a$- WPR has a positive bias of 0.79 mm/day, as compared to ET$_a$-MSG, for both dekads shown. The correlation is 0.41 and 0.56 for dekad 1810 and dekad 1830 respectively. The R^2 is low for both dekad 1810 and 1830, 0.17 and 0.31, however the general trend increasing ETI$_a$-WPR with increasing ET$_a$-MSG.

The differences between the data sets can probably be found in the data sources used and also in the land cover classifications and associated model parameterizations used for both ET$_a$ products.
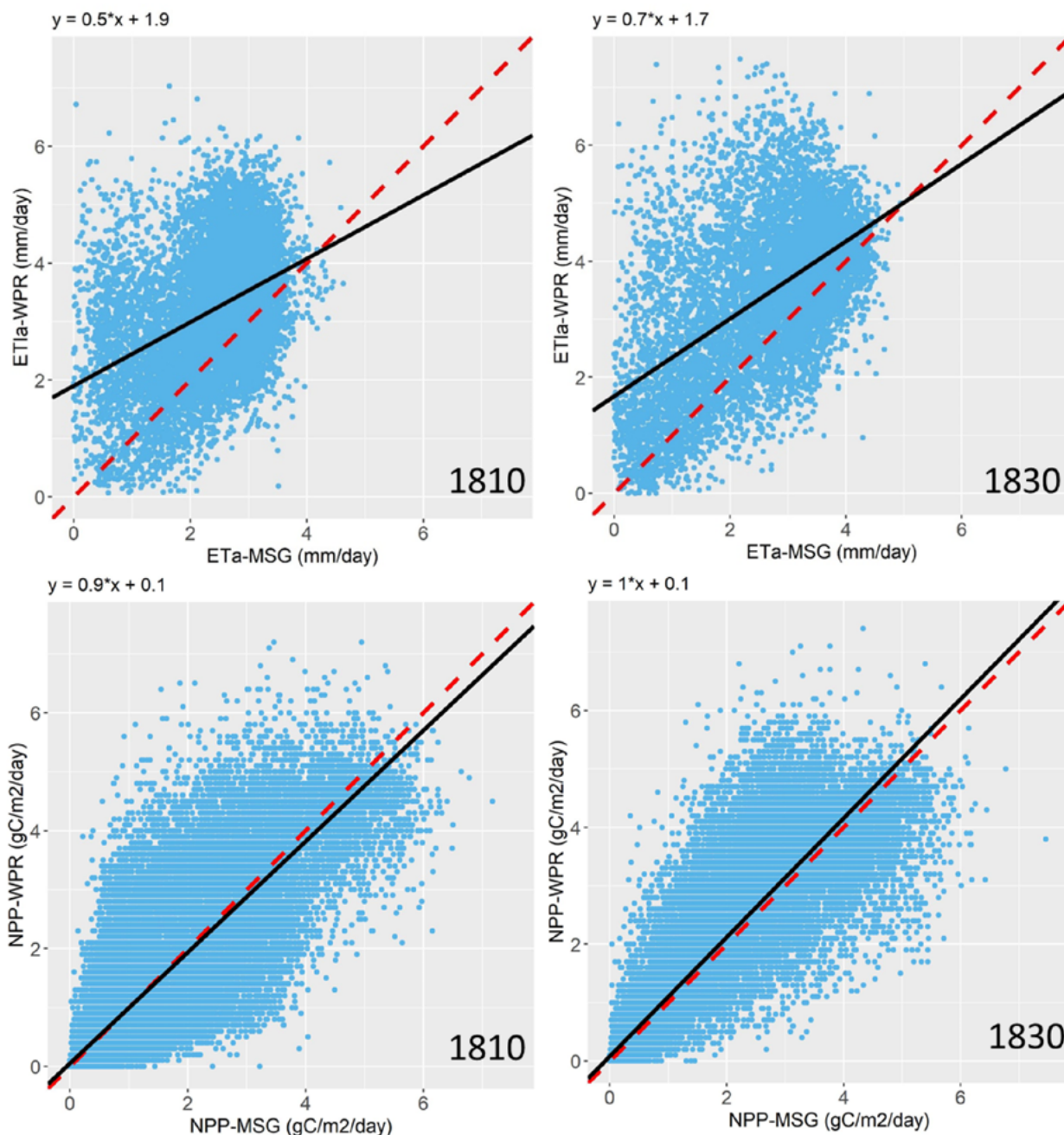
Figure 3-10. Density plots of continental ETI$_a$ - WPR and ET$_a$ - MSG (upper) and NPP - WPR with NPP - MSG (GPP*0.5) (lower) on 01-10 April 2018 (dekad 1810) and 21-31 Oct 2018 (dekad 1830).

The spatial NPP patterns for MSG-NPP (GPP*0.5) and NPP-WPR can be seen in Figure 3-11. Patterns and map value ranges coincide well, although differences are clearly visible e.g. in the humid tropical (Congo basin). As for the ET$_a$ products, the NPP-MSG shows more "nodata" pixels as more stringent data quality criteria are used in the production of this data set (and more gap filling through smoothing is used for L1 NPP-WPR).

The NPP-WPR and NPP-MSG products show a very good agreement, with no significant bias evident for any dekads compared. For example dekad 1810 NPP-WPR has a positive bias of 0.11 and dekad 1830 has a negative bias of -0.02 as compared to NPP-MSG. The linear regression between products has a high R^2, 0.81 and 0.72 for dekad 1810 and 1830 respectively, and high correlations, 0.90 and 0.85 for dekad 1810 and 1830 respectively (Figure 3-10).

The differences can probably be found in the data sources used, but more probably in the land cover classifications and model parameterizations of both GPP (NPP) product developments. In our opinion, also here the differences can best be explained by the LCC and radiation models or data and the assumptions for

LUE and $_a$. Also the down-regulation factors (scalars) and approaches used for calculating temperature and moisture effects on photosynthesis and primary production are different in both data.
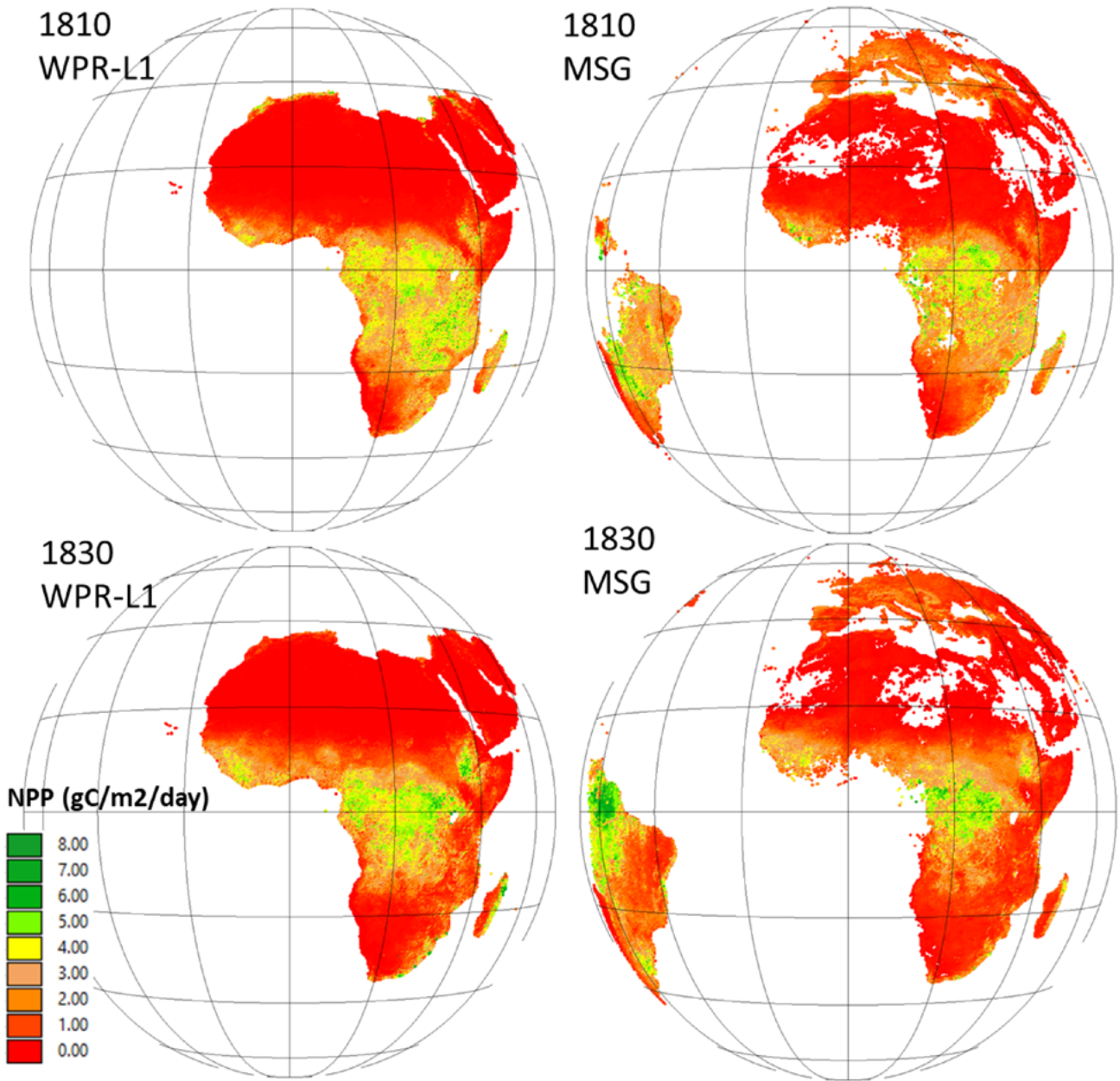
Figure 3-11. Views of NPP-WPR L1 and NPP-MSG (GPP*0.5) on 01-10 April 2018 (dekad 1810) and 21-31 Oct 2018 (dekad 1830). *Source: this study*

As both data sets are 10-day products, a time series comparison of L1 NPP-WPR vs. NPP-MSG was also done for a number of sample locations in the field of view. Overall the similarity in the temporal series of NPP-MSG and NPP-WPR is positive. Figure 3-12 shows timeseries comparisons of NPP-MSG (GPP*0.5) and L1 NPP-WPR for 16 randomly selected locations for dekads 1810 (01-April) to 1836 (31-Dec 2018). The location show the 8 locations with data continuity (least gaps) in the LSA SAF NPP dataset. Like the previous comparison (Figure 3-11), the NPP-MSG is taken as the GPP-MSG multiplied by 0.5 (R$_a$ adjustment). Most of the locations show similar temporal trends and capture the same seasonal variation. The WaPOR NPP is typically higher than the MSG-NPP in wetter climates (e.g. n13 and n3). However, the MSG-NPP is frequently higher than the WaPOR NPP in more arid climates and conditions, reflected by low NPP. For example n5 is in an arid environment, with low values for both MSG-NPP and WaPOR-NPP, and MSG-NPP is greater than WaPOR NPP throughout

the timeseries. Another example in n2 and n18, where WaPOR is demonstrating higher NPP peaks and lower NPP troughs. Geostationary sensors (MSG) on (sub)daily scale capture fluctuations better. WaPOR data is smoothed with 10-day averaged data which leads to typically lower values, and possible underestimations in drier regions. This is due in part to use of non-linear down-regulating functions (accounting for moisture, temperature) and how smoothing is done (e.g. exponential, linear, etc.).

The location in the Nile Delta (n15) is in irrigated agriculture and the only site not showing any temporal consistency, showing almost an inverse trend. As NPP-MSG has a much lower spatial resolutions than L1 NPP-WPR and is capturing more fields and even possibly extending slightly beyond the irrigated area, and is therefore likely not capturing the NPP increase in agricultural land and the irrigated season.
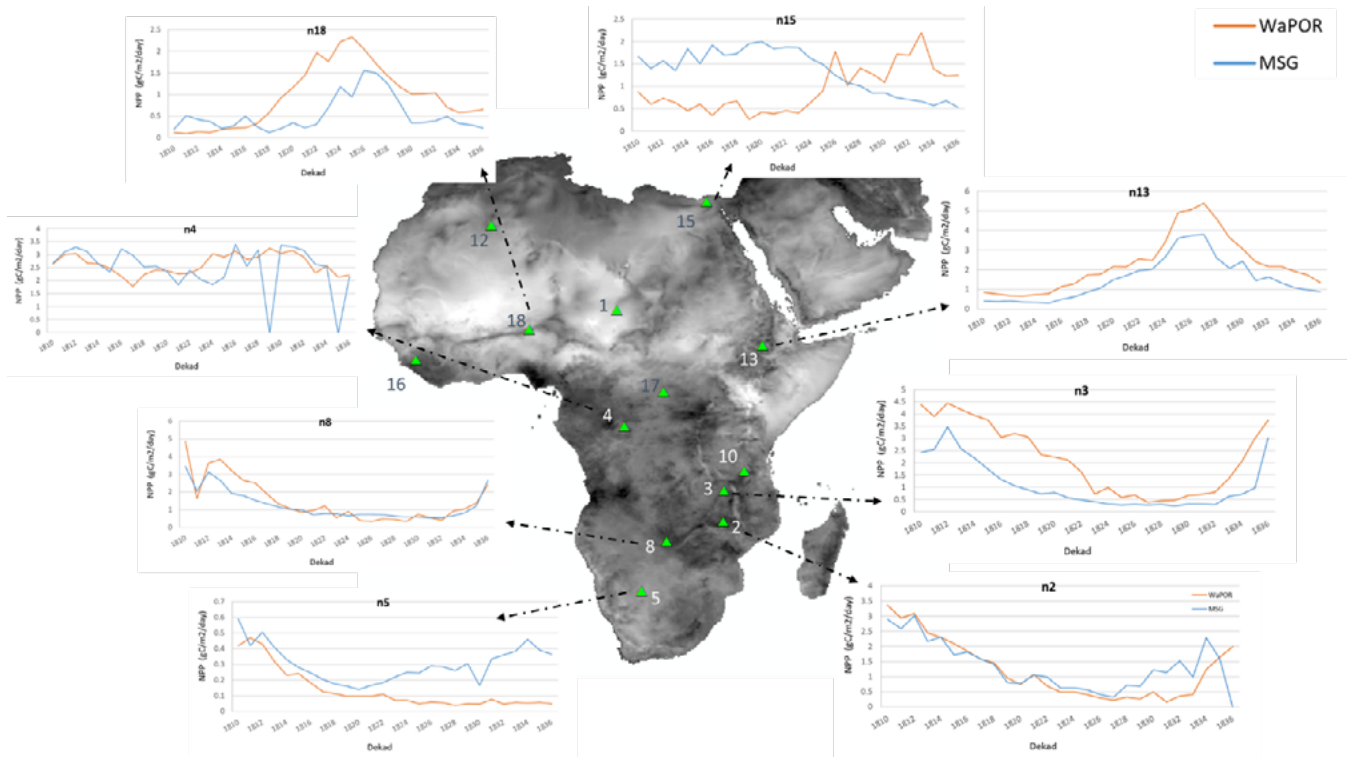
Figure 3-12. Time series (April-December 2018) comparison of L1 NPP-WaPOR to LSASAF MSG-NPP (as GPP*0.5) for selected random locations across Africa.

Source: this study

3.2.3.   Comparison of Bekaa Valley level-3 area ETI$_a$-WPR to literature reference data

The Level-3 30-m resolution ETI$_a$ results from WaPOR were cross—validated through comparison with literature reference data for the Bekaa valley, Jordan (Table 3-2). The ETI$_a$ was estimated on a dekadal and annual scale for the Upper Litani Basin L3 extent and for the Upper Litani Basin agricultural areas as defined by Jaafar and Ahmad (2019)we derive a novel time series of field-scale actual evapotranspiration for the Bekaa Valley using two one-source energy balance models for the period 1984–2017, utilizing local weather data and all available original Level 1 Landsat thermal imagery and Level 2 surface reflectance products. We compare a modified METRIC model with an automated hot and cold pixel identification procedure run in batch mode to pySEBAL, a new version of SEBAL, which also has its automated anchors pixel selection algorithm. Analysis of 1200 cloud-masked and gap-filled Landsat-derived ET products show that the two models give comparable water use estimates at the seasonal and annual time steps. We estimate an average annual ET of 652 ℗ 53 mm (or 800 mcm in Lebanon. The agricultural area excludes part of the non-cultivated mountains on either side of the valley and extends a little further north and south than the L3 Bekaa Valley area extent. The peak agricultural period in the Upper Litani Basin is in summer, May-October, which is reflected by the higher evapotranspiration. This is possibly low considering the high summer temperatures, and that most fields in the summer receive supplemental irrigation and that transpiration should dominate the ETI$_a$-WPR when the crop cover is high, which is common in June.

Table 3-2. Comparison of ETI$_a$ estimates from literature and remote sensing in the Bekaa Valley.

Source	May-Oct 2016 (mm)	May-Oct 2013 (mm)	Annual av. (mm)	Reference
Literature	600			Jafar and King-Okumu (2016)
Literature		391; 741	700-800 (2016)	Jafar and King-Okumu (2016)
pySEBAL			921 (2001-2017)	Jaafar and Ahmad 2019
METRIC			798 (2001-2017)	Jaafar and Ahmad 2019
MODIS			361 (2001-2017)	Jaafar and Ahmad 2019
WPR L1 V2	357	406	515 (2009-2018)	-

In the agricultural area, the annual ETI$_a$-WPR values range from 410 mm in 2014 to 602 mm in 2010. Jaafar and Ahmad (2019)we derive a novel time series of field-scale actual evapotranspiration for the Bekaa Valley using two one-source energy balance models for the period 1984–2017, utilizing local weather data and all available original Level 1 Landsat thermal imagery and Level 2 surface reflectance products. We compare a modified METRIC model with an automated hot and cold pixel identification procedure run in batch mode to pySEBAL, a new version of SEBAL, which also has its automated anchors pixel selection algorithm. Analysis of 1200 cloud-masked and gap-filled Landsat-derived ET products show that the two models give comparable water use estimates at the seasonal and annual time steps. We estimate an average annual ET of 652 Ⓟ 53 mm (or 800 mcm estimated the annual and ecadal ETI$_a$ values in the agricultural areas for the period of 1984-2017 using both the METRIC and pySEBAL remote sensing based energy balance models. As compared to this study, WaPOR has lower ETI$_a$-WPR values. Both METRIC and pySEBAL estimated maximum daily ETI$_a$ of 4-5 mm/day and in the summer periods for 2009-2017. The annual values for 2009-2017 were estimated to be approximately 700-900 mm/year for various years in the 2009-2017 period. On an annual basis, these values are up to 50% larger than estimates by WaPOR. However, on the long term average ETI$_a$-WPR was still larger than the MODIS derived ET$_a$. This is also in contrast to another study that estimated using an NDVI approach and the DisAlexi energy balance model, which reported ET$_a$ of 741 mm and 391 mm, respectively for 2013 and 2016 (Jaafar and King-okumu, 2016). The WaPOR annual estimate in 2013 falls closer to the DisAlexi value.

3.3. Internal validation of spatial and temporal consistency

In order to verify the internal consistency of the WaPOR data, an analysis was performed per climate class to verify the coherence of the evaporative flux components (E,T,I) of ETI$_a$-WPR and the biomass NPP-WPR. Data were inspected using time series visualization and also scatter plots (per climate zone) were used to appraise the clustering per climate class.

3.3.1. Internal consistency of ETI$_a$–WPR and NPP–WPR data components

The 10-day values of total ETI$_a$-WPR, transpiration (T), evaporation (E), NPP-WPR, SR, SMC and NDVI were plotted for all climate zones for the northern and southern hemisphere. Figure 3-13 shows some examples of ETI$_a$-WPR, transpiration, evaporation, SMC and NDVI for the largest sub-zones per main climate; wet tropical-savanna (Aw), arid-desert-hot (Bwh) and temperate-dry winter-warm summer (Cwb). The average ETI$_a$-WPR (y-axis on the left), and SMC and NDVI (y-axis on the right) are reported from dekad 0901 (2009 – dekad 1) to 1836 (2018 – dekad 36).

The temporal trend for each climate zone is inversed between hemispheres, reflecting the opposite seasons between hemispheres. For example, peak ETI$_a$-WPR values occur around dekad 19 and through values occur around dekad 01 in the northern hemisphere. Conversely, in the southern hemisphere, peak ETI$_a$-WPR

values occur around dekad 01 and through values occur around dekad 19. The inverse pattern highlights the need to separate climate zones based on hemisphere to view continental data of Africa, as these trends would otherwise cancel out and flatten out temporal trends.

The Aw zones are maintaining the highest ETI_a-WPR values and shows the lowest relative variability throughout the year. The BWh zones consistently have lower ETI_a-WPR values. The BWh in the southern hemisphere is higher than in the northern hemisphere, and the relative intra-annual variation is greater. The ETI_a-WPR in these zones follows a clear seasonal pattern, that is not evident from the NDVI or the SMC. The ETI_a-WPR is predominantly governed by evaporation in these arid zones, which is indicated by the low NDVI all-year-round. The temperate zone, Cwb, shows the greatest intra-annual variability in ETI_a-WPR, which reflects the more dramatic climatic seasonal variations in these years. ETI_a-WPR in Cwb in the northern hemisphere shows two peaks per year. The two seasons are consistent with the zones' location in the Rift Valley of Eastern Africa. Several regions in the Rift Valley experience two wet seasons as influenced by the seasonal migration of the intertropical convergence zone (Hills, 1978) and usually experience a long and short wet season.

ETI_a is controlled either by available solar energy or by available water for evaporation. All zones, other than BWh and Aw in the northern hemisphere, show clear relationships between the ETI_a-WPR, the NDVI and relative SMC. The Aw zone in the northern hemisphere shows two ETI_a-WPR peaks a year, however, the SMC and NDVI show one. Therefore, the ETI_a-WPR during this period, in this zone, the ETI_a-WPR appears to be limited by solar radiation, as despite NDVI being high and SMC being available, there is a drop in ETI_a-WPR. Although not shown here – ETI_a-WPR in BWh in the northern hemisphere follows the same seasonal trend as solar radiation (Figure 3-13). In the Aw zone in the northern hemisphere, the net radiation peaks several dekads before the NDVI and SMC, resulting in a double-peaked ETI_a-WPR. The ETI_a-WPR in BWh zone shows a clear seasonal trend, despite no clear seasonal NDVI or SMC trend. Therefore it is governed by the amount of solar radiation which has a clear yearly trend at the latitudes within the BWh zone.
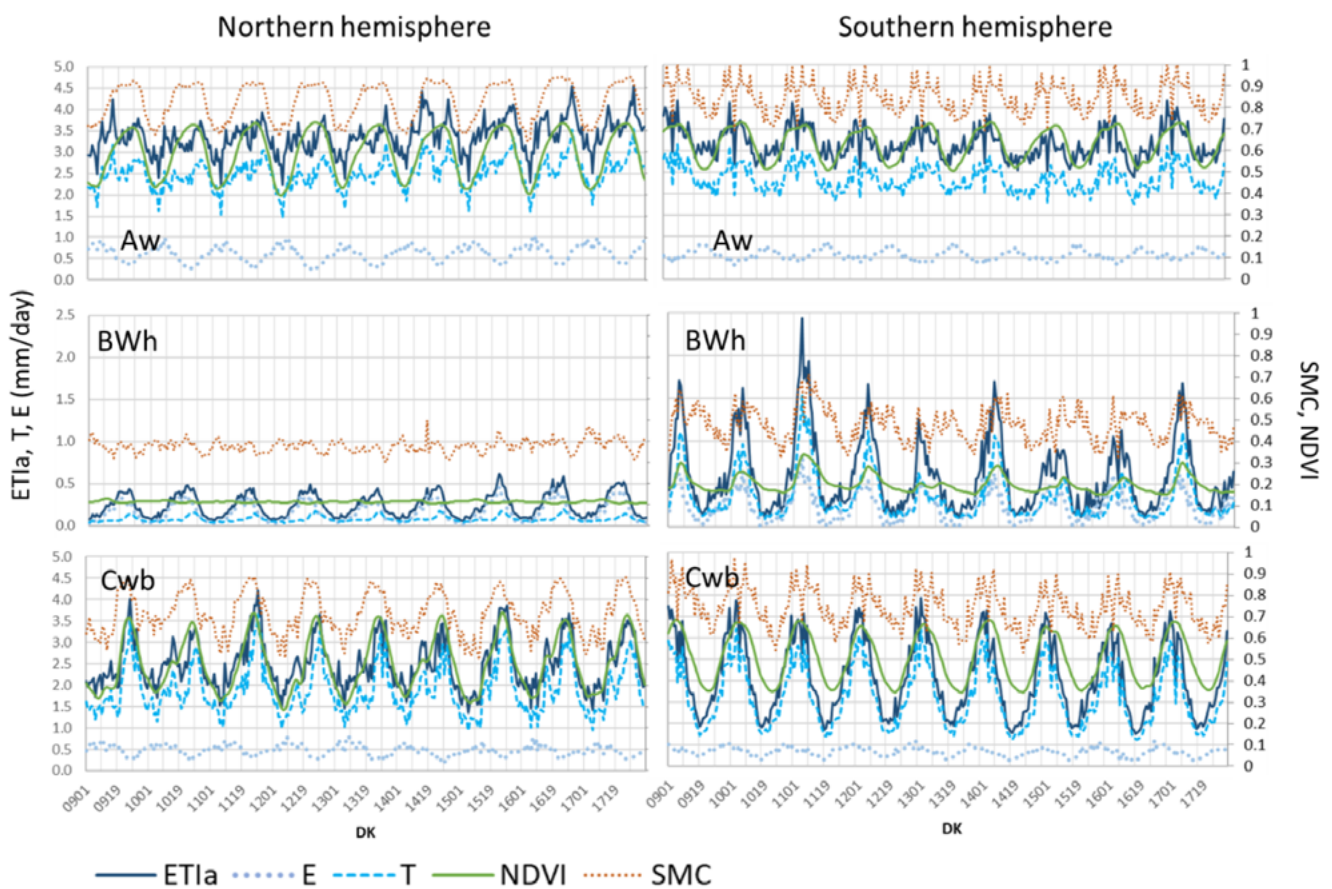
Figure 3-13. Times series of ETI_a-WPR (orange line), SMC (blue line) and NDVI (green line) in tropical wet savanna (Aw), hot arid desert (BWh) and sub-tropical highland climate classes (Cwb) in the northern hemisphere (left) and southern hemisphere (right). Note that BWh has a different ETI_a-WPR y-axis range to Aw and Cwb.

Evaporation and transpiration have inverse trends in temperate and tropical climates. However, in the arid zones, the transpiration and evaporation follow the same seasonal variations. In the dry and hot (BWh) zones in the southern hemisphere, this is due to available soil moisture and NDVI trends. The zone-averaged NDVI, even at peak seasonal NDVI, never exceeds 0.4. Therefore, transpiration does not dominate at peak NDVI and both soil evaporation and transpiration are being driven by soil water availability. The average transpiration minimum and maximum values vary considerably by climate. However, the evaporation component has much less variation between climate zones. For example, the mean evaporation across climates varies from 0.20-0.63 mm/day with coefficients of variation (CV= SD/mean) of 0.28-0.98. However, the mean transpiration between climates ranges from 0.05-2.9 mm/day with a CV of 0.14-2.50. The mean evaporation across the major climate classes is 0.56 mm/day, 0.21 mm/day and 0.31 mm/day for tropical, arid and temperate zones respectively. The mean plant transpiration rates for the major climate classes is 2.52 mm/day, 0.19 mm/day and 1.14 mm/day for tropical, arid and temperate zones respectively.

The relative SMC appears rather high in the arid zones, particularly considering such low NDVI in these regions. For example, in BWh in the northern and southern hemisphere, the mean SMC for the climate zone, across all dekads in the study period, never drops below 0.3 and 0.32 respectively. These regions have high potential energy and are typically strongly water constrained. As the relative SMC is high in these areas with high energy availability, a resulting higher than expected ETI_a-WPR is observed in these zones. The SMC, NDVI or ETI_a-WPR do not seem to be responding to the droughts in the region, where decreasing PCP values should result in reduced SMC and ETI_a-WPR during the 2014-2015 period. The low NDVI values indicate that it is the evaporation component (driven by SMC, solar radiation and soil resistance) that is being overestimated in these dry regions.

The NPP, transpiration and SR are plotted in Figure 3-14. The NPP trend is following the transpiration trend closely in all zones. This is expected as the carbon assimilation is directly dependent on transpiration. In the tropical zone, Aw, in the Northern hemisphere the NPP peaks when the transpiration either flattens or dips slightly.
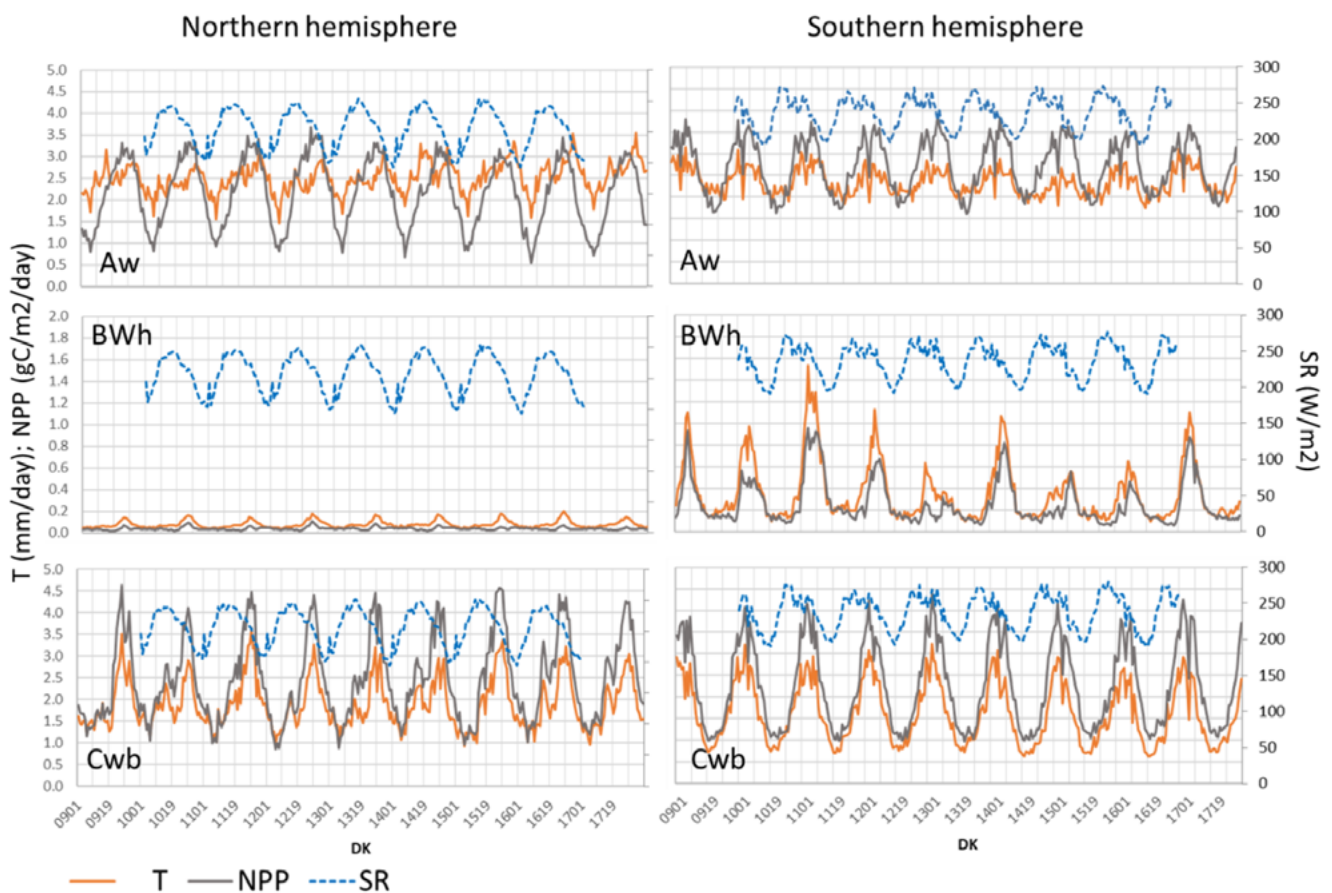
Figure 3-14. Times series of climate zone averaged Transpiration (orange line), NPP (grey line) and SR (blue dashed line) in tropical wet savanna (Aw), hot arid desert (BWh) and sub-tropical highland climate classes (Cwb) in the northern hemisphere (left) and southern hemisphere (right). Note that BWh has a different ETI_a-WPR y-axis range to Aw and Cwb.

3.3.2. Internal consistency of Water Productivity

The mean above ground biomass productivity (AGBP) was plotted against the mean annual ETI_a-WPR for the major Köppen-Geiger climate zones (Figure 3-15). The mean annual AGBP WP water productivity was also plotted against the mean annual AGBP. The AGBP plotted against the ETI_a-WPR shows an increasing AGBP with increasing ETI_a. The relationship between the average annual ETI_a-WPR and the average annual AGBP per climate class had an overall correlation of 0.93 and an R^2 if 0.87. All the desert zones showed a correlation between ETI_a-WPR and AGBP of between 0.95-0.99. The tropical zones surprisingly showed a negative correlation. The temperate zones showed mixed results, with little relationship shown in e.g. the temperate regions without dry season and hot summer or Cfa (r=0.27) and a high correlation in temperate regions with dry winters and hot wetter summers or Cwa (r=0.96). None of the tropical zones showed a correlation between the AGBP and the ETI_a-WPR. The lack of correlation in the tropical zones is in spite of good temporal trends between ETI_a-WPR, transpiration and NPP shown in section 5. However, these areas are non-water limited and may suggest that the relationship between AGBP and ETI_a-WPR behaves differently under these conditions (high humidity and no water limitation, etc).

The AGBP WP is typically increasing with increasing AGBP. The temperate zones showed both high AGBP and high AGBP WP. The tropical zone shows a large range of AGBP and fairly low AGBP -WP for the given AGBP, i.e. for the same AGBP, the temperate zones have higher AGBP WP. The arid strong water-limited regions typically show low AGBP and low ETI_a-WPR, and consequently low water productivity or AGBP WP. The zones with snow show low AGBP and low ETI_a-WPR, however, the AGBP WP is reasonably high given the AGBP.
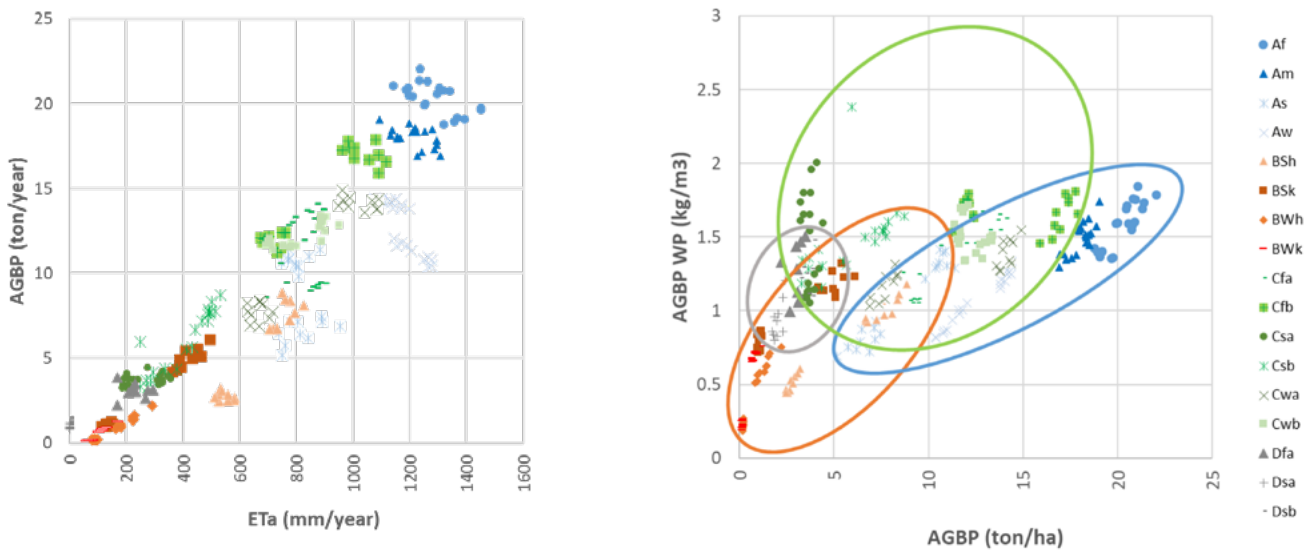
Figure 3-15. Annual AGBP plotted against annual ETI_a-WPR (upper) and annual AGBP WP plotted against annual AGBP (lower) for climate zones. The circles represent the clusters of AGBP WP for each major climate class (Equatorial – blue; arid – orange; temperate – green; snow – grey).

Main findings of Chapter 3.1, 3.2 and 3.3:

- ETI$_a$-WaPOR appears to be overestimated at basin and climatic zone level

- The intermediate relative SMC data component appears to be too high under prolonged dry and hot conditions, leading to the overestimation of the WaPOR evaporation component; especially the soil evaporation (E) component is affected

- The spatial and temporal consistency between ETI$_a$-WPR and NPP-WPR and MOD16-ET and MOD17-NPP is good; WaPOR values are significantly higher than MODIS;

- The spatial and temporal consistency between ETI$_a$-WPR and NPP-WPR and ET$_a$-MSG and NPP - MSG is good;

  - NPP-WPR shows no bias compared to the NPP-MSG

  - ETI$_a$-WPR is consistently higher than the ET$_a$-MSG.

- The 10-year ecadal time series of 10-day averaged ETI$_a$ and NPP show consistent seasonality and show valid relationships with solar radiation, rainfall and temperature variations in both the northern and southern hemispheres

- The spatial correlation and consistency between ETI$_a$ and NPP are high for agricultural cropland classes LCC but low for taller and tree vegetation LCCs.

- The ETI$_a$ and NPP data, averaged per Koppen-Geiger climate class, show consistent behaviour;

- At the individual 250-m pixel level and at certain locations, some unexplained breaks and anomalies (e.g. 2013-2015 period) in both the ETI and NPP time series were detected in the time series. This merits some further analysis and investigation.

3.4. Direct validation to in-situ ground observations

The WaPOR main data components were also directly compared to *in-situ* and ground truth observations. This was achieved using data from Eddy Covariance flux towers, own field surveys in two WaPOR L3 areas, and supplemental ground data, reported by local stakeholders and other information sources.

3.4.1. Comparison to eddy covariance flux tower data

Latent heat flux and Evapotranspiration

The ETI$_a$-WPR component was compared to data from 14 in-situ flux tower observation sites. We refer to Section 2.5.1 for more information on the sites. The agreement between ETI$_a$-WPR and ET$_a$-EC is shown in Figure 3-16 and Table 3-3. Figure 3-16 shows the time series of ETI$_a$-WPR and ET$_a$-EC for all available in-situ data from all EC stations. Table 3-3 shows the corresponding metrics for each station, including r, RMSE, bias, the R2 and the average NDVI and LST quality for the comparison period. A good overall correlation (r=0.71) was found between the site ET$_a$ observations and L1 WaPOR ETI$_a$. However, substantial variations were observed among the sites. Consistency in results is seen between years for most sites. The ETI$_a$-WPR captures seasonality well at most sites.

The best-performing sites are the Senegal SN-DHR and the Sudan SD-DEM sites. The SN-DHR and SD-DEM sites are characterised by a semi-arid climate and a tree savannah and seasonal short vegetation. The ETI$_a$-WPR closely follows the ET$_a$-EC at the SN-DHR and SD-DEM sites. ETI$_a$-WPR is also performing well at ES-SCL, ZM-MON, CG-TCH, EG-ZAN, EG-SAA, EG-SAB and SA-SKU. Excluding CG-TCH, all these sites have high-quality LST and NDVI layers (the average LST quality for the comparison period is equal to or less than 1).

At the irrigated agriculture sites, EG-ZAN, EG-SAA and EG-SAB (Egypt), the ETI$_a$-WPR overestimates ET$_a$-EC during certain time intervals, although correlations and R2 between ET$_a$-EC and ETI$_a$-WPR are good. This induces a daily bias as for example in the EG-Zankalon station (Table 3-3). The seasonal ETI$_a$-WPR, ET$_a$-EC, applied water (irrigation water + PCP) and lysimeter ET$_a$ (ET$_a$-lys) are shown in Figure 3-17 for crop seasons

at EG-ZAN and EG-SAA. If no value is given, no data was available for that crop/season. The ETI_a-WPR values are larger than the ET_a-EC, except wheat in 2011 at EG-SAA. The ET_a-WPR is also larger than the applied water for all crop rotations except fava bean in 2012 and maize in 2013. Shallow groundwater is a water-contributing factor to crops in the several parts of the Nile Delta, due to the shallow groundwater levels in the Nile Delta. Therefore, it is possible that the ETI_a is higher than applied irrigation water at these fields. The seasonal values ETI_a-WPR and ET_a-EC for the summer maize 2012 crop at EG-ZAN are 682 mm and 424 mm, respectively. ET_a-lys is 543mm, as cited in literature (Atta *et al.*, 2015), at EG-ZAN for the same crop and period. This analysis suggests that the ET_a at the irrigated sites in the Nile delta fall somewhere between the ET_a-EC and L1 ETI_a-WPR.

Table 3-3. Statistics comparing ETI_a-WPR with ET_a-EC at 14 EC locations.

EC site	Dekad Count	r	RMSE (mm/day)	Bias (mm/day)	R^2	NDVI QUAL*	LST QUAL*
SA-SKU	63	0.46	1.1	0.1	0.465	5.5	0.9
SN-DHR	72	0.96	0.4	0.0	0.924	2.0	0.9
SD-DEM	33	0.90	0.6	0.3	0.799	1.7	0.5
EG-ZAN	95	0.68	2.2	1.7	0.691	1.3	0.2
EG-SAA	108	0.75	0.9	0.8	0.716	1.4	0.3
EG-SAB	93	0.54	1.3	1.6	0.899	1.3	0.3
NE-WAF	49	0.56	1.2	-0.5	0.314	7.4	1.3
NE-WAM	118	0.63	0.9	-0.3	0.397	6.3	1.3
ES-SCL	45	0.72	0.9	-0.3	0.519	NA	NA
GH-ANK	80	0.34	1.0	0.6	0.119	99.5	18.0
BN-NAL	36	0.52	1.8	-0.0	0.267	11.3	2.1
CG-TCH	36	0.74	0.6	0.2	0.552	227.0	23.8
ZM-MON	20	0.69	0.8	0.2	0.478	7.0	1.0
KWSTI	98	0.53	0.8	0.1	0.262	1.5	0.8
Overall	946	0.71	1.0	0.3	0.61	-	-

* The NDVI quality layer provides the gap, in days, to the nearest valid observation for that variable. The LST quality layer provides the number of the days between the date of the data file and the earlier remote sensing observation on which the data is based.

The overestimation of peak ETI_a rates at the Egypt sites are not easily explained. These errors might lie in the FAO-PM method's and may be associated with local advection effects. Local advection may increase ET_a over a water-limited field by up to 30% (De Bruin *et al.*, 2016; Trigo *et al.*, 2018). There is an underlying assumption of no advection in the RET definition for a reference grass field (Allen *et al.*, 1998). However, in small fields, under arid conditions with high temperatures, local advection effects may occur when warm, dry air formed over an upwind, adjacent field is advected horizontally over the well-watered fields (De Bruin & Trigo, 2019). This horizontal advection of sensible heat increases the evapotranspiration of water from well-watered areas but will result in the overestimation of evapotranspiration in water-limited fields or areas. The Zankalon irrigated area, where EG-ZAN is located, has small fields, ~0.2ha (Table 1-4), as does the EG-SAA and EG-SAB. Therefore these sites may be particularly influenced by this effect as 0.2ha is 3% of an L1 -250m pixel, 20% of an L2 -100m pixel and 200% of an L3 -30m pixel.

Figure 3-16. Time series comparison of 10-day averaged (dekad) ETI$_a$-WPR (solid blue line) and ET$_a$-EC (solid black line) for all available flux tower data observations (variable for the different sites). Note that the dates are reported in YYYY-MM format.
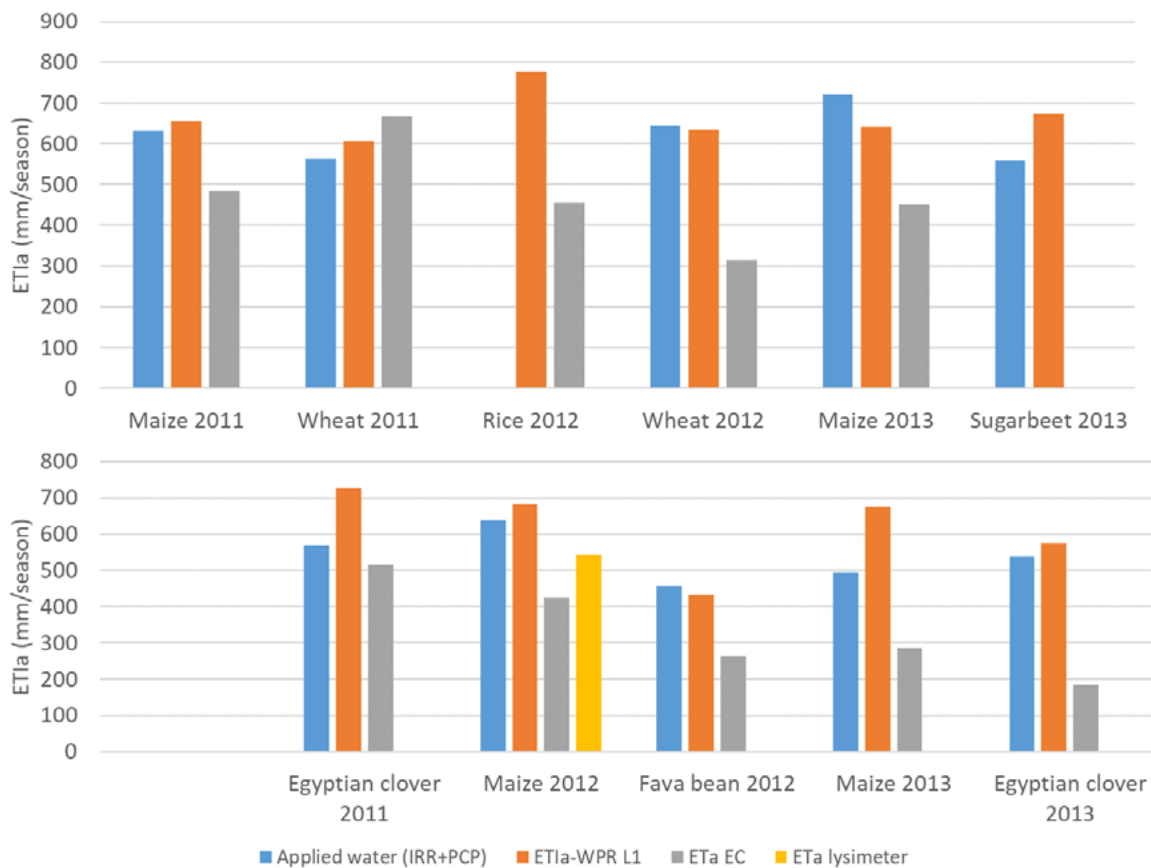
Figure 3-17. Seasonal values of ETI$_a$-WPR, ET$_a$-EC, ET$_a$-lys and applied water for crops at the Egypt EG-SAA (upper) and EG-ZAN (lower) sites. IRR is irrigation water. Applied water, crops, and seasons taken from Sugita *et al.*, (2017).

The SN-DHR and SD-DEM ETI$_a$ respond quickly to the onset of the rainfall season. At these sites, the WaPOR SMC and NDVI are well related to both the ET$_a$-EC and ETI$_a$-WPR (Figure 3-18). For example, the R^2 for the SMC or NDVI and ET$_a$-EC or ETI$_a$-WPR ranges between 0.82-0.87 at SN-DHR and 0.69-0.86 at SD-DEM. SD-DEM does overestimate ETI$_a$-WPR when ET$_a$-EC is low and the NDVI is low.

The good performance at the CG-TCH site may be because the variation in CG-TCH station ET$_a$-EC and ETI$_a$-WPR is strongly related to the vapor pressure deficit (VPD) derived from the EC station and RET, with R^2=0.62 and 0.66 respectively. The VPD and RET in WaPOR are derived from the GEOS-5 model (VPD and RET) and MSG (RET only), as compared to being derived from satellite images. GEOS-5 and MSG are continuously available at sub-daily level and satellite image gaps do not influence the quality of the VPD and RET quality.
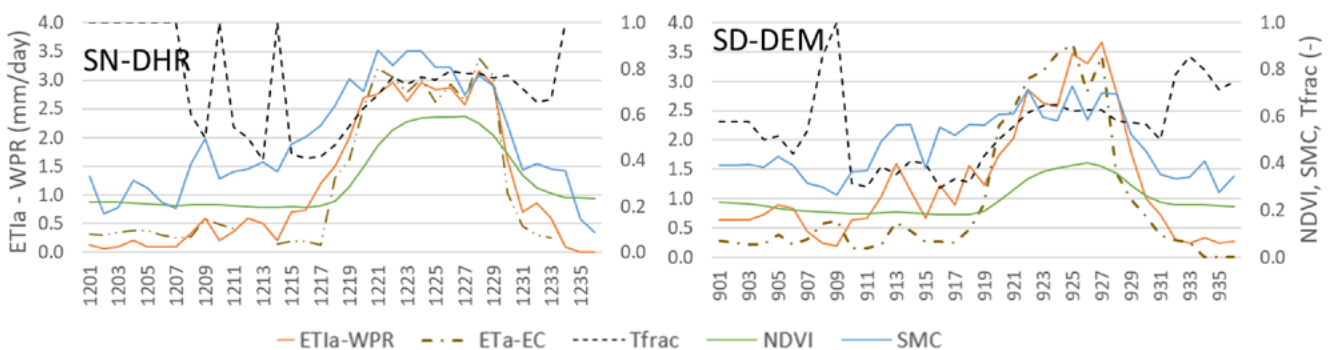
Figure 3-18. WaPOR ETI$_a$, SMC, NDVI and fraction of transpiration (Tfrac) at SN-DHR (2012) and SD-DEM (2009).

The differences at the NE-WAM and NE WAF sites are likely related to the low-quality NDVI and LST layers during the summer (average annual values LST and NDVI gaps appear low in Table 3-3, however major gaps are concentrated in the summer season). These sites are not highly correlated with the site VPD or RET and therefore the lower quality LST and NDVI is expected to have a great impact on the quality of ETI_a-WPR here. The ETI_a-WPR is strongly related to the SMC at these sites (e.g. R^2=0.73 at NE-WAM); however, the ET_a-EC shows no relationship with the WaPOR SMC (R^2=0.37 at NE-WAM). Both of these sites are dominated by soil evaporation (in WaPOR) for most of the year – as indicated by low NDVI all year. The MOD17A2 NCEP II GPP 8-day, 1km product similarly overestimated in-situ GPP at peak vegetation periods (Sjöström et al., 2013). While authors suggested underestimations may be due to data used in the GPP product, they also noted possible uncertainties due to scale mismatch. As the vegetation in the NE-WAM and NE-WAF is quite heterogeneous and the pixels used for comparison extends beyond the vegetation of the EC sites. As ETI_a-WPR does not seem responding well to precipitation, it may be due to the NDVI resolution being too low to pick-up on vegetation increase around the EC site during wet periods. A detailed look into the NE-WAM site tower data can be seen in Appendix C. The ETI_a-WPR at this site more closely follows air temperature, rather than responding to available water.

At the BN-NAL site, the WaPOR SMC and NDVI layers have a stronger relationship with the ET_a-EC than the ETI_a-WPR. For example, the R^2 between the WaPOR NDVI and the ET_a-EC and the WaPOR NDVI and the ETI_a-WPR are 0.87 and 0.56 respectively. At this location the transpiration fraction appears overestimated (Figure 3-19) for much of the season, and not responding well to the NDVI. Therefore, pointing to an overestimation of both the WaPOR evaporation and transpiration component when the ETI_a-EC is low and an underestimation of the transpiration component when the ETI_a-EC is high.
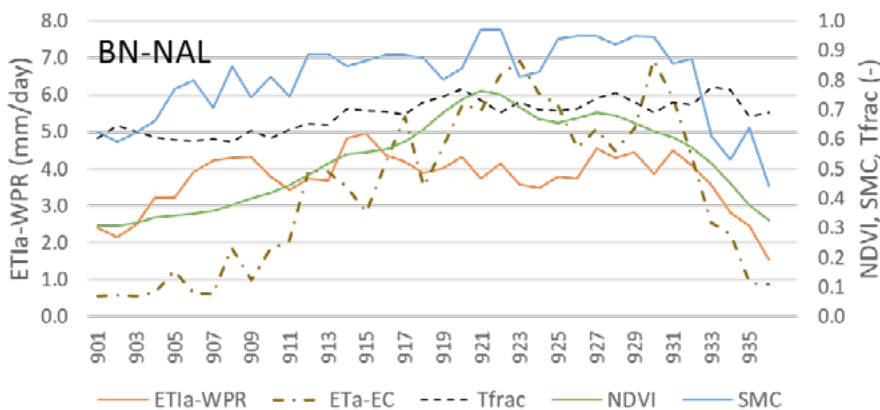
Figure 3-19. WaPOR ETI_a, SMC, NDVI and fraction of transpiration (Tfrac) at BN-NAL (2009).

The Ghana GH-ANK site is characterised by a tropical climate and high vegetation height (evergreen forest). The KWSTI site is located in Naivasha and the Rift Valley, between the Aberdares Ranges to the east and the Mau escarpment to the west. This setting creates a complex micro-climate with significant diurnal variation in temperature and wind speed, among other meteorological variables. The ET_a-EC is not strongly related to the VPD or the RET at both GH-ANK and KWSTI. Therefore, large gaps in the NDVI and LST quality layers will highly influence the quality of the ETI_a-WaPOR at these site. As a result, errors in the input meteorological data may highly influence ET_a-EC estimates at these sites.

The results improve slightly for all sites on a monthly scale. The monthly mean daily ETI_a-WPR plotted against monthly mean daily ET_a-EC is shown in Figure 3-20. The R^2 metric improves the most. The RMSE improves at all stations except EG-SAA, where the RMSE increases by 63%. The correlation and R^2 improved slightly at all stations. The correlation and R^2 increase on average, across stations – not weight, by 9% and 8% respectively. The absolute bias increases slightly at 5 of the 14 stations.

The ETI_a-WPR results are comparable to the improved MODIS global terrestrial evapotranspiration algorithm, with a MAPE of 24.6% as compared to in-situ EC measurements, when driven by flux tower meteorological data (Mu, Zhao & Running 2011). The ETI_a-WPR error estimates, on average, are also close the average errors in EC measurements (20-30%) (Allen et al, 2011; Blatchford et al, 2019).
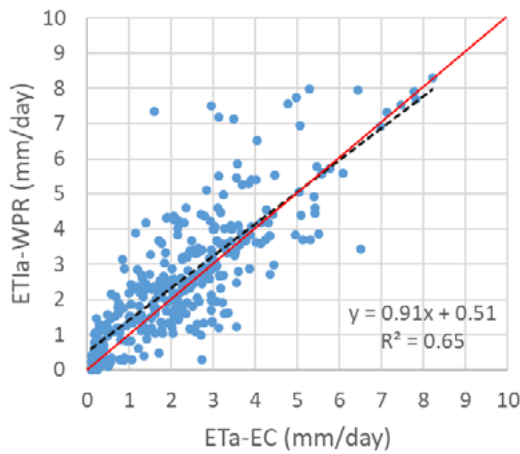
Figure 3-20. The relationship between monthly mean daily ETI_a-WPR plotted against monthly mean daily ET_a-EC. Only months with valid daily observations for all dekads within that month are included. The dotted black line represents the linear regression, and the red line represents the 1:1 line.

CO_2 fluxes and Net primary productivity

The agreement between the NPP-WPR and the NPP-EC is mixed (Figure 3-21). The SN-DHR and SD-DEM sites have a high agreement with the *in-situ* flux tower CO_2 gas exchange data. The NPP-WPR appears overestimated at the GH-ANK, ZM-MON and CG-TCH sites. The seasonal variation was captured fairly well at the SD-DEM, ZM-MON and CH-TCH sites, despite the strong bias. This is indicated by high correlations and R^2 values, particularly at SD-DEM and ZM-MON. The sites in which NPP-WPR performed best are those where the ETI_a-WPR also performed well.

A strong relationship between the ET_a-EC and the WaPOR NDVI was found at sites where there was good agreement between NPP-WPR and NPP-EC (Table 3-4). For example, the SN-DHR and SD-DEM sites had correlations of 0.89 and 0.90 respectively between the NPP-EC and the NDVI from WaPOR. The ZM-MON site had a correlation of 0.32 while no correlation was found between the NPP-EC and the WaPOR NDVI at CH-TCH or GH-ANK. These sites had very low NDVI quality values. The low NDVI quality is expected to influence the NPP-WPR quality more than the ETI_a-WPR, as the NPP relies heavily on the NDVI. The NDVI is the only parameter used to estimate fAPAR, and NPP has a linear dependency on fAPAR.

The MOD17A2 NCEP II GPP 8-day, 1km product was compared to EC at the SD-DEM, ZM-MON and CG-TCH sites in 2007-2009 and 2007-2008 respectively by Sjöström *et al.*, (2013). Similarly, they captured the seasonality well. However, MOD17A2 typically underestimates the GPP in peak vegetation growth periods. The underestimations by MOD17A2 as compared to in-situ GPP were of a similar magnitude as the NPP-WPR and shown in Figure 3-21. This was particularly evident at ZM-MON, where the in-situ GPP often exceeded in the MOD17A2 GPP by up to 80% during peak periods. However, the MOD17A2 product captured the low vegetation period better than WaPOR at these sites. This may be as the in-situ data available for the WaPOR comparison at this site does not cover the entire year. It may also be due to the scalars used that are capturing VPD or other stressors is slightly better with MOD17A2. Conversely, the WaPOR represents the NPP-EC much better than the MOD17A2 at SD-DEM. MOD17A2 greatly underestimated in-situ GPP at peak vegetation growth, where NPP-WPR shows a very good match during the same period.
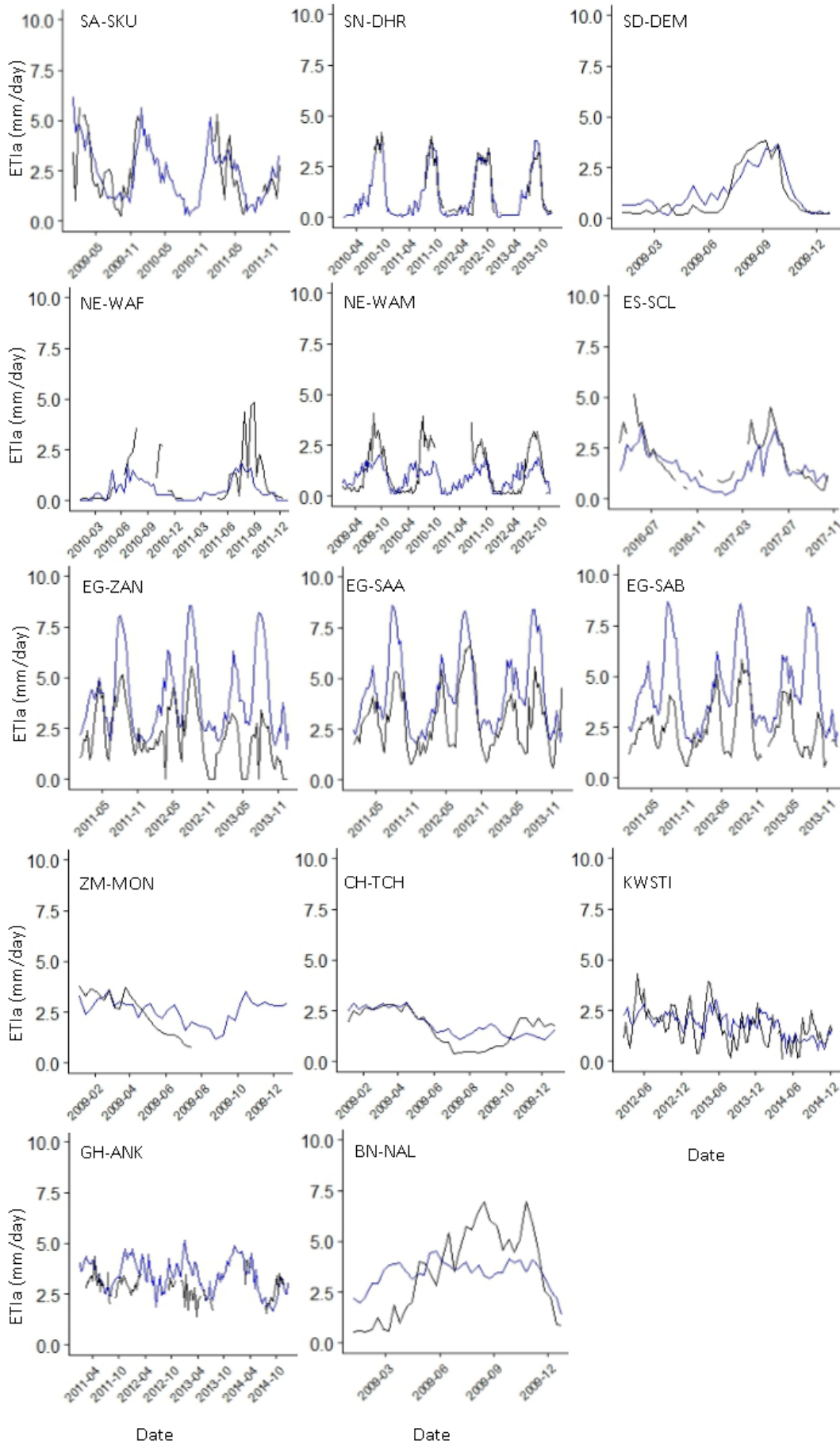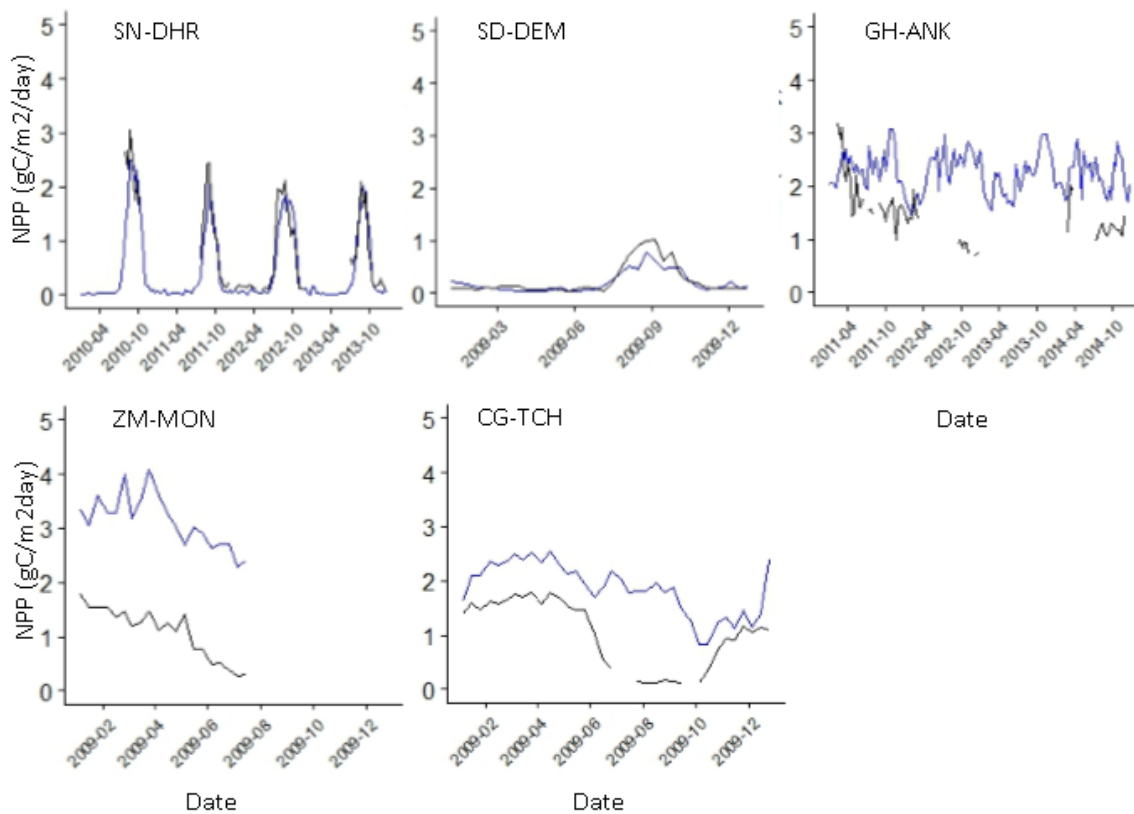
Figure 3-21. Time series comparison of 10-day averaged (dekad) NPP-WPR (solid blue line) and NPP-EC (solid black line) for the available period which varies for different sites. Note that the dates are reported in YYYY-MM format.

Table 3-4. Statistics comparing NPP-WPR with NPP-EC in 5 locations EC locations.

EC site	Dekad Count	r	RMSE (gC/m^2/day)	Bias (gC/m^2/day)	R^2	NDVI QUAL*
SN-DHR	72	0.92	0.3	-0.1	0.85	2.0
SD-DEM	36	0.92	0.1	-0.0	0.86	1.7
GH-ANK	63	0.10	1.0	0.8	0.01	99.5
CG-TCH	33	0.56	1.0	0.8	0.38	227.0
ZM-MON	20	0.75	2.1	2.1	0.56	7.0
Overall	227	0.69	0.5	-0.5	0.46	

* The NDVI quality layer provides the gap, in days, to the nearest valid observation for that variable.

Reference Evapotranspiration to flux tower in-situ (RET-EC)

The RET-WPR generally has good agreement with the RET-EC estimated from *in-situ* meteorological measurements at the Eddy Covariance sites (Figure 3-22 and Table 3-5). The RET-WPR captures the seasonal variations well, however, it did frequently overestimate RET-EC particularly at peak RET-EC periods. This was less pronounced at the agricultural cropping sites. The primary drivers of RET are the available energy or net radiation and the VPD. Therefore, uncertainties are likely primarily attributed to the radiation component or the input meteorological dataset.

The correlation at all sites was reasonable to very good (0.59-0.87). The R^2 was more mixed ranging from 0.35 (ZM-MON) to 0.79 (SN-DHR, EG-ZAN and EG-SAA). The RET-WPR performs better at sites with grasslands and croplands than at sites with taller vegetation canopy (e.g. GH-ANK and ZM-MON). Generally,

sites where the agreement between RET-WPR and RET-EC is high, the agreement between the ETI_a-WPR and ET_a-EC is also high. This indicates that RET is a good indicator of model performance.
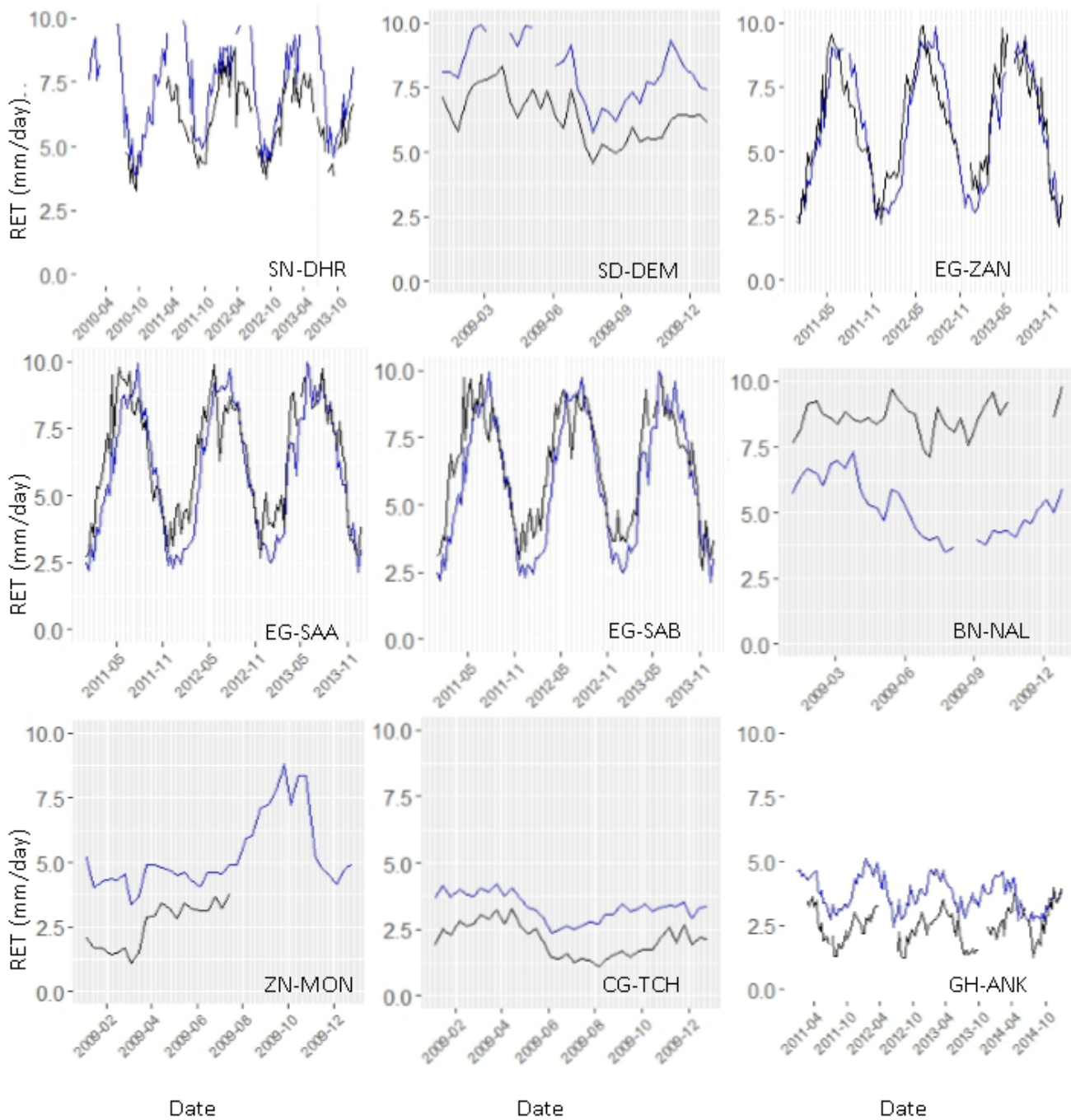
Figure 3-22. Time series of dekad RET-WPR (solid blue line) and dekad RET-EC (solid black line) for the available period which varies for different sites. Note that the dates are reported in YYYY-MM format.

Table 3-5. Statistics comparing daily RET–WPR with RET–EC at 9 EC locations.

EC site	Observation Count (# of days)	r	RMSE (mm/day)	Bias (mm/day)	R^2	NDVI QUAL*
SN-DHR	1112	0.87	0.1	-0.1	0.75	2.0
SD-DEM	365	0.77	2.0	-1.6	0.65	1.7
EG-ZAN	1062	0.87	2.9	2.7	0.76	1.3
EG-SAA	1096	0.87	3.2	3.0	0.64	1.4

EG-SAB	1053	0.80	3.5	3.2	0.75	1.3
GH-ANK	1120	0.71	2.3	-2.1	0.50	99.5
BN-NAL	364	0.68	6.2	6.1	0.46	11.3
CG-TCH	364	0.79	4.8	-4.1	0.64	227.0
ZM-MON	203	0.59	1.1	1.0	0.35	7.0
Overall	6720	0.68	3.1	12.0	0.52	

* The NDVI quality layer provides the gap, in days, to the nearest valid observation for that variable.

3.4.2. Comparison of WaPOR to farmer-reported in-situ crop yields

The comparison in this section considers only shows the results of L3 and L1, as there are discrepancies between L3 and L1 results. However, L1 and L2 show very high consistency (see section 3.6.1), so L1 was considered representative of both L1 an L2.

Wheat and potato – Bekaa Valley (Lebanon)

The mean wheat and potato yields, derived from WaPOR, were compared to the mean reported wheat and potato yields reported by farmers in the Bekaa valley. The precision of farmer reported yields in the region were considered to be too low for a plot-by-plot comparison. For example, of the 19 reported potato tuber yields, only 3 values were given; 35 ton/ha was reported by four farmers, 40 ton/ha was reported by 13 farmers and 45 ton/ha was reported by two farmers. The mean farmer reported potato tuber yield was 39.5 ton/ha. The mean L3 and L1 WaPOR derived potato tuber yield was 32.2 ton/ha and 35.8ton/ha. The standard deviation for the farmer reported, L3 WaPOR and L1 WaPOR derived potato tuber yields was 2.8 ton/ha, 2.9 ton/ha and 6.5ton/ha respectively. The higher standard deviation in the L1 WaPOR derived potato yields may be due to the varying field sizes in the Bekaa. The reported potato field sizes varied from 2 ha to 50 ha. A 2 ha field is only 0.32 of a 250m L1 pixel.

The mean farmer reported wheat (grain + straw) yield was 1.3 ton/ha. The mean farmer reported, L3 and L1 WaPOR derived wheat (grain + straw) yield was 1.32 ton/ha, 1.1 ton/ha and 1.0 ton/ha. The standard deviation of the farmer reported and L3 WaPOR derived wheat yields was 0.2 ton/ha and 0.1 ton/ha respectively. The L3 WaPOR derived mean yields were less than the farmer reported mean yields and the standard deviations were slightly higher. It is suggested that the mean derived WaPOR values are reasonable compared to the reported values.

The temporal trends of the potato and wheat field (plot) NDVI and SMC can be seen in Appendix B for the growing seasons (for the fields included in the comparison). The SMC was high for the entire wheat growing season, with a minor dip in late February and early March (dk 1706). These trends align with the transition to a lower rainfall period (wet season late Oct-Mar) and onset of irrigation in the summer. The NPP-WPR over time was highly correlated to the NDVI for all plots. The NDVI trend aligns with the growing season for both wheat and potato. The wheat and potato NDVI drops at the end of the season, before harvest. For wheat this is associated with graining phase. For potato this is associated with the tuber maturation phase where the leaves turn yellow and lose colour (eventually dying). The wheat peak NDVI ranges from 0.55-0.9, which is in the expected range of wheat NDVI (Duchemin *et al.*, 2006; Guan *et al.*, 2019)this study investigates the feasibility of using the normalised difference vegetation index (NDVI. The potato NDVI peaks are reasonably compared to other studies which reach up to 0.9 mid-season (Blatchford *et al.*, 2018; Geng *et al.*, 2015). Therefore, discrepancies may be due to scaling parameters on NPP, such as temperature stress, or solar radiation. The L3 wheat and potato bias were 21 and 19% respectively, which fall within the range. Some discrepancies are also likely found in the farmer reported estimates, that typically have errors of 10-30% (Blatchford *et al.*, 2019). The homogeneity of the farmer reported yields suggest that the farmer reported yield errors are on the high end of the typical error range.

Sugarcane – Awash (Ethiopia)

The sugarcane AGBP, derived from WaPOR and the AGBP reported by farmers in both the Wonji and Metehara irrigation schemes is shown in Figures 3-23 and 3-24. The WaPOR estimated AGBP and the farmer reported AGBP are often within the same range. The fields in the north-west (top-left) of the Wonji scheme have higher AGBP. While the fields in the centre and the south-west (bottom-left) have a lower AGBP for both farmers reported and WaPOR derived estimates. The performance of the fields in the east is mixed. The farmer reported yields also show more variation between plots and years, with a standard deviation in reported AGBP being 47 ton/ha compared to a standard deviation of 26 ton/ha found for the WaPOR derived AGBP.
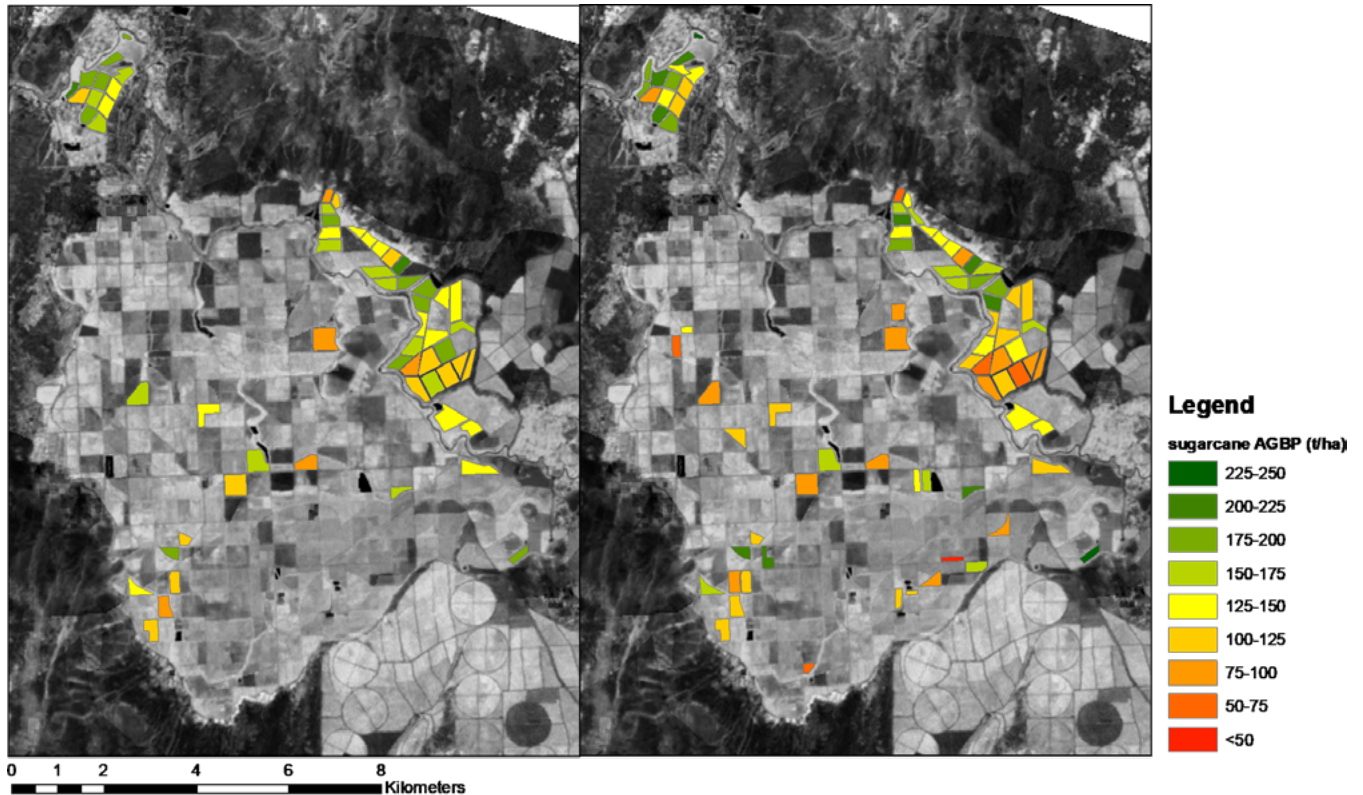
Figure 3-23. WaPOR derived (left) and reported (right) AGBP (ton / ha per full ratoon cropping period) for available plots in the Wonji – with SOS and EOS between 2009-2016. Full ratoon cropping periods range from 0.8 to 2.8 years (and can explain the high ranges of total sugarcane productivity ABGP in ton/ha).

Source: this study

Overall, the agreement between the in-situ and WaPOR derived AGBP is high in the Wonji and is good in the Metehara (Figure 3-25 and Table 3-6). The correlation in the Wonji is high (0.84) and the R^2 is high, 0.71. However, in general the WaPOR AGBP is underestimated as compared to the in-situ data. In the Metehara the correlation is 0.71, though the R^2 is only 0.5. Based on the standard parameters used to convert NPP to sugarcane AGBP, the WaPOR derived AGBP continuously underestimates in-situ AGBP by 58% in the Metehara. The lower AGBP in Metehara is likely due to the land cover being classified as a C3 crop (Crops in classified as both 41 and 42 are classified as C3 crops) in LCC in WaPOR. While the LCC is the same in the Wonji, the Wonji does not reach the same high average maximum daily temperatures as the Metehara. For example, average maximum daily temperatures reach 36C, 33C and 32C in June, Jul, Aug in the Metehara as compared to 29C, 26C and 26C in June, Jul, Aug in the Wonji. As C3 crops are more sensitive to temperature stress, this may be influencing the biomass production.

The comparison of the Metehara AGBP for harvest years 2012, 2014 and 2016 are shown Figure 3-24. The in-situ data is consistently lower in the Metehara. The average reported AGBP is higher in the Metehara than the Wonji. The standard deviation and CV estimated through WaPOR was 30.1 ton/ha and 0.33 respectively and

the standard deviation and CV estimated reported by farmers estimates was 62.8 ton/ha and 0.36 respectively. Though the standard deviation is lower for AGBP-WPR, the CV is similar suggesting the datasets have similar spatial variation. The temporal variation was similar for both products, i.e. the mean values and spatial variation over time remained consistent between the L3 AGBP-WPR and the farmer estimates. E.g. years when the farmer reported AGBP spatial variation was higher, the AGBP-WPR was proportionately higher and years where the farmer reported mean AGBP was higher, the AGBP-WPR was higher. For example, Figure 3-24 shows that in 2016, both the reported AGBP and AGBP-WPR are lower than the previous years.
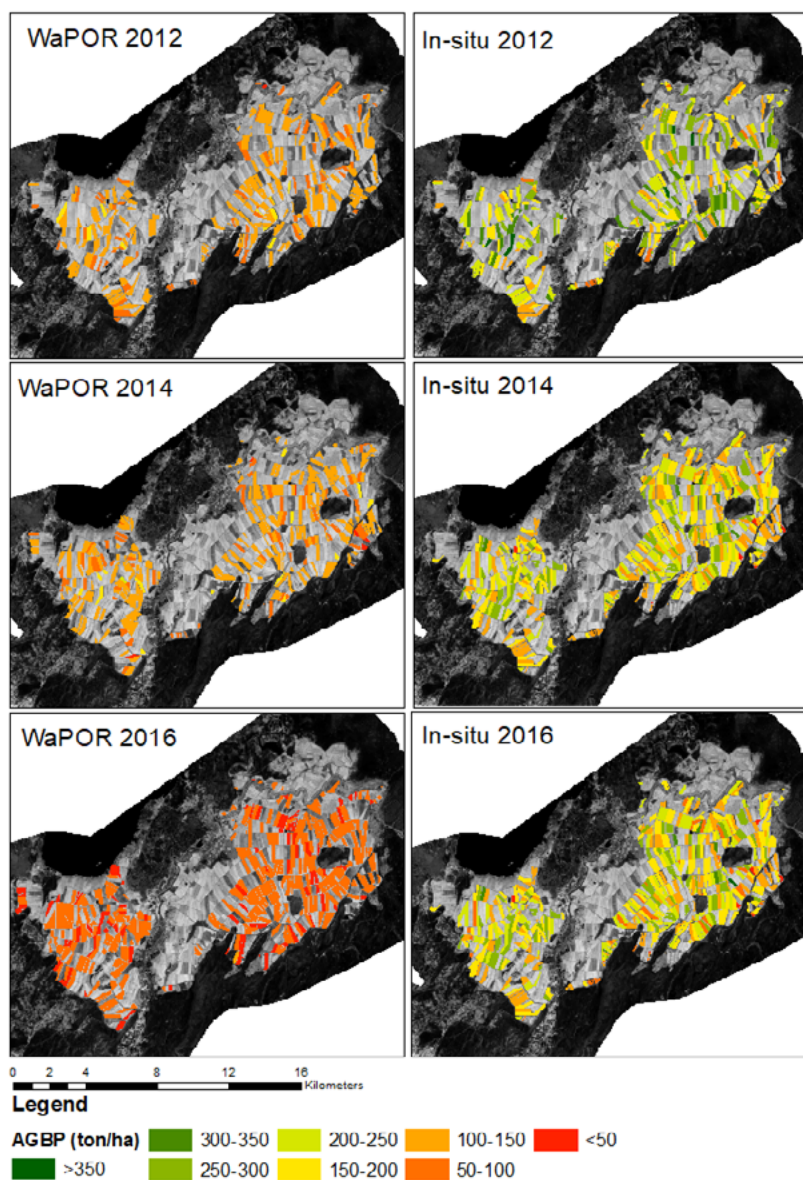
Figure 3-24. WaPOR derived (left) and reported (right) AGBP in ton/ha for full ratoon cropping cycle [variable per plot, ranging from 0.8-2.8 yrs]) for available plots in the Metehara with EOS between in 2012, 2014 and 2016.

Source: this study
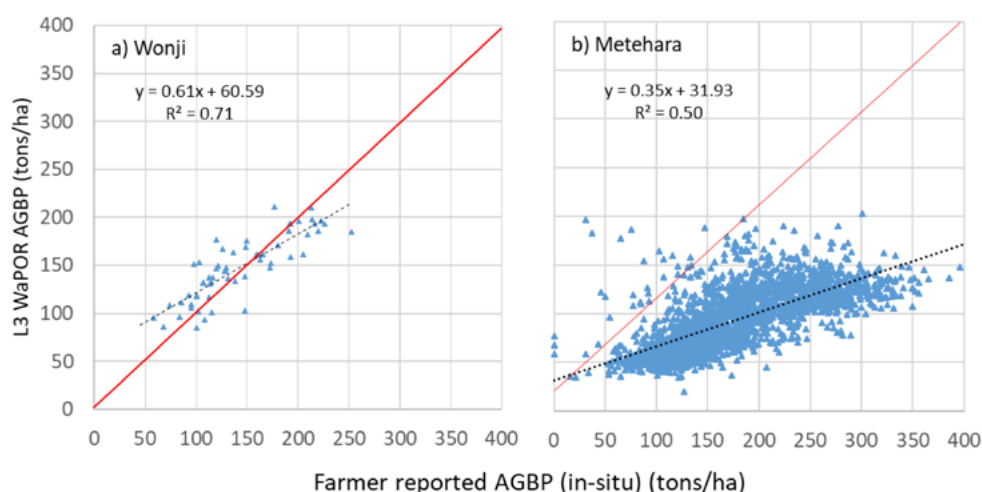
Figure 3-25. Comparison of farmer reported sugarcane AGBP and sugarcane AGBP derived from L3 NPP-WPR data in the Wonji (left) and Metehara (right). ABGP are in ton.ha-1.full ratoon cycle [range: 0.8 to 2.8 years].

Table 3-6. Summary statistics of WaPOR derived sugarcane AGBP compared to farmer reported sugarcane AGBP.

Metric	Wonji (AGBP)			Metehara (AGBP)		
	L3 - WPR	L1 - WPR	Reported	L3 - WPR	L1 - WPR	Reported
RMSE (ton/ha)	33.9	48.2		83.2	96.8	
Correlation	0.84	0.68		0.71	0.70	
R^2	0.72	0.46		0.50	0.49	
Bias (%)	0.4	-3.3		-48.4	-57.4	
Bias (ton/ha)	0.55	-4.91		-84.0	-99.5	
Mean (ton/ha)	150.6	141.1	147.3	92.9	76.5	173.5

Both the reported and estimated yields are high in the Wonji compared to global averages, but the biomass was reported in ton/ha over the total ratoon cycle and growing period. The AGBP-WPR is comparable to the average global cane yields. According to FAO 66, global sugarcane average biomass yield is 69.8 t/ha per year (Steduto *et al.*, 2012)and relying on a network of several scientific institutions, FAO has packaged a set of tools in this Irrigation and Drainage Paper to better appraise and enhance crop yield response to water. These tools provide the means to sharpen assessment and management capacities required to: compare the result of several water allocations plans: improve soil-moisture control-practices under rainfed conditions; optimize irrigation scheduling (either full, deficit or supplementary. FAO WATER reports that the cane yield varies from 50 to 150 t/ha for depending on the variety and ratooning stages, which suggest that the WaPOR derived values are with-in the typical range, while the farmer estimates are on the high side. The harvested biomass is related to the growing period. The average total growing period of sugarcane in the Awash L3 area is 585 days with a range of 305-1037 days or 0.8-2.8 years.

The results of the AGBP-WPR in the Wonji and Metehara are highly promising, considering a user can adjust paramaters, including fraction of above ground biomass and moisture content, to reduce bias, and retain the spatial and temporal representativeness of the dataset. Converse to the comparison with EC data, where the NPP-WPR was sometimes overestimated, the NPP-WPR at the Metehara location and Wonji appears underestimated. This may be due to the NPP being compared in section 6.1.2, compared to the AGBP being compared in this section. It is difficult to assert the true bias, when the conversion factors taken to convert the NPP-WPR to AGBP are standard parameters for sugarcane with a linear relationship. Similarly, farmer estimates are reported to have typical errors of up 10-30% (Blatchford *et al.*, 2019).

3.5. Analysis of interactions between NPP and ETI$_a$

When interpreting agricultural water productivity data, it is useful to analyse interactions and relationships between biomass productivity and evapotranspiration processes. Hereunder a succinct analysis is done, using the in-situ datasets (flux towers, field surveys and farmer reported data), and contrasting these with the WaPOR estimates at the in-situ flux tower locations.

3.5.1. Contrasting EC flux tower NPP: ETI$_a$ ratios with WaPOR estimates

The relationship between ETI$_a$-WPR and NPP-WPR was often similar to the relationship between ET$_a$-EC and NPP-EC at SN-DHR and SD-DEM (Figure 3-26). In terms of WP this is important, as the ratio between the two products is as important than the magnitude of each component individually. The sites where the relationship was not well replicated are the sites where both variables were not well represented by in-situ data (e.g. GH-ANK, andCG-TCH). The ZM-MON and CG-TCH in-situ data suggest a much lower water use efficiency (NPP-ET$_a$ ratio) than the data from WaPOR. This is due to an overestimation of the NPP-WPR data at these sites. The SN-DHR site, has a large cluster of very low NPP-WPR values when ETI$_a$-WPR is below 2 mm/day. At this site, during these time periods with very low ET values, also the NDVI and SMC are very low. The resolution of the L1 images may not be capturing the vegetation including the ephemeral dynamics during the rainfall season well at this site.

We also note that, although a simple linear regression was used to evaluate the relationship between biomass production and water consumption, these relations are probable more non-linear, as can be observed for some sites in the figures.
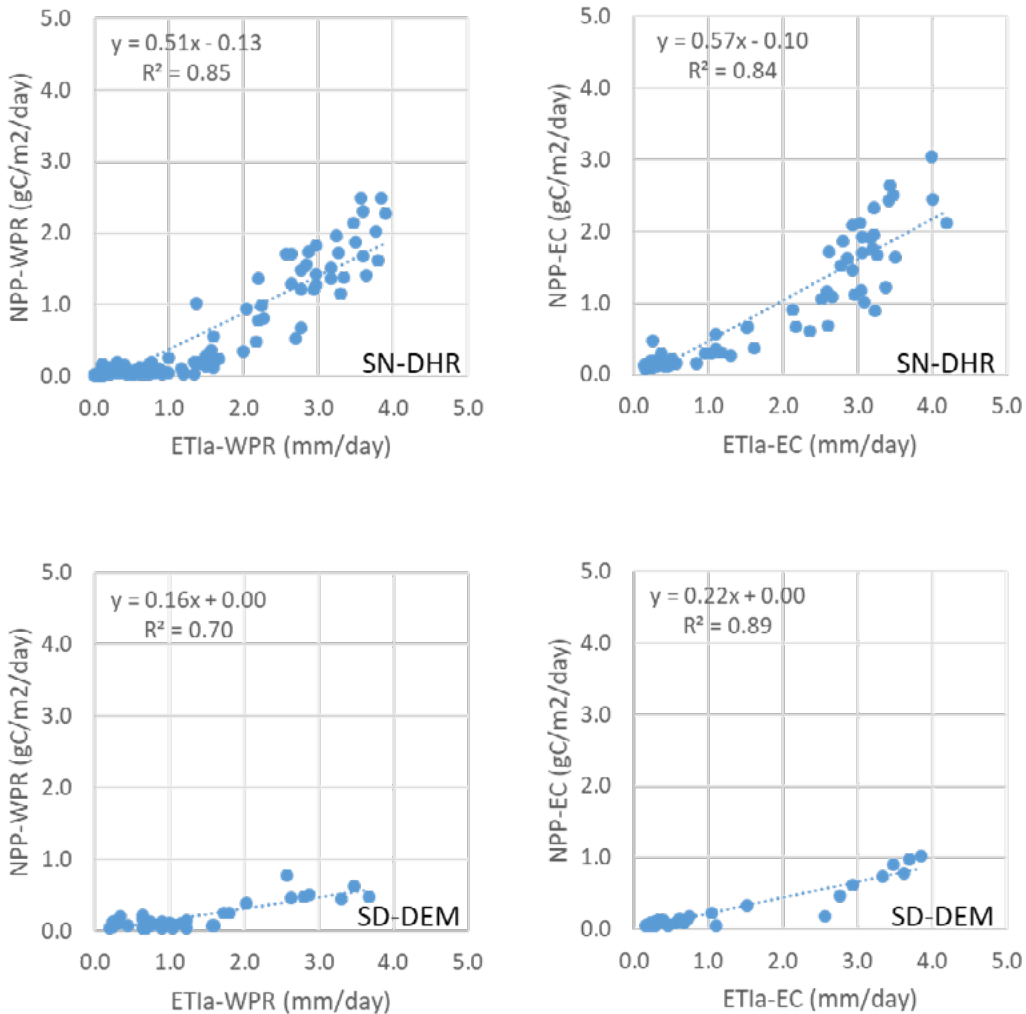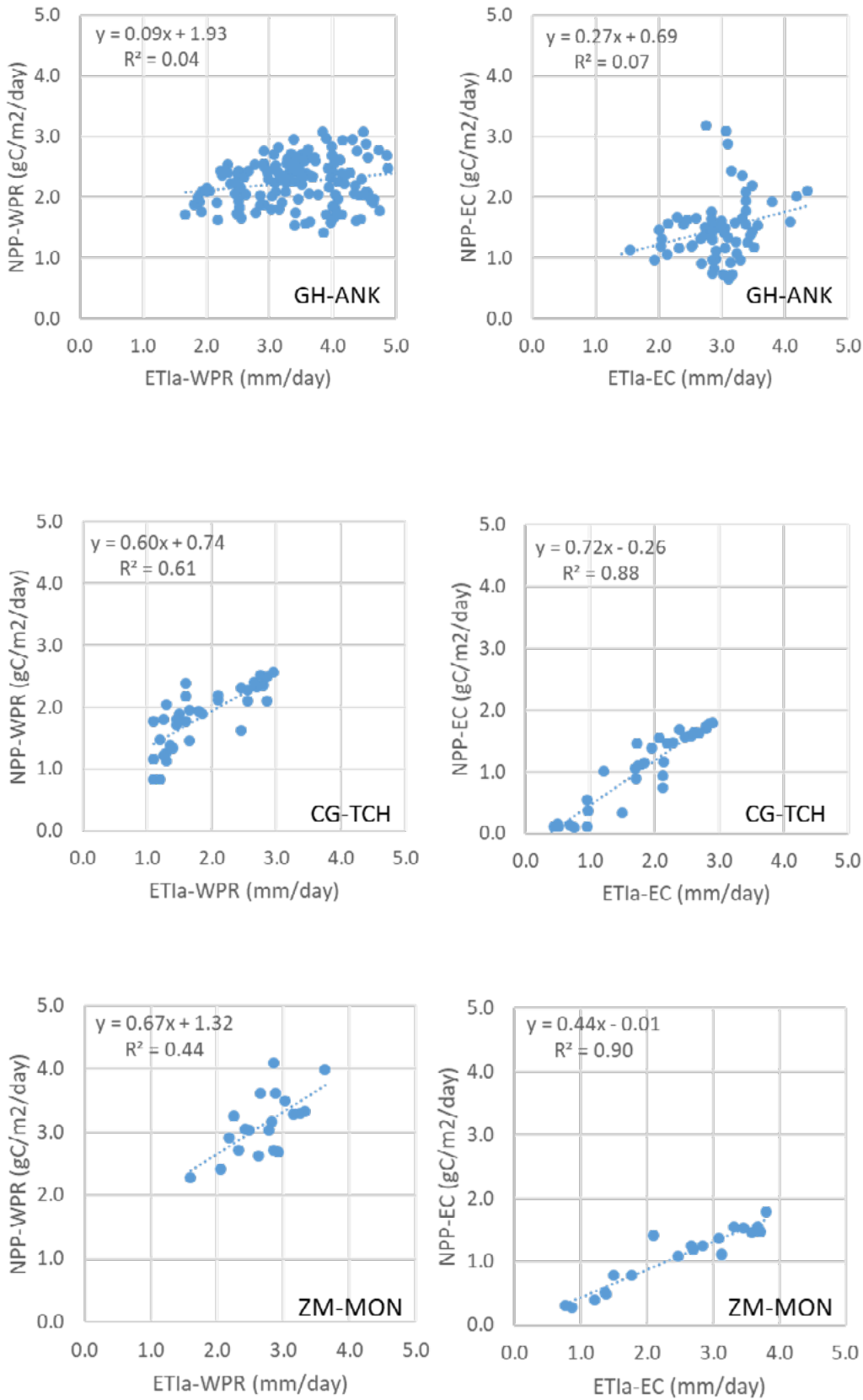
Figure 3-26. NPP-WPR plotted against ETI$_a$-WPR (left) and NPP-EC plotted against ET$_a$-EC (right) for 5 eddy covariance stations with both latent energy and carbon flux observations.

Figure 3-27 shows the NPP-WPR plotted against the ETI$_a$-WPR and the NPP-EC plotted against the ETI$_a$-EC for all stations and for all dekads where in-situ data exists. The slope between the NPP-WPR and ETI$_a$-WPR is greater than the slope between the NPP-EC and ET$_a$-EC. This relates to the overestimation of NPP, as compared to in-situ data, shown in Figure 6-12. The NPP-WPR also has more very low values (<0.2gC/m^2/day)

as compared to the NPP-EC. When all the dekads for all stations are combined the relationship between NPP-WPR and ETI_a-WPR is less clear. A couple of identified causes are the cluster identified in the orange circle. These values have low NPP-WPR considering the high ETI_a-WPR.

The values highlighted in the circle are located in the Nile Delta and represent the dry hot summer. The Egypt EC tower and irrigation sites are not affected by soil moisture stress or VPD stress and therefore may be excessively constrained by temperature stresses, especially considering the high NDVI values (0.7-0.8) during these periods of lower NPP-WPR. This is highlighted in the time series of ETI_a, NPP, NDVI and SMC at EG-ZAN shown in Figure 3-28. The NDVI and ETI_a show two distinct seasons, associated with the winter (clover and fava) and summer (maize) crops grown in the plot. The relative SMC is high when the NDVI and ETI_a are high. However, the NPP is not responding to the increased NDVI and ETI_a despite available soil moisture. This suggests that the temperature is down regulating the NPP too strongly. The sites have an irrigated maize summer crop (a C4 crop) rotation which may be resulting in a lower NPP for two reasons; C4 crops have a higher resistance to high temperatures which may not be accounted for, and C4 crops have a higher maximum LUE than C3 crops. The standard LUE used in WaPOR is based on the L2 LCC map from the portal (as L3 LCC is not yet available). These sites are classified as irrigated cropland, which uses a maximum LUE of 2.7 gDM/MJ or 1.21 gC/MJ, as compared to a more appropriate C4 LUE of 4.32 gDM/MJ or 1.94 gC/MJ, suggesting it is undercalculated by up to 62.5% based on LUE differences alone.

This is further supported when compared to other studies. The WaPOR maize values are low (1-3 gC/m2/day) compared to maximum NPP peak rates (taken as 0.5 x GPP) values for maize based on the EC flux tower measurements found in Saudi Arabia (21 gC/m2/day), China (7.5 gC/m2/day) and France (~12.5 gC/m2/day) (Madugundu *et al.*, 2017)[1]. Therefore, while this highlights the importance of converting the maximum LUE based on the vegetation type when using NPP-WPR, it does not completely account for the low NPP-WPR values for the C4 crops in the region. On top of converting LUE, different temperature stress factors that are associated with C3 and C4 crops (which are incorporated in the NPP-WPR). NPP will decrease much faster in higher temperatures for C3 than C4, resulting in NPP estimates which are too low for Maize in arid regions. As this area is classified as C3 and not C4, the temperature stress function is associated with C3, resulting in observed crop stress through NPP-WPR which is not actually present on the ground (this was also seen in sugarcane in the Metehara – section 3.4.2).
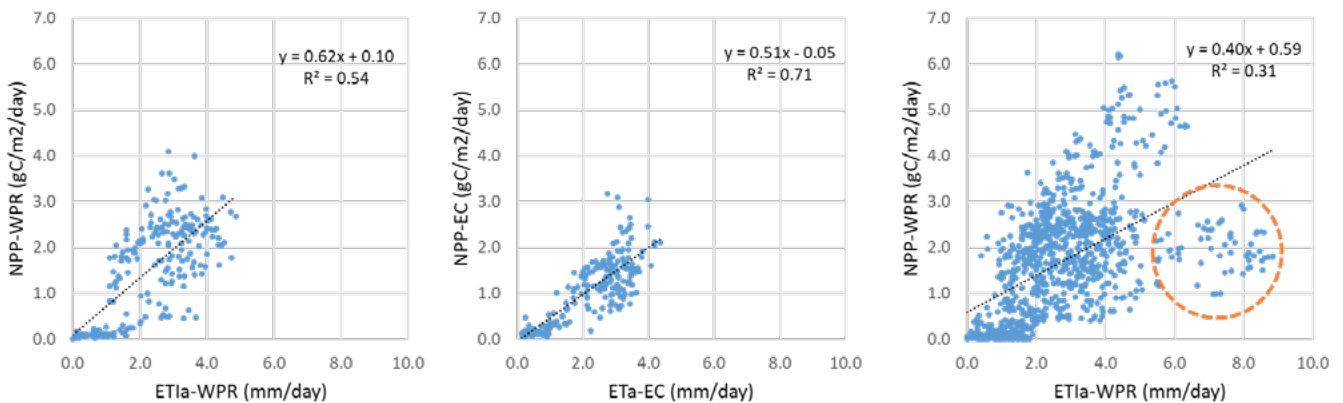
Figure 3-27. NPP-WPR plotted against ETI_a-WPR for 5 EC stations with in-situ NPP data (left) and NPP-EC plotted against ET_a-EC (Near) for 5 eddy covariance stations and NPP-WPR plotted against ETI_a-WPR for all EC stations (right) where ET_a-EC data exists. Orange dashed circle highlights NPP-WPR that may be responding to temperature stress.

---

1. We mention that the LUE and GPP, NPP values reported by Madugundu et al (2017) from Eddy Covariance and other field experiments in Saudi Arabia represent high values and represent observed maximum values during the growth cycle. We must mention that there are large differences between instantaneous (e.g. maximum) and crop cycle averaged light use efficiency and NPP values.
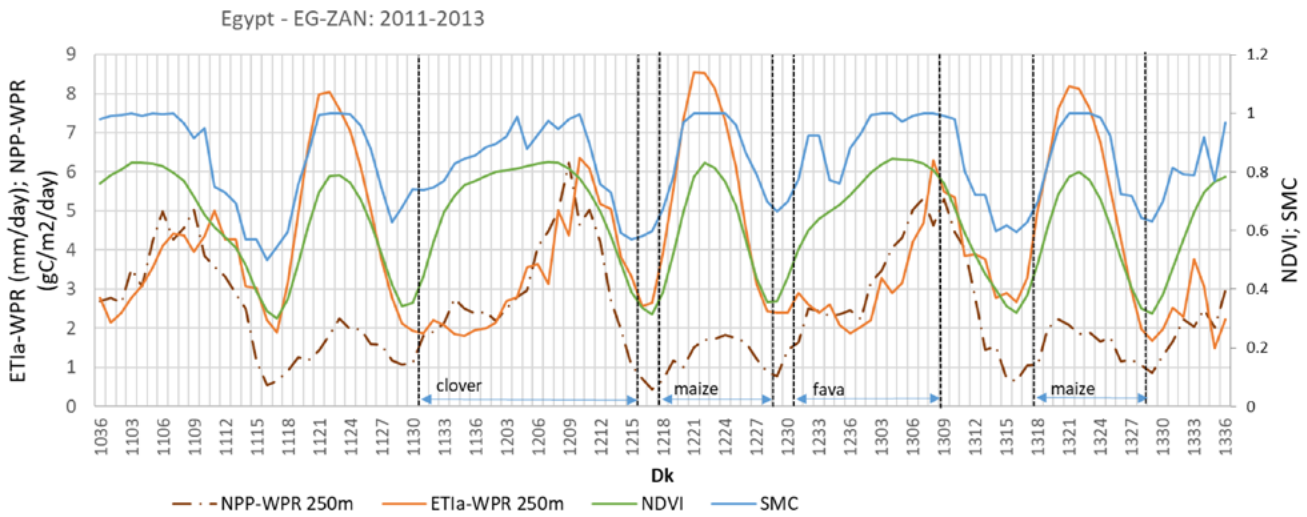
Figure 3-28. NPP - WPR, ETI$_a$ - WPR, NDVI and SMC time series at EG - ZAN station 2011-2013.

3.5.2. Farmer reported *in-situ* yield estimates

The relationship between the L3 WaPOR yield and L3 WaPOR transpiration shows a positive linear trend for wheat (Figure 3-29), with a high R^2, 0.81. The potato relationship shows an increasing yield with increasing transpiration, however, the linear fit shows poor correlation , R^2 =0.27. The range of transpiration to Carbon ratio – T(g):C(g) – is 62-134 g/g for potato and 79-130 g/g for wheat. This is lower than the range expected for C3 crops (160-245 gH_2O/gC), the transpiration rates for potato and wheat. The WaPOR transpiration rates for potato and wheat range from 220-430 mm/season and 383-616 mm/season respectively, and the ETI$_a$-WPR ranges from 427-720 mm/season and 437-781 mm/season respectively. The transpiration ratio (T/ETI$_a$) seems low and does not follow NDVI trends well. No relationship was observed between Tfrac and NDVI over time for any field in the Bekaa valley. However, a strong relationship was observed between plant transpiration and NDVI, NDVI and NPP-WPR, NDVI and ETI$_a$-WPR, and transpiration and NPP-WPR. This suggests that the evaporation component is overestimated or, the evaporation fraction is being overestimated.

The Awash L3 sugarcane AGBP plotted against the L3 transpiration showed a positive linear relationship with a R^2 of 0.66 and the transpiration to carbon assimilation ratio is within the expected ratio of C4 crops (60-100 gH_2O/gC). The transpiration rates ranged between 1342-3112 mm/season (or mm/ratoon) and the ETI$_a$-WPR rates ranged from 1658-3688 mm/season (or mm/ratoon). These values are much higher and represent a longstanding green crop. These values are high, because the total planting season and ratoon periods for sugarcane are near 2-years or more. Converse to the Bekaa, a clear relationship was seen between Tfrac and NDVI in the Awash during the seasons. For example, plots ADU-17-A2 and MIA-1-C1 showed positive linear relationships, R^2=0.86 and R^2=0.51, during their respective growing seasons. A strong relationship was also seen between transpiration and NDVI, NDVI and NPP-WPR, NDVI and ETI$_a$-WPR, and transpiration and NPP-WPR.
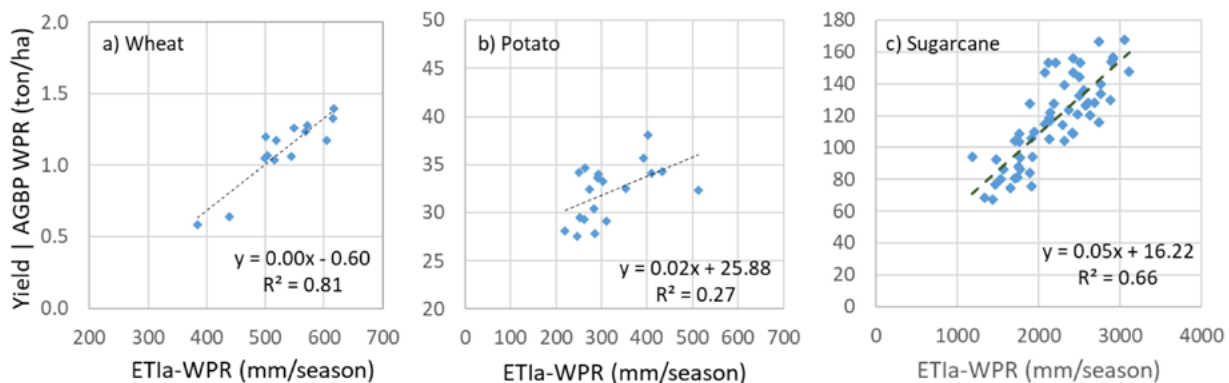
Figure 3-29. Wheat and potato yield and sugarcane AGBP plotted against seasonal evapotranspiration.

Main findings of Chapter 3.4 and 3.5:

- Comparison of WaPOR ETI$_a$ and NPP to Eddy Covariance flux tower data is generally satisfactory, with some good to very good performances. Some locations, typically with more dense tall vegetation (tree cover classes) show poor correlation for all data (ETI$_a$, RET, NPP)

- Good performance of ETI$_a$ in agricultural crop (rain fed and irrigated) sites; but overestimation of ETI$_a$ in some irrigated area sites in the Nile Delta

- Mixed performance in dry savannah – rain fed agriculture sites (very high to medium)

- NPP is performing well at the same locations where ETI$_a$ is performing well

- RET is performing well at the same locations ETI$_a$ is performing well

- Good correlations of farmer reported yields versus seasonal ETI$_a$ for wheat (cereals) in Bekaa and sugarcane (Ethiopia); poor correlation for potato (tubers) in Lebanon

- Selecting the correct maximum LUE correction factor is important for L3 site level comparisons. Temperature stress down regulating may be reducing NPP too much in the C4 crops in hot, arid areas (as they considered as a C3 crop).

3.6. Evaluation of consistency among spatial resolution levels

3.6.1. Consistency between level-1 and level-2 resolutions

The consistency between the evapotranspiration and NPP-WPR data products for the L1 and L2 data products is high (Figure 3-30 and Appendix D). Due to high consistency between L1 and L2, for both ETI$_a$ and NPP, much of the values overlapping in Figure 3-30. The ETI$_a$-WPR RMSE, between L1 and L2, for each dekad for the 2009-2018 period ranged from 0.01 to 0.11mm/day with a median of 0.03mm/day, while the correlation ranged from 0.95 to 1.00 with a median of 0.98. The median R^2 over the period is 0.96 while the median bias is 7%. The consistency between layers dropped slightly after 2014. In 2014 the PROBA-V was introduced for L2, as compared to resampling of MODIS to 100m before 2014. The median correlation dropped from 1.0 to 0.96 for the ETI$_a$-WPR and dropped from 0.98 to 0.93 for the NPP-WPR. The median ETI$_a$ RMSE increased from 0.01 mm/day to 0.04 mm/day and the NPP RMSE increased from 0.10 to .0.11 gC/m^2/day. A slight positive systematic bias, in favour of L2 for ETI$_a$-WPR, is evident after 2013, with median bias increasing from 4% to 9%. No bias is evident between the L1 and L2 NPP products. The consistency between layers dropped slightly after 2014, due to the use of an additional satellite data source (PROBA-V). The median correlation dropped from 1.0 to 0.96, and the median RMSE increased from 0.01 mm/day to 0.04 mm/day. A slight positive systematic bias, in favour of L2, is evident after 2013, with median bias increased from 4% to 9%.
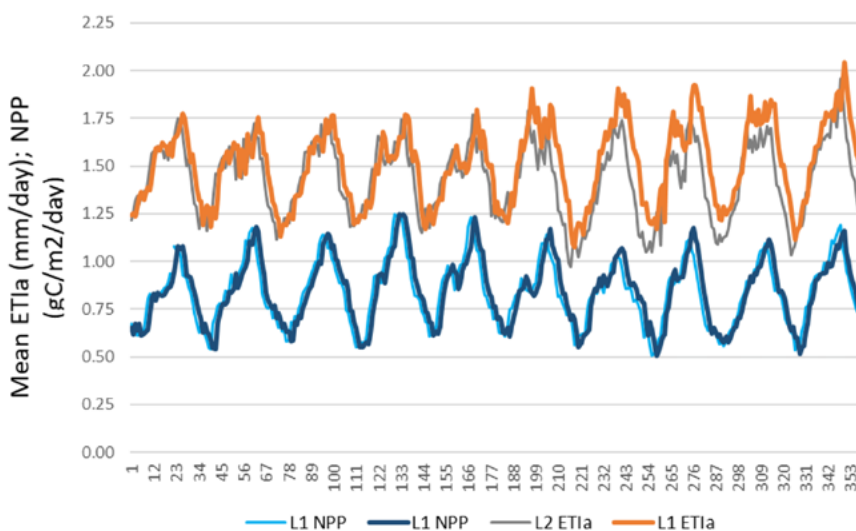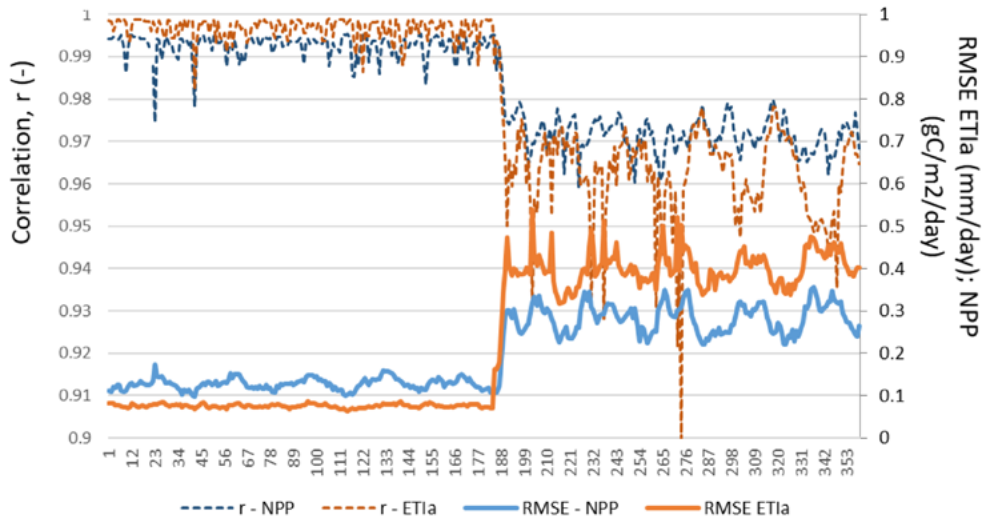
Figure 3-30. Level consistency between L1 and L2 ETI$_a$ and NPP.

The resulting level consistency between the L1 and L2 AGBP WP (AGBP/ETI$_a$) is shown in Figure 3-31. Due to the high consistency in the ETI$_a$-WPR and NPP-WPR products the AGBP WP consistency is also very high. The same small drop in consistency is seen in 2014 that was seen for ETI$_a$-WPR and NPP-WPR. However, the correlation remains high, and is above 0.75 on 95% of dekads. The median RMSE increases from 0.07 kg/m^3 before 2014 and 0.09 kg/m^3 after.
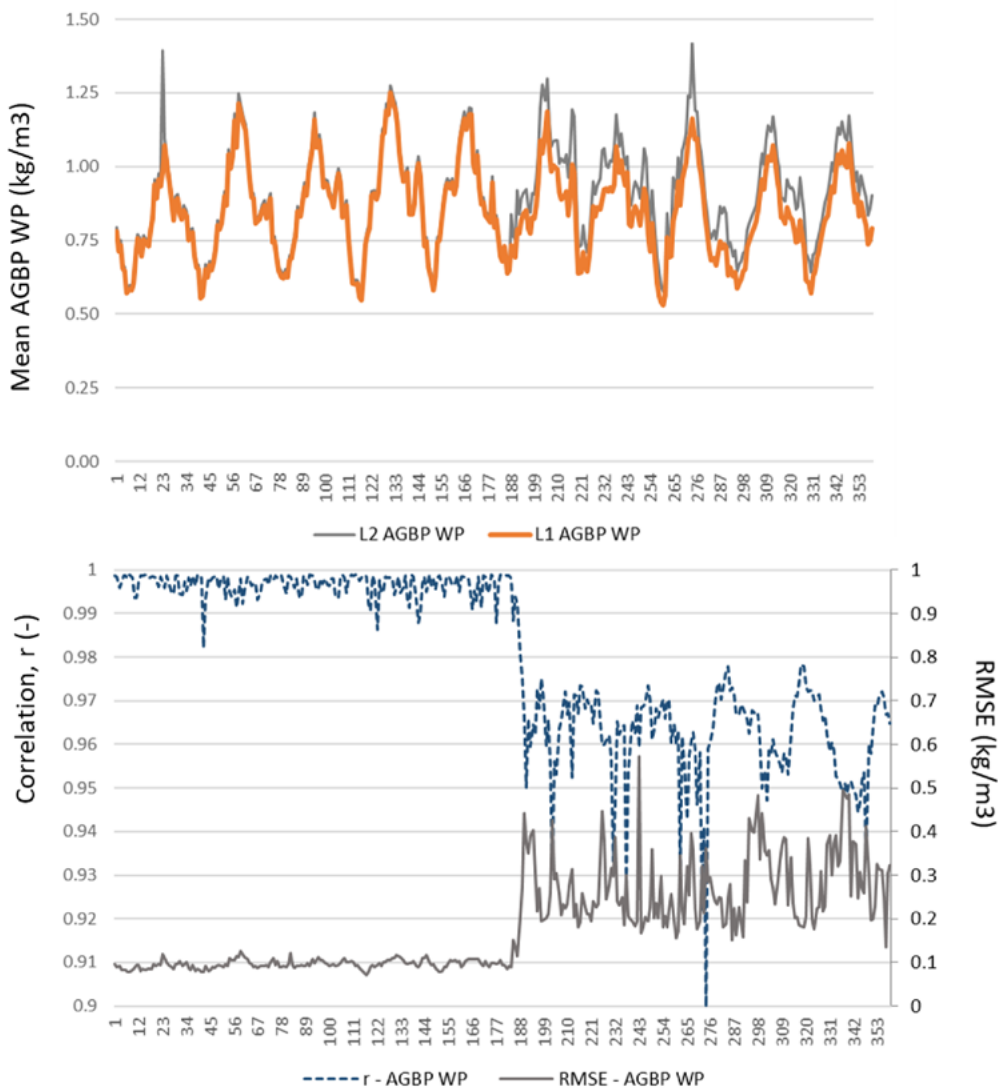
Figure 3-31. Level consistency between L1 and L2 AGBP WP.

3.6.2. Consistency between level-1 and level-3 resolutions

The agreement between the L1 and L3 ETI_a-WPR and the NPP-WPR products are shown in Figure 3-32 for each scheme (see Appendix E for detailed metrics). The L1 and L3 ETI_a-WPR and NPP products-WPR have a lower consistency as compared to the L1 and L2 products in the five irrigation areas. The Awash area has the highest consistency, for both ETI_a and NPP, of all L3 scheme areas, which is reflected in the highest correlation and R^2.

The RMSE between L1 and L3 in the Awash (AWA) ranges from 0.42-1.01 mm/day and 0.30-1.03 gC/m^2/day for ETI_a-WPR and NPP-WPR respectively. The correlation ranges from 0.63-0.92 and 0.54-0.92 for ETI_a-WPR and NPP-WPR respectively. The median correlation for all dekads in the study period is 0.84 (ETI_a-WPR) and 0.83 (NPP-WPR), and the median R^2 is 0.84 (ETI_a-WPR) and 0.7 (NPP-WPR). The RMSE is highest when the ETI_a-WPR and NPP-WPR is highest. The RMSE temporal trends are in line with the seasonal trend in the Awash and displays the two seasons associated with the intertropical convergence zone. The correlation is above 0.73 (ETI_a-WPR) and 0.7 (NPP-WPR) on 95% of dekads, and lowest on dekads when the mean ETI_a-WPR is highest.

The Koga has the lowest consistency of the schemes. Although the RMSE between L1 and L3 is lower, ranging from 0.26-0.71 mm/day and 0.07-1.52 gC/m^2/day for ETI_a-WPR and NPP-WPR respectively. The median correlation and R2 for 0.67 and 0.45 respectively for ETI_a-WPR and 0.69 and 0.48 for NPP. Zankalon ETI_a-WPR and NPP-WPR performed slightly better, with a median correlation of 0.71 and a median R2 of 0.51 for ETI_a-WPR and 0.67 and 0.44 for NPP. The RMSE is higher in Zankalon than in the Koga for ETI_a-WPR, but is lower for NPP-WPR. This reflects the higher ETI_a-WPR values found in the area. The ODN has the same RMSE (ETI_a-WPR RMSE = 0.64mm/day) as Zankalon and the highest range of RMSE (0.15-1.62mm/day). However, the RMSE for NPP-WPR is lowest in ODN. All schemes show similar per cent bias medians (9-12%). The only scheme that shows a systematic bias in ETI_a-WPR is ZAN, where the L1 shows consistently higher ETI_a-WPR values than L3. However, a systematic bias in NPP, with L1 being greater than L3, was present for three irrigation areas (Awash, Zankalon and Koga). The Bekaa Valley has low bias for both NPP and ETI_a-WPR, and performed similar to other schemes in terms of the RMSE, correlation and R^2.
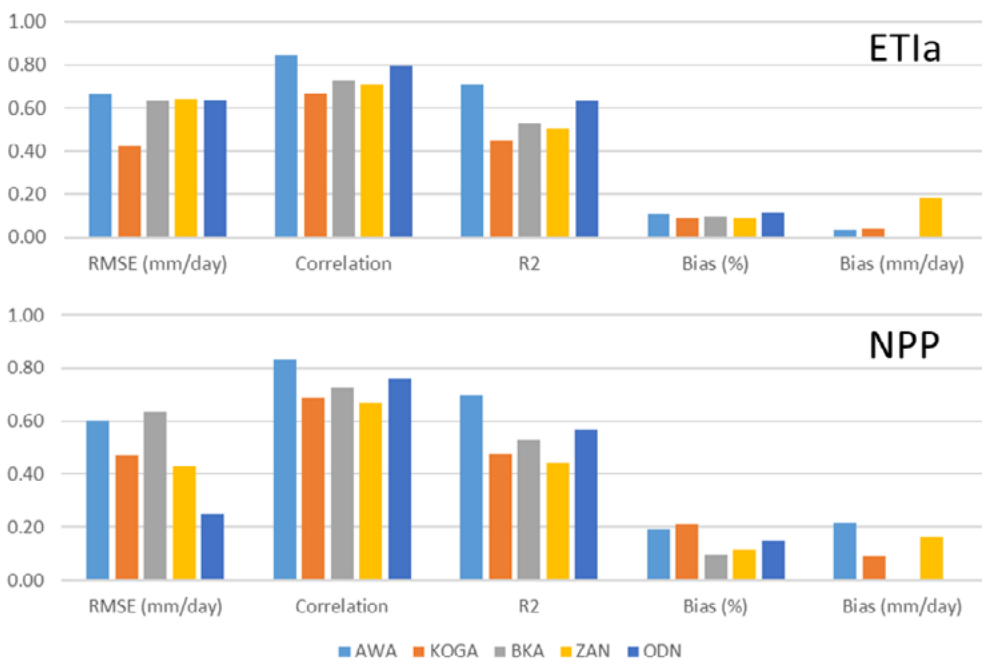
Figure 3-32. Level consistency of 250m, 100m and 30m ETI_a-WPR resolution against ETI_a-EC at EG-ZAN.

The three spatial resolutions were compared to the EC in the Zankalon irrigation scheme. The 10-daily average ET_a-EC and ETI_a-WPR for all three spatial resolutions at EG-ZAN are shown in Figure 3-33. The L1 and L2 ETI_a-WPR show high consistency with each other. The L3 ETI_a-WPR is consistently sitting between the ET_a-EC and the L1 and L2 ETI_a-WPR. All levels capture the overall ET_a-EC seasonal trends. The L3 data shows a slightly lower R^2 (L3=0.66 and L1=0.69) and correlation (L3=0.53 and L1=0.68), but a much lower bias (L3=1.06 mm/day and L1=1.68 mm/day) and a lower RMSE (L3=0.99 mm/day and L1=2.19 mm/day) when compared with

ET_a-EC. The better R^2 and correlation reflect the L1 and L2 ETI_a-WPR ability to capture the temporal fluctuations of ET_a-EC better than L3 ETI_a-WPR. An example of this is at dekad 1117 or 2011-17, where L1 and L2 ETI_a-WPR capture the ET_a-EC dip, whereas L3 ETI_a-WPR stays flat. The L3 ETI_a-WPR have a better seasonal agreement with the ET_a-lys for the summer maize crop in 2012 (L3=487mm, L1=682mm and ET_a-lys=543mm).
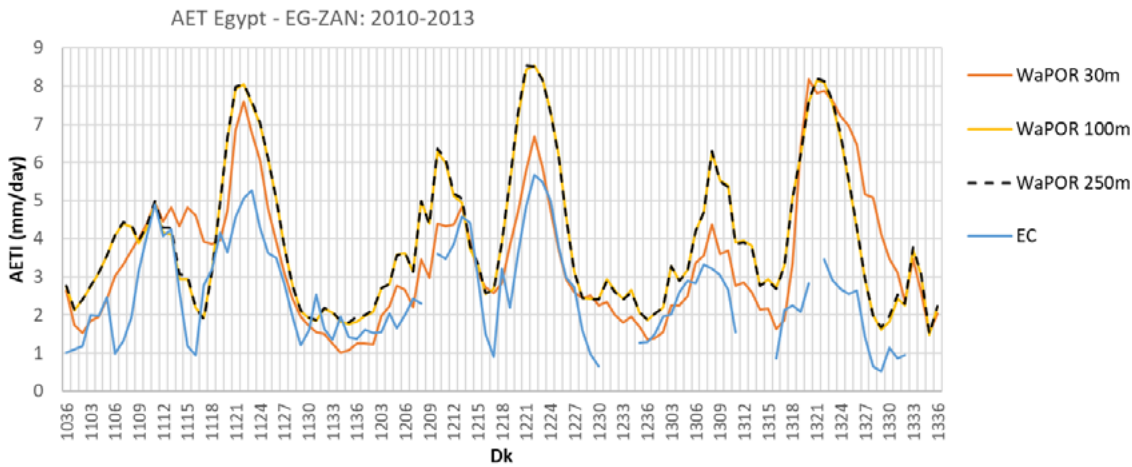
Figure 3-33. Level consistency of 250m, 100m and 30m ETI_a-WPR resolution against ETI_a-EC.

3.6.3. Resolution level consistency implications on water productivity

On an annual plot-by-plot basis the WP is very inconsistent between L1 and L3 for each location. The correlation between levels, on a plot-by-plot basis, is close to zero for all years between 2009-2018 (<0.30) for each of the Wonji, the ODN and the Koga. However, for a single plot over time the consistency was good. An example of this is shown in Figure 3-34 in the Wonji. For a single dekad (2nd dekad of Jan 2009), the mean L1 AGBP WP and L3 AGBP WP of each plot is compared. A poor agreement is found (no correlation). However, when the AGBP WP for a single plot is plotted over time for all dekads, a much better agreement is found (av. R = 0.62, with a r =0.81 at BOKU-11-A2).This suggests that on a plot-by-plot basis, the temporal consistency between levels is good, however, the spatial consistency is low.

The long-term crop water productivity and AGBP WP are shown for the Wonji, ODN and the Koga are shown in Figure 3-35. The Wonji has the largest average field size, followed by ODN and then the Koga (Table 1-4). The Wonji showed the largest consistency of the three schemes, both temporally and spatially. For all three schemes the L3 area captured the most spatial variability. However, all three levels captured the temporal variability well. While long term trends and annual means at scheme level show good consistency.

The selection and use of a WaPOR spatial resolution level (1,2,3) have implications for the interpretation of WP values. This is important for the use of the data. For example, the smaller Koga irrigation scheme, although shown with a plot overlay (shape file) is covered by a mere 6x6 250m L1 pixels, and scheme sector and field variability cannot be distinguished. One needs 100-m or even 30-m data to decipher real WP in the scheme. Due to the larger field sizes in the ODN and Wonji sugarcane estate schemes, this resolution effect is less visible, although always attention should be given when interpreting WP values for crops at a certain spatial resolution.
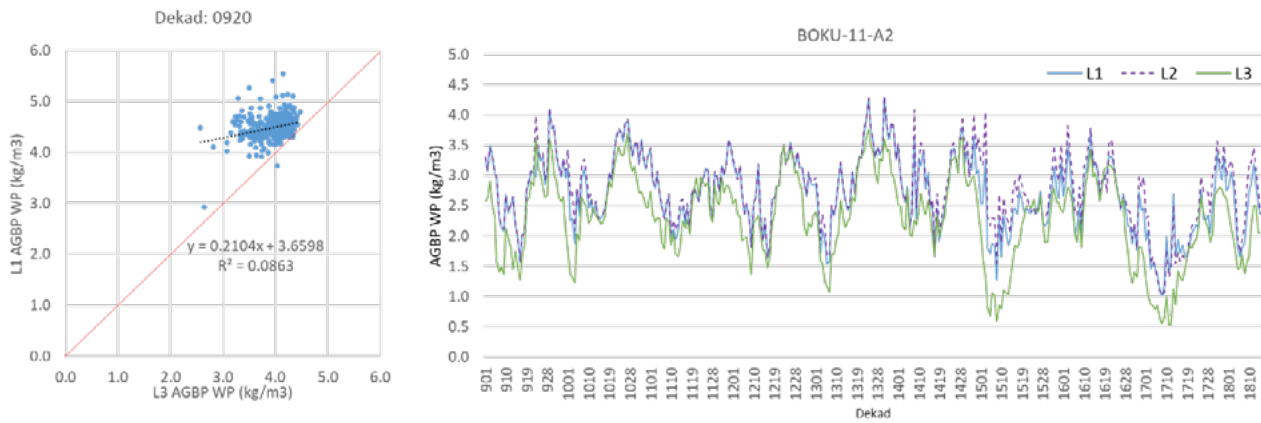
Figure 3-34. Plot average AGBP WP derived from L1 NPP-WPR plotted against plot average AGBP WP derived from L3 NPP-WPR for all plots (left) and mean dekadal L1 NPP-WPR, L2 NPP-WPR and L3 NPP-WPR timeseries for plot BOKU-11-A2.

Main findings of Chapter 3.6:

- Level consistency between L1 and L2 ETI_a and NPP is very high for all data components
- Level consistency between L1 and L3 ETI_a and NPP is decent, with highest consistency in Awash and ODN.
- Scheme level WP temporal and spatial consistency is good.
- Plot-by-plot dekadal WP consistency (plot temporal consistency) is good; however, plot-by-plot annual WP consistency (plot spatial consistency) is poor.
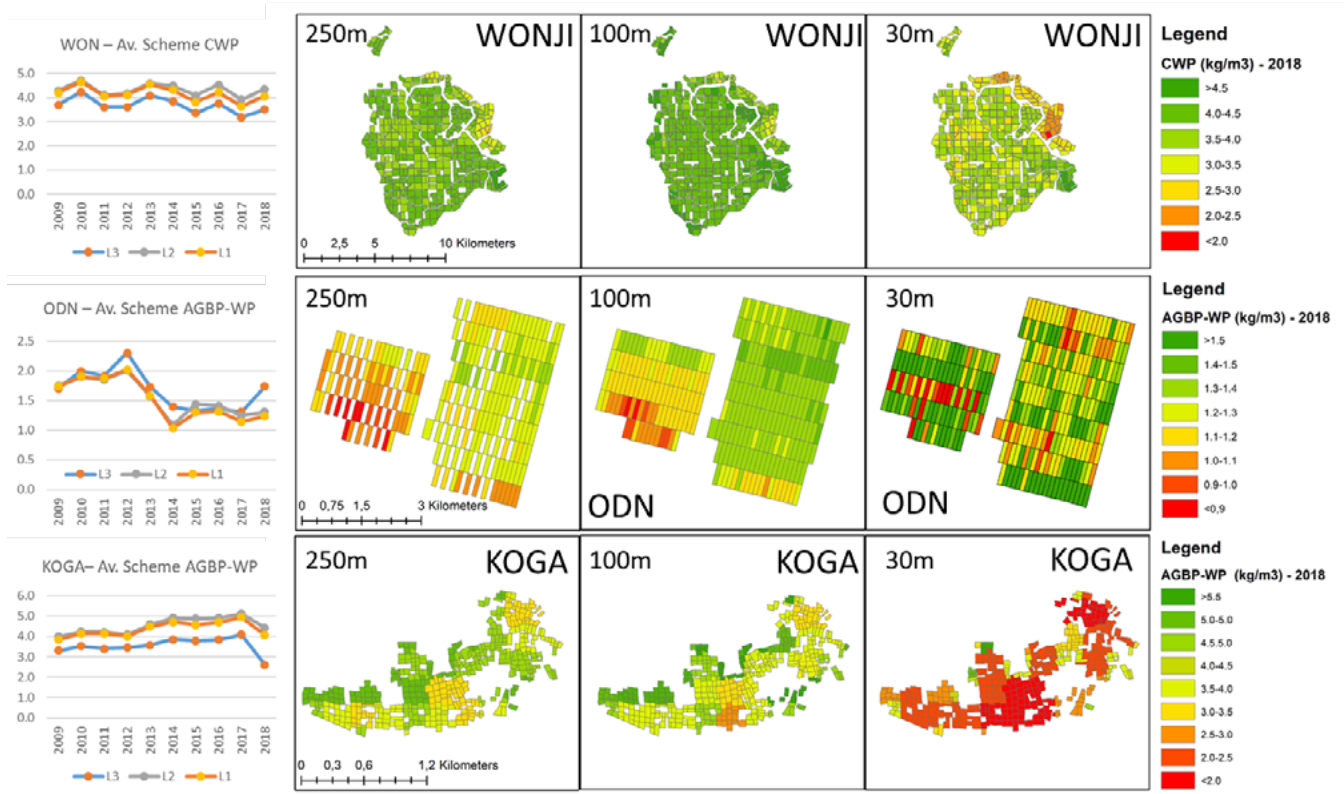
Figure 3-35. Annual average crop WP and AGBP WP plotted over time (left) and average long-term crop WP and AGBP WP (2009-2018) for irrigated fields for three spatial resolutions in the Wonji – WON (upper), ODN (Near) and the Koga (bottom).

Source: this study

3.7.   Comparison between WaPOR Version-1 and Version-2

Comparison of ETI_a-WPR V1 and V2 were made and aggregated per climate class, and for the 22 hydrological river basins. On a long-term (2009-2018 average annual), and large basin scale (Figure 3-36) the ETI_a-WPR has increased slightly from V.1.0 to V2 in 19 out of 22 basins. . The largest changes were in the Central West Coast and Congo River Basins with a 14% increase and 15% increase respectively. Other moderate changes (5-8% increases) were noted for 12 basins. The other 5 basins had increases of 0-5%. Three basins had a decrease of 6% from V1 to V2.
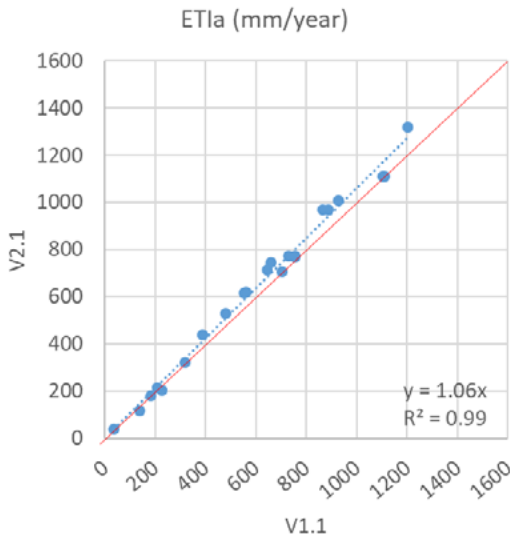
Figure 3-36. Annual ETI_a (mm/year) for the 22 major African river basins, compared for V1 and V2. The dotted line is the regression line and the red line is the 1:1 line.

When considering the version changes based on climate, there are some obvious trends and changes between WaPOR V1 and V.2.0. (Figure 3-37). The NPP-WPR, ETI_a-WPR and soil evaporation (T) have generally increased. For NPP-WPR and ETI_a-WPR, this is irrespective of climate, with the exception of the ETI_a–WPR component in the temperate climate zones in the northern hemisphere. These changes in ETI_a–WPR are primarily driven by changes in the soil evaporation (T) component. In the arid and tropical zones, the soil evaporation component has increased, while in the temperate zone it has increased in the southern hemisphere and decreased in the northern hemisphere. The plant transpiration component has changed the least. These changes are likely primarily a result of changes to the SMC algorithm. However, this does not explain the reduction to the evaporation in the temperate zone in the northern hemisphere. The evaporation component was the largest contribution to change in ETI_a-WPR in some climate zones, while transpiration was a larger contributing factor then others. The other source of changes in versions is the LCC. This will affect the transpiration and NPP components the most as look-up tables are used to assign number of parameters. For example in the transpiration algorithm the soil and canopy surface roughness and minimum stomatal resistance and in the NPP algorithm the maximum LUE is derived from landcover.

The ETI_a-WPR and NPP-WPR V2 are plotted against V1 in Figure 3-38 for the EC sites described in section 2.5. The consistency between both WaPOR versions is high at all stations. The largest changes occur at ZM-MON (R^2=0.79) and EG-ZAN (R^2=0.81). All other sites have a R^2 between versions >= 0.95. The lowest consistency between versions for NPP-WPR is SD-DEM (R^2=0.67), followed by ZM-MON (R^2=0.80). NPP-WPR V2 and V1 have an even higher agreement than ETI_a-WPR V2 and V1. The NPP-WPR V2 is greater than NPP-WPR V1 at all sites for all dekads. The overall R^2 is 0.97. The correlations ranged from 0.90 at ZM-MON up to 1.0 at GH-ANK, SN-DHR, SA-SKU and NE-WAM sites.
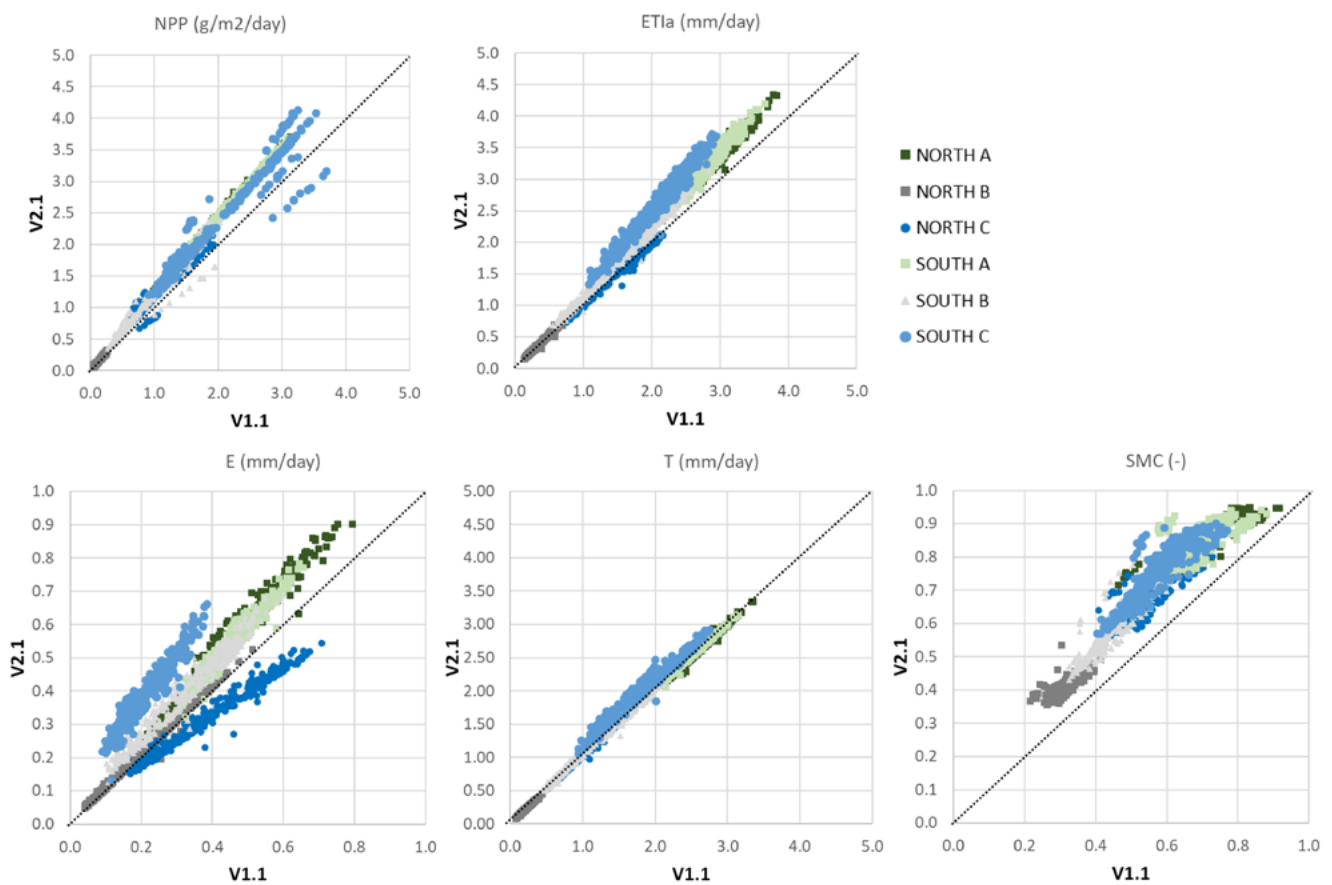
Figure 3-37. WaPOR V2 NPP, ETI_a, evaporation (E), transpiration (T) and SMC plotted against WaPOR V1 NPP, ETI_a, evaporation(E), transpiration (T) and SMC for major climate classes. NORTH is northern hemisphere, SOUTH is southern hemisphere, A is tropical, B is arid and C is temperate. Note that the evaporation and SMC graphs have a different X and Y-axis.
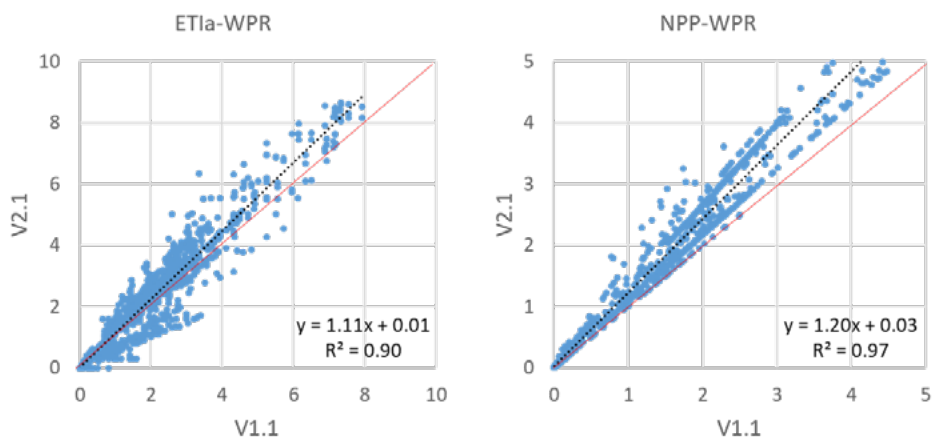
Figure 3-38. ETI_a-WPR (mm/day) V2 plotted against V1 and NPP-WPR (gC/m^2/day) V2 plotted against V1 (right) NPP-EC. The dotted line is the regression line and the red line is the 1:1 line.

Main findings of Chapter 3.7:

- The major difference between V1 and V2 was observed in the soil evaporation (E) component (significant increase in V.2.0) and slightly in NPP.

- Soil evaporation changes seem due to the behaviour of the relative SMC intermediate data component (under prolonged dry and hot weather & climate conditions)

- Changes have resulted in an overall increase in ETI_a and NPP across most climate zones

4.   Conclusions and recommendations

4.1.   Conclusions and findings

The FRAME project validation team earlier carried out the validation work and reported on the WaPOR beta-(2017) and version-1 (2018) data. Based on the quality control reports and information from data users and experts, improvements were continuously implemented by the product development team (eLEAF and VITO), leading to the current version-2, released mid-2019 by FAO. The ITC validation team performed the validation and verification of the current WaPOR version-2. This document reports on the findings of this v.2.0 validation.

In total, 11 data components (core data components: T, E, I, NPP, ABGP, WP, LCC and intermediate data components: RET, PCP, SMC, NDVI) were subjected to data quality control and validation (Table 1-1). Emphasis was laid upon the core data, representing evapotranspiration processes (E, T, I) and biomass growth processes (NPP, AGBP), constituting the building blocks of agricultural water productivity (WP).

Five different validation protocols mentioned (in section 1.3.1 and shown in Figure 2-1) were applied to the different data sets. This concerned the following methods:

- Rule- or model-based physical consistency evaluation (e.g., mass balance appraisal)
- Cross validation using inter-product comparison to reference data
- Internal validation of spatial and temporal consistency (e.g. of time series)
- Direct validation against measured *in-situ* data and observations
- Consistency of data components among the three spatial resolutions Levels

At the end of all the paragraphs of the validation results Chapter 3, detailed conclusions of the specific validation work is reported. These concern the individual data analysis and results on all five methods, described above. We refer the reader to these pages for details on the validation results. In Table 4.1, we summarized the main conclusions and findings of the validation of version-2.

We fully acknowledge that in most validation work, except e.g. entirely controlled laboratory experiments, the absolute "error-free" true value of estimates (e.g. plant transpiration, soil moisture and evaporation, and biomass productivity and other variables) is not known or achieved by any method.

For example, the appraisal of the water balance closure for the major African river basins holds uncertainties, especially in the large basin runoff and rainfall figures. The uncertainties around the energy and water balance of the large Congo basin, one of the core convection regions in the global tropics, next to the Amazon basin and the equatorial maritime region in SE-Asia and West-Pacific are high (Washington et al, 2013). The Congo basin latent heating from convection exceeds 120 $W.m^{-2}$ (Jury et al, 2009). This makes any evaluation of Africa-wide water balances awkward. In addition, the data sets used as spatial reference data (i.e. MODIS and MSG), although peer-reviewed, have internal data quality issues and uncertainties. In any cross-validation, errors and uncertainties from both data sets come into play and are confounded, as is also the case here. We can make a similar remark for the *in-situ* validation of the WaPOR remote-sensing derived ET and NPP estimates with ground truth Eddy Covariance flux tower data. EC measurements concern high time frequency measurements with sonic anemometers and in-situ gas analysers, with relatively low signal to noise ratios and subject to local meteorological conditions and phenomena. We can mention tower measurement footprint and energy balance closure issues, making use and interpretation of in-situ EC fluxes fairly complicated. They remain however one of the few ground-based counterparts of the geospatial WaPOR data.

We judged therefore that the confrontation of the WaPOR v.2 data with the numerous independent data sources and procedures, as done in this document can provide valuable information for further use and interpretation of the WaPOR data by end-users and agricultural water productivity evaluators.

Table 4-1. Summary of the findings and conclusions on the validation of the WaPOR V2 data components and spatial levels.

#	Dataset (Level)	Validation Method	Scale	Performance (a)	Key findings
1	ETI_a (L1)	Inter-product consistency - cross validation	basin (AF)	G	ETI_a-WPR is performing well at river basin level. However, the fraction of ETI_a/PCP appears to be on average too high and ETI_a-WPR is overestimating on average at basin scale compared to the physical water balance.
2	ETI_a (L1)	Inter-product consistency Cross validation	AF+ ME[(b)]	P-G	General overestimation of ETI_a-WPR compared to MOD16 irrespective of climate or land use. Higher overestimation in semiarid and arid climates. High correlations in grasslands, shrublands and croplands, despite large biases.
3	NPP (L1)	Inter-product consistency Cross validation	AF+ME	G	General overestimation of NPP-WPR compared to MOD17 in arid and tropical climate classes, however bias is less than ETI_a-WPR. High correlations in grasslands, shrublands and croplands.
4	WP (L1)	Inter-product consistency Cross validation	AF+ME	G	Water use efficiency (NPP/ETI_a ratio) is similar between WaPOR and MODIS products. The linear relationship between NPP and ETI_a is most evident for grasslands, shrublands and croplands.
5	Multiple[(c)] (L1)	Internal consistency & validation	AF+ME	G	ETI_a-WPR is showing good spatial and temporal consistency between T, E and NPP-WPR. Linear trend between NPP-WPR and T is consistent. SMC appears overestimated in arid zones, driving overestimation of evaporation.
6	ETI_a (L1)	Product accuracy Direct validation In-situ	point	P-VG	ETI_a-WPR shows mixed results at point scale as compared to EC flux towers. At some sites the performance is very good. The performance appears to be highest when the NDVI and LST quality layer show high quality, when the site is water limited rather than energy limited and when consistency between the NPP-WPR and ETI_a-WPR data is high. ETI_a-WPR is overestimating ETI_a and in irrigation areas in the Nile Delta.
7	NPP (L1)	Product accuracy In-situ	point	P-VG	NPP-WPR has mixed results at point scale as compared to EC flux towers. NPP is overestimated compared to flux measurements at some locations. At some sites the performance is very good. The performance appears to be highest when the NDVI and LST quality layers show high quality.
8	NPP (L3)	Product accuracy In-situ	plot - Awash	VG	The reported sugarcane AGBP agreed well with WaPOR derived yields in the Wonji. The agreement was less in the Metehara, but the correlation was still strong. The NPP:T ratio from WaPOR is good in the expected range for C4 crop.
9	NPP (L3)	Product accuracy In-situ	plot -Bekaa	P	WaPOR did not capture spatial variation of potato and wheat fields (Bekaa). The NPP:T ratio is OK for both crops and is in the expected range for C3 crops.

10	RET (L1)	Product accuracy In-situ	point	P-VG	RET-WPR performance varied between sites. Typically overestimated, but captured seasonality well with high correlations between WaPOR and in-situ estimates. RET-WPR performs less in dense and tall vegetation
11	ETI_a, NPP, WP (L1, L3)	Product level consistency	scheme	P-G	Varied between schemes for ETI_a-WPR and NPP-WPR. Highest consistency at Awash. Highest bias in Zankalon.
12	ETI_a, NPP, WP (L1, L2)	Product level consistency	basin	VG	Very high consistency between L1 and L2 product for NPP-WPR and ETI_a-WPR in the full L2 extent.

(a) Performance Indicator: VG – Very Good; G – Good; P – Poor; VP – Very Poor. No average class is included (considered non-informative);

(b) AF-Africa; ME-Near East;

(c) ETI_a, NPP, SMC, SR, NDVI, T, E

4.2.   Recommendations

Hereafter, we give a brief summary of data issues, encountered during the validation analysis. FAO and the WaPOR product development team may judge to further take-up the following data issues, which can possibly still improve the WaPOR database quality.

In dry and warm semiarid climatic zones, such as the Sahel region (Western Africa), where very high land surface and air temperatures (> 30-40 °C) are observed during prolonged periods of the year, the surface energy balance ET and satellite LST retrieval approach may become problematic. We recommend to verify the ETI_a-WPR data production and behaviour of the source data i.e. the GEOS-5 model meteorological near surface data, and the satellite data e.g. MODIS-LST in these cases. This issue is most probably the reason that ET estimates in the semiarid Sahel region, during the prolonged dry season, are much higher (> 1 mm/day) than observed values (~0.1 mm/day) from flux towers and field data. This sub-regional data flaw results in higher annual and regional (i.e. river basin) ETI_a-WPR totals, when compared to water mass balance checks of river basins located in drier regions. Appendix E further illustrates this through a comparison of the EC flux tower observations for the NE-WAM site (13 degree North, Niger, Sahel region) with ETI_a-WaPOR data for that location.

The autotrophic plant respiration fraction used to generate NPP from GPP used currently by WaPOR is a single value for all Land cover classes (LCC). At this stage, we also judge this is the best possible choice for a single value (as shown in this report). We recommend however investigating this parameter further, and eventually making plant maintenance and growth respiration dependent from LCC (as done in many GPP-NPP models).

We also recommend to verify the behaviour of the relative SMC intermediate data component (soil moisture content index). The SMC relative moisture index is currently derived using a method based on land surface temperature and vegetation cover (NDVI) data. A verification to more physically based satellite soil moisture observations (e.g. passive a/o active microwave sensors on-board Sentinel-1A, METOP, SMAP, SMOS, etc.) can be advised. WaPOR currently also uses a single SMS or soil moisture stress function for all LCC. This function might be made LCC specific in the future.

Comparison to independent data and information, as pursued throughout this report, lies at the heart of validation. The availability of *in-situ* validation data sources in Africa and the Near East remains a problematic issue when doing validation work in these regions, although increasing data gathering efforts are made in the last decades. We are convinced that independent control of data quality by peers remains an essential part of any geospatial database development, and can lead to improving data quality, and thereby increase data usability and end-user satisfaction.

References

Allen, R.G., Pereira, L.S., Howell, T.A., Jensen, M.E. 2011. Evapotranspiration information reporting: I. Factors governing measurement accuracy. *Agricultural Water Management*. 98, 899–920. https://doi.org/10.1016/j.agwat.2010.12.015

Allen, R.G., Pereira, L.S., Raes, D., Smith, M. 1998. FAO Irrigation and Drainage Paper No. 56: *Crop Evapotranspiration*. Food and Agriculture Organization of the United Nations (FAO), Rome, Italy.

Ardö, J., Mölder, M., El-Tahir, B.A., Elkhidir, H.A.M. 2008. Seasonal variation of carbon fluxes in a sparse savanna in semi arid Sudan. *Carbon Balance Management*. 3, 1–18. https://doi.org/10.1186/1750-0680-3-7

Atta, Y., Gaafar, I., Hassan, W., El, A. 2015. *Validation of Accurate Determination of Maize Water Requirements in Nile Delta*, in: International Commission on Irrigation and Drainage 26th Euro-Mediterranean Regional Conference and Workshops, Innovate to Improve Irrigation Performances. Montpellier, p. 4.

Baldocchi, D.D. 2003. Assessing the eddy covariance technique for evaluating carbon dioxide exchange rates of ecosystemes: past, present and future. *Global Change Biology*. 9, 479–492. https://doi.org/10.1046/j.1365-2486.2003.00629.x

Bastiaanssen, W.G.M., Cheema, M.J.M., Immerzeel, W.W., Miltenburg, I.J., Pelgrum, H. 2012. Surface energy balance and actual evapotranspiration of the transboundary Indus Basin estimated from satellite measurements and the ETLook model. *Water Resources Research*. https://doi.org/10.1029/2011WR010482

Beck, H.E., de Roo, A., van Dijk, A.I.J.M. 2015. Global Maps of Streamflow Characteristics Based on Observations from Several Thousand Catchments*. *Journal of Hydrometeorology*. 16. https://doi.org/10.1175/jhm-d-14-0155.1

Blatchford, M.L., Karimi, P., Bastiaanssen, W.G.M., Nouri, H. 2018. From Global Goals to Local Gains — A Framework for Crop Water Productivity. *ISPRS International Journal of Geo-Information*. 7. https://doi.org/10.3390/ijgi7110414

Blatchford, M.L., Mannaerts, C.M., Zeng, Y., Nouri, H. and Karimi, P. 2019. Status of accuracy in remotely sensed and in-situ agricultural water productivity estimates: A review. *Remote Sensing of Environment*. 234 (2019) 111413. https://doi.org/10.1016/j.rse.2019.111413

Boulain, N., Cappelaere, B., Séguis, L., Favreau, G., Gignoux, J. 2009. Water balance and vegetation change in the Sahel: A case study at the watershed scale with an eco-hydrological model. *Journal of Arid Environments*. 73, 1125–1135. https://doi.org/10.1016/j.jaridenv.2009.05.008

Budyko, M.I. 1974. *Climate and life*. Volume 18. ed. Academic Press.

Budyko, M.I. 1958. *The Heat Balance of the Earth's Surface*. 5417, 255. https://doi.org/10.1080/00385417.1961.10770761

Chishugi, J.B., Alemaw, B.F. 2009. The Hydrology of the Congo River Basin: A GIS-Based Hydrological Water Balance Model. *World Environmental and Water Resources Congress*. 1–16.

Chiti, T., Certini, G., Grieco, E., Valentini, R. 2010. The role of soil in storing carbon in tropical rainforests: The case of Ankasa Park, Ghana. *Plant and Soil*. 331, 453–461. https://doi.org/https://doi.org/10.1007/s11104-009-0265-x

De Bruin, H., Trigo, I., Bosveld, F., & Meirink, J. 2016. Thermodynamically based model for actual evapotranspiration of an extensive grass field close to FAO reference, suitable for remote sensing application. *Journal of Hydrometeorology*. 17 (5): 1373–1382. https://doi.org/10.1175/JHM-D-15-0006.1

De Bruin, H. A. R., & Trigo, I.F. 2019. A new method to estimate reference crop evapotranspiration from geostationary satellite imagery: Practical considerations. *Water*. 11 (2): 382. https://doi.org/10.3390/w11020382

Dembélé, M., Zwart, S.J. 2016. Evaluation and comparison of satellite-based rainfall products in Burkina Faso, West Africa. *International Journal of Remote Sensing*. 37, 3995–4014. https://doi.org/10.1080/01431161.2016.1207258

Dinku, T., Funk, C., Peterson, P., Maidment, R., Tadesse, T., Gadain, H., Ceccato, P. 2018. Validation of the CHIRPS satellite rainfall estimates over eastern Africa. *Quarterly Journal of the Royal Meteorological Society.* 144, 292–312. https://doi.org/10.1002/qj.3244

Duchemin, B., Hadria, R., Erraki, S., Boulet, G., Maisongrande, P., Chehbouni, A., Escadafal, R., Ezzahar, J., Hoedjes, J.C.B., Kharrou, M.H., Khabba, S., Mougenot, B., Olioso, A., Rodriguez, J.C., Simonneaux, V. 2006. Monitoring wheat phenology and irrigation in Central Morocco: On the use of relationships between evapotranspiration, crops coefficients, leaf area index and remotely-sensed vegetation indices. *Agricultural Water Management.* 79, 1–27. https://doi.org/10.1016/j.agwat.2005.02.013

FAO. 2020a. *WaPOR, FAO's portal to monitor Water Productivity through Open access of Remotely sensed derived data.* Food and Agriculture Organization of the United Nations. https://wapor.apps.fao.org/. Database accessed on [2019/11/30].

FAO. 2020b. *WaPOR Database methodology, V2 release.* Food and Agriculture Organization of the United Nations, Rome.

FAO. 2019. *WaPOR quality assessmentWaPOR quality assessmentTechnical report on the data quality of the WaPOR FAO database version 1.0*, Food and Agriculture Organization of the United Nations, Rome, 2019.

FAO. 2018a. *WaPOR Database Methodology: Level 1.* Remote Sensing for Water Productivity Technical Report: Methodology Series. FAO, Licence: CC BY-NC-SA 3.0 IGO, Rome, Italy.

FAO. 2018b. *Using Remote Sensing in support of solutions to reduce Agricultural water productivity gaps, Database methodology: Level 2 data WaPOR Version 1.* FAO, Rome.

FAO. 2018c. *Using Remote Sensing in support of solutions to reduce Agricultural water productivity gaps, Database methodology: Level 3 data WaPOR Version 1.* FAO, Rome.

FAO. 1997. *Irrigation potential in Africa: A basin approach.* FAO, Rome.

Fu, B. 1981. On the calculation of the evaporation from land surface. *Chinese Journal of Atmospheric Sciences.* 1, 23–31.

Funk, C., Peterson, P., Landsfeld, M., Pedreros, D., Verdin, J., Shukla, S., Husak, G., Rowland, J., Harrison, L., Hoell, A., Michaelsen, J. 2015. The climate hazards infrared precipitation with stations—a new environmental record for monitoring extremes. *Scientific Data.* 2, 150066. https://doi.org/10.1038/sdata.2015.66

Gebrechorkos, S.H., Hülsmann, S., Bernhofer, C. 2018. Evaluation of multiple climate data sources for managing environmental resources in East Africa. *Hydrology and Earth System Sciences.* 22, 4547–4564. https://doi.org/10.5194/hess-22-4547-2018

Geng, L., Ma, M., Yu, W., Wang, X., Jia, S. 2015. *Validation of the MODIS NDVI Products in Different Land-Use Types Using In Situ Measurements in the Heihe River Basin.* https://doi.org/10.1109/LGRS.2014.2314134

Glenn, E.P., Doody, T.M., Guerschman, J.P., Huete, A.R., King, E.A., Mcvicar, T.R., Van Dijk, A.I.J.M., Van Niel, T.G., Yebra, M., Zhang, Y. 2011. Actual evapotranspiration estimation by ground and remote sensing methods: the Australian experience. *Hydrological Processes.* 25, 4103–4116. https://doi.org/10.1002/hyp.8391

Guan, S., Fukami, K., Matsunaka, H., Okami, M., Tanaka, R. 2019. *Assessing Correlation of High-Resolution NDVI with Fertilizer Application Level and Yield of Rice and Wheat Crops using Small UAVs.* https://doi.org/10.3390/rs11020112

Hills, R.C. 1978. The Structure of the Inter-Tropical Convergence Zone in Equatorial Africa and Its Relationship to East African Rainfall. *Transactions of the Institute of British Geographers.* 4, 329–352. https://doi.org/ https://www.jstor.org/stable/622055

Hobbins, M.T., Ramírez, J.A., Brown, T.C. 2001. The complementary relationship in regional evapotranspiration: the CRAE model and the Advection-Aridity approach. *Water Resources Research.* 37, 1389–1403. https://doi.org/10.1029/2000WR900359

Jaafar, H., King-okumu, C. 2016. *Water resources within the Upper Orontes and Litani Basins.*

Jaafar, H.H., Ahmad, F.A. 2019. Time series trends of Landsat-based ET using automated calibration in MET-RIC and SEBAL: The Bekaa Valley, Lebanon. *Remote Sensing of Environment.* 0–1. https://doi.org/10.1016/j.rse.2018.12.033

Jury MR, Matari E, Matitu M. 2009. Equatorial African climate teleconnections. *Theoretical and Applied Climatology.* 95, 407-416. doi:10.1007/s00704-008-0018-4

Kooman, P.L., Rabbinge, R. 1996. An Analysis of the Relation between Dry Matter Allocation to the Tuber and Earliness of a Potato Crop. *Annals of Botany.* 77, 235–242. https://doi.org/10.1006/anbo.1996.0027

Kottek, M., Grieser, J., Beck, C., Rudolf, B., Rubel, F. 2006. World map of the Köppen-Geiger climate classification updated. *Meteorologische Zeitschrift.* 15, 259–263. https://doi.org/10.1127/0941-2948/2006/0130

LBPTC. 2010. *Joint Limpopo River Basin Study Scoping Phase: Final Report.* Limpopo Basin Permanent Technical Committee (LBPTC).

Limpopo Basin Permanent Technical Committee (**LBPTC**), **Lehner, B., Grill, G.** 2013. Global river hydrography and network routing: baseline data and new approaches to study the world's large river systems. *Hydrological Processes.* 27, 2171–2186. https://doi.org/https://doi.org/10.1002/hyp.9740

Li, K.Y., Coe, M.T., Ramankutty, N. 2005. Investigation of hydrological variability in West Africa using land surface models. *Journal of Climate.* 18, 3173–3188. https://doi.org/10.1175/JCLI3452.1

Liu, W., Wang, L., Zhou, J., Li, Y., Sun, F., Fu, G., Li, X., Sang, Y.F. 2016. A worldwide evaluation of basin-scale evapotranspiration estimates against the water balance method. *Journal of Hydrology.* 538, 82–95. https://doi.org/10.1016/j.jhydrol.2016.04.006

Lobell, D.B., Hicke, J.A., Asner, G.P., Field, C.B., Tucker, C.J., Los, S.O. 2002. Satellite estimates of productivity and light use efficiency in United States agriculture, 1982-98. *Global Change Biology.* 8, 722–735. https://doi.org/10.1046/j.1365-2486.2002.00503.x

Madugundu, R., Al-Gaadi, K.A., Kayad, A.G., Tola, E., Jha, C.S. 2017. Estimation of gross primary production of irrigated maize using Landsat-8 imagery and Eddy Covariance data. *Saudi Journal of Biological Sciences.* 24, 410–420. https://doi.org/10.1016/j.sjbs.2016.10.003

Majozi, N.P., Mannaerts, C.M., Ramoelo, A., Mathieu, R., Nickless, A., Verhoef, W. 2017. Analysing surface energy balance closure and partitioning over a semi-arid savanna FLUXNET site in Skukuza, Kruger National Park, South Africa. H*ydrology and Earth Systems Sciences.* 21, 3401–3415. https://doi.org/https://doi.org/10.5194/hess-21-3401-2017

Mamadou, O., Cohard, J.M., Galle, S., Awanou, C.N., Diedhiou, A., Kounouhewa, B., Peugeot, C. 2014. Energy fluxes and surface characteristics over a cultivated area in Benin: Daily and seasonal dynamics. *Hydrology and Earth Systems Sciences.* 18, 893–914. https://doi.org/https://doi.org/10.5194/hess-18-893-2014

Mannaerts, C.M., Blatchford, M.L. 2017. *FRAME ß version Data Validation Report.* Enschede.

Matondo, J.I., Mortensen, P. 1998. Water resource assessment for the Zambezi River Basin. *Water International.* 23, 256–262. https://doi.org/https://doi.org/10.1080/02508069808686780

McDonald, J.E. 1961. On the Ratio of Evaporation to Precipitation. *Bulletin of the American Meteorological Society.* 42, 185–189. https://doi.org/10.1175/1520-0477-42.3.185

Merbold, L., Ardö, J., Arneth, A., Scholes, R.J., Nouvellon, Y., Grandcourt, A., De Archibald, S., Bonnefond, J.M., Boulain, N., Brueggemann, N., Bruemmer, C., Cappelaere, B., Ceschia, E., El-Khidir, H.A.M., El-Tahir, B.A., Falk, U., Lloyd, J., Kergo, W. 2009. Precipitation as driver of carbon fluxes in 11 African ecosystems. *Biogeosciences.* 6, 1027–1041. https://doi.org/https://doi.org/10.5194/bg-6-1027-2009

Mu, Q., Heinsch, F.A., Zhao, M., Running, S.W. 2007. Development of a global evapotranspiration algorithm based on MODIS and global meteorology data. *Remote Sensing of Environment.* 106, 285–304. https://doi.org/10.1016/j.rse.2006.07.007

Mu, Q., Zhao, M., Running, S.W. 2013. *Algorithm Theoretical Basis Document: MODIS Global Terrestrial Evapotranspiration (ET) Product (NASA MOD16A2/A3) Collection 5.* NASA Headquarters.

Mu, Q., Zhao, M., Running, S.W. 2011. Improvements to a MODIS global terrestrial evapotranspiration algorithm. *Remote Sensing of Environment*. 115, 1781–1800. https://doi.org/10.1016/j.rse.2011.02.019

Muthoni, F.K., Odongo, V.O., Ochieng, J., Mugalavai, E.M., Mourice, S.K., Hoesche-Zeledon, I., Mwila, M., Bekunda, M. 2019. Long-term spatial-temporal trends and variability of rainfall over Eastern and Southern Africa. *Theoretical and Applied Climatology*. 137, 1869–1882. https://doi.org/10.1007/s00704-018-2712-1

Odongo, V.O., Van der Tol, C., Becht, R., Hoedjes, J.C.B., Ghimire, C.P., Su, Z. 2016. Energy partitioning and its controls over a heterogeneous semi-arid shrubland ecosystem in the Lake Naivasha Basin, Kenya. *Ecohydrology*. 9, 1358–1375. https://doi.org/https://doi.org/10.1002/eco.1732

Odongo, V.O., Van der Tol, C., Van Oel, P.R., Meins, F.M., Becht, R., Onyando, J., Su, Z. 2015. Characterisation of hydroclimatological trends and variability in the Lake Naivasha basin, Kenya. *Hydrological Processes*. 29, 3276–3293. https://doi.org/10.1002/hyp.10443

Pelgrum, H., Miltenburg, I.J., Cheema, M.J.M., Klaasse, A., Bastiaanssen, W.G.M. 2012. ET Look: A novel continental evapotranspiration algorithm. *International Association of Hydrological Sciences Publications*. 352, 120–123.

Pieroux D., Debal F., Gellens-Meulenberghs F., Quinet A. 2001. *Estimation of evapotranspiration all over Europe using MSG remote sensing.* Proceedings of The 2001 EUMETSAT Meteorological Satellite Data Users'Conference (Antalya, October 2001), pp 121-128.

Ramier, D., Boulain, N., Cappelaere, B., Timouk, F., Rabanit, M., Lloyd, C.R., Boubkraoui, S., Métayer, F., Descroix, L., Wawrzyniak, V. 2009. Towards an understanding of coupled physical and biological processes in the cultivated Sahel - 1. Energy and water. *Journal of Hydrology*. 375, 204–216. https://doi.org/https://doi.org/10.1016/j.jhydrol.2008.11.045

Rienecker, M.M., Suarez, M.J., Gelaro, R., Todling, R., Bacmeister, J., Liu, E., Bosilovich, M.G., Schubert, S.D., Takacs, L., Kim, G.K., Bloom, S., Chen, J., Collins, D., Conaty, A., Da Silva, A., Gu, W., Joiner, J., Koster, R.D., Lucchesi, R., Molod, A., Owens, T., Pawson, S., Pegion, P., Redder, C.R., Reichle, R., Robertson, F.R., Ruddick, A.G., Sienkiewicz, M., Woollen, J. 2011. MERRA: NASA's modern-era retrospective analysis for research and applications. *Journal of Climatology*. 24, 3624–3648. https://doi.org/https://doi.org/10.1175/JCLI-D-11-00015.1

Rodell, M., Famiglietti, J.S., Wiese, D.N., Reager, J.T., Beaudoing, H.K., Landerer, F.W., Lo, M.H. 2018. Emerging trends in global freshwater availability. *Nature*. 557, 651–659. https://doi.org/https://doi.org/10.1038/s41586-018-0123-1

Rubel, F., Kottek, M. 2010. Observed and projected climate shifts 1901-2100 depicted by world maps of the Köppen-Geiger climate classification. *Meteorologische Zeitschrift*. 19, 135–141. https://doi.org/10.1127/0941-2948/2010/0430

Running, S., Mu, Q., Zhao, M. 2017. MOD16A2 MODIS/Terra Net Evapotranspiration 8-Day L4 Global 500m SIN Grid V006 [Data set]. https://doi.org/https://doi.org/10.5067/MODIS/MOD16A3.006

Sebhat, M.Y., Wenninger, J. 2014. Water balance of the Juba and Shabelle Rivers basins the Horn of Africa. *International Journal of Agricultural Policy and Research*. 2, 238–255.

Sjöström, M., Zhao, M., Archibald, S., Arneth, A., Cappelaere, B., Falk, U., de Grandcourt, A., Hanan, N., Kergoat, L., Kutsch, W., Merbold, L., Mougin, E., Nickless, A., Nouvellon, Y., Scholes, R.J., Veenendaal, E.M., Ardö, J. 2013. Evaluation of MODIS gross primary productivity for Africa using eddy covariance data. *Remote Sensing of Environment*. 131, 275–286. https://doi.org/10.1016/j.rse.2012.12.023

Steduto, P., Hsiao, T.C., Fereres, E., Raes, D. 2012. Crop yield response to water, Fao Irrigation and Drainage Paper Issn.

Sugita, M., Matsuno, A., El-Kilani, R.M.M., Abdel-Fattah, A., Mahmoud, M.A. 2017. Crop evapotranspiration in the Nile Delta under different irrigation methods. *Hydrological Sciences Journal*. 62, 1618–1635. https://doi.org/10.1080/02626667.2017.1341631

Tagesson, T., Fensholt, R., Guiro, I., Rasmussen, M.O., Huber, S., Mbow, C., Garcia, M., Horion, S., Sandholt, I., Holm-Rasmussen, B., Göttsche, F.M., Ridler, M.E., Olén, N., Lundegard Olsen, J., Ehammer, A., Madsen, M., Olesen, F.S., Ardö, J. 2015. Ecosystem properties of semiarid savanna grassland in West Africa and its relationship with environmental variability. *Global Change Biology*. 21, 250–264. https://doi.org/https://doi.org/10.1111/gcb.12734

The Nile Basin Initiative Secretariat. 2014. *Understanding Nile Basin Hydrology Mapping Actual Evapotranspiration over the Nile Basin.* Nile Waters Technical Bulletin from The Nile Basin Initiative Secretariat. Entebbe.

Trigo I. F., De Bruin H., Beyrich F., Bosveld F. C., Gavilán P., Groh J., & López-Urrea R. 2018. Validation of reference evapotranspiration from Meteosat Second Generation (MSG) observations. *Agricultural and Forest Meteorology.* 259 (15 September 2018): 271–285. https://doi.org/10.1016/j.agrformet.2018.05.008

Turner, D.P., Ritts, W.D., Cohen, W.B., Gower, S.T., Running, S.W., Zhao, M., Costa, M.H., Kirschbaum, A.A., Ham, J.M., Saleska, S.R., Ahl, D.E. 2006. Evaluation of MODIS NPP and GPP products across multiple biomes. *Remote Sensing of Environment*. 102, 282–292. https://doi.org/10.1016/j.rse.2006.02.017

USAID. 2016. Southern Africa Drought - Fact Sheet #4 - Fiscal Year (FY) 2016. https://doi.org/https://www.usaid.gov/sites/default/files/documents/1866/southern_africa_dr_fs02_05-06-2016.pdf

Voisin, N., Wood, A.W., Lettenmaier, D.P. 2008. Evaluation of Precipitation Products for Global Hydrological Prediction. *Journal Hydrometeorology.* 9, 388–407. https://doi.org/10.1175/2007JHM938.1

Wang, D., Alimohammadi, N. 2012. Responses of annual runoff, evaporation, and storage change to climate variability at the watershed scale. *Water Resources Research.* 48. https://doi.org/https://doi.org/10.1029/2011WR011444

Washington, R., James, R., Pearce, H., Pokam, W. and Moufouna-Okia W. 2013. Congo basin rainfall climatology: can we believe climate models? *Philosophical Transactions of the Royal Society B: Biological Sciences*. 368: 20120296.

Weerasinghe, I., Van Griensven, A., Bastiaanssen, W., Mul, M., Jia, L. 2019. Can we trust remote sensing ET products over Africa? *Hydrology and Earth System Sciences.* Discuss. 1–27. https://doi.org/10.5194/hess-2019-233

Zhang, L., Hickel, K., Dawes, W.R., Chiew, F.H.S., Western, A.W., Briggs, P.R. 2004. A rational function approach for estimating mean annual evapotranspiration. *Water Resources Research.* 40, W025021–W02502114. https://doi.org/10.1029/2003WR002710

Zhang, L., Potter, N., Hickel, K., Zhang, Y., Shao, Q. 2008. Water balance modeling over variable time scales based on the Budyko framework - Model development and testing. *Journal of Hydrology.* 360, 117–131. https://doi.org/10.1016/j.jhydrol.2008.07.021

Zhang, Y., Leuning, R., Chiew, F.H.S., Wang, E., Zhang, L., Liu, C., Sun, F., Peel, M.C., Shen, Y., Jung, M. 2012. Decadal Trends in Evaporation from Global Energy and Water Balances. *Journal of Hydrometeorology.* 13, 379–391. https://doi.org/https://doi.org/10.1175/JHM-D-11-012.1

Appendixes

Appendix A. Metrics used in validation

Metric	Equation	Unit
Bias	$Bias = \dfrac{\Sigma\,(\,y_i + x_i\,)}{n}$	Same as input
RMSE	$RMSE = \sqrt{\dfrac{1}{n}\,\Sigma\,(\,y_i + x_i\,)^2}$	Same as input
r	$COR = \dfrac{n\,(\,\Sigma xy\,)\,-\,(\,\Sigma x\,)\,(\,\Sigma y\,)}{\sqrt{[\,n\,\Sigma x^2 - (\,\Sigma x\,)^2\,][\,n\,\Sigma y^2 - (\,\Sigma y\,)^2\,]}}$	(-)
NRMSE	$NRMSE = \dfrac{RMSE}{\bar{x}}$	Fraction
MAE	$MAE = \dfrac{\Sigma ABS\,(\,x_i + y_i\,)}{n}$	Same as input
R²	$R^2 = \dfrac{S_{xy}}{n\,S_x\,S_y}$	(-)
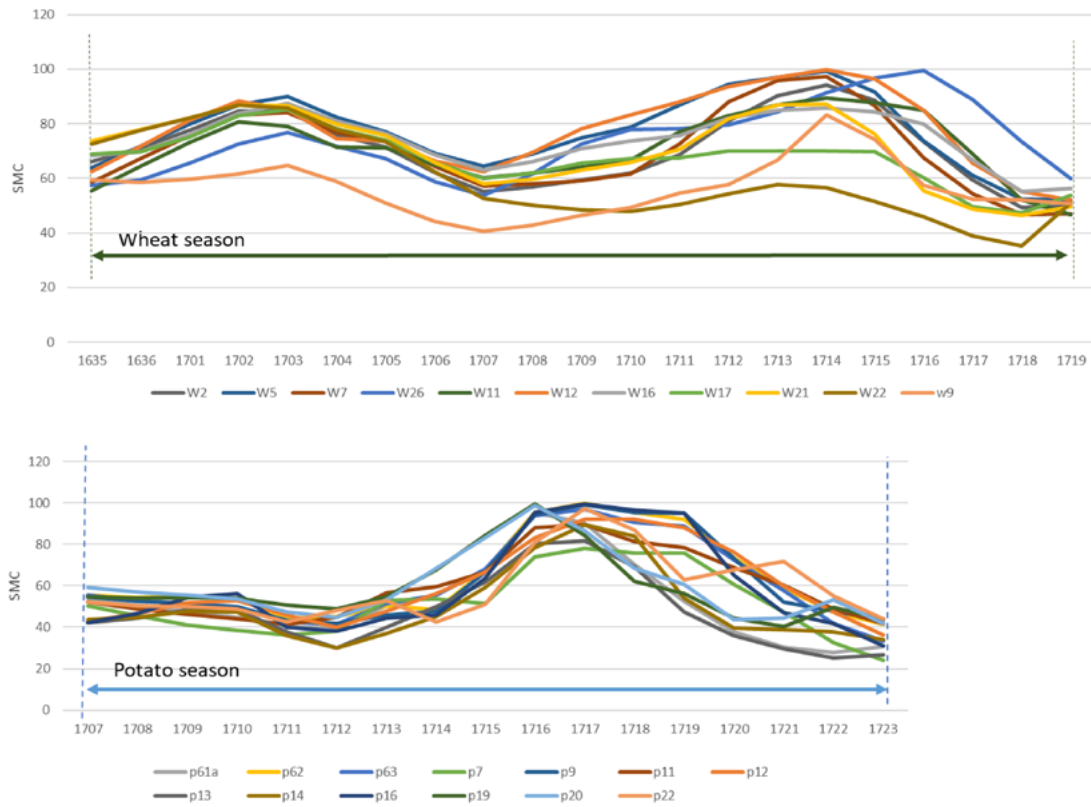
Figure B1. Dekadal SMC for each plot for wheat potato. Trends shown are for the earliest plant date (SOS) of all farmer reported SOS to the last harvest date (EOS) of all EOS reported by farmers. Note that aggregation for yield was taken from the actual SOS and EOS per plot reported by farmer.
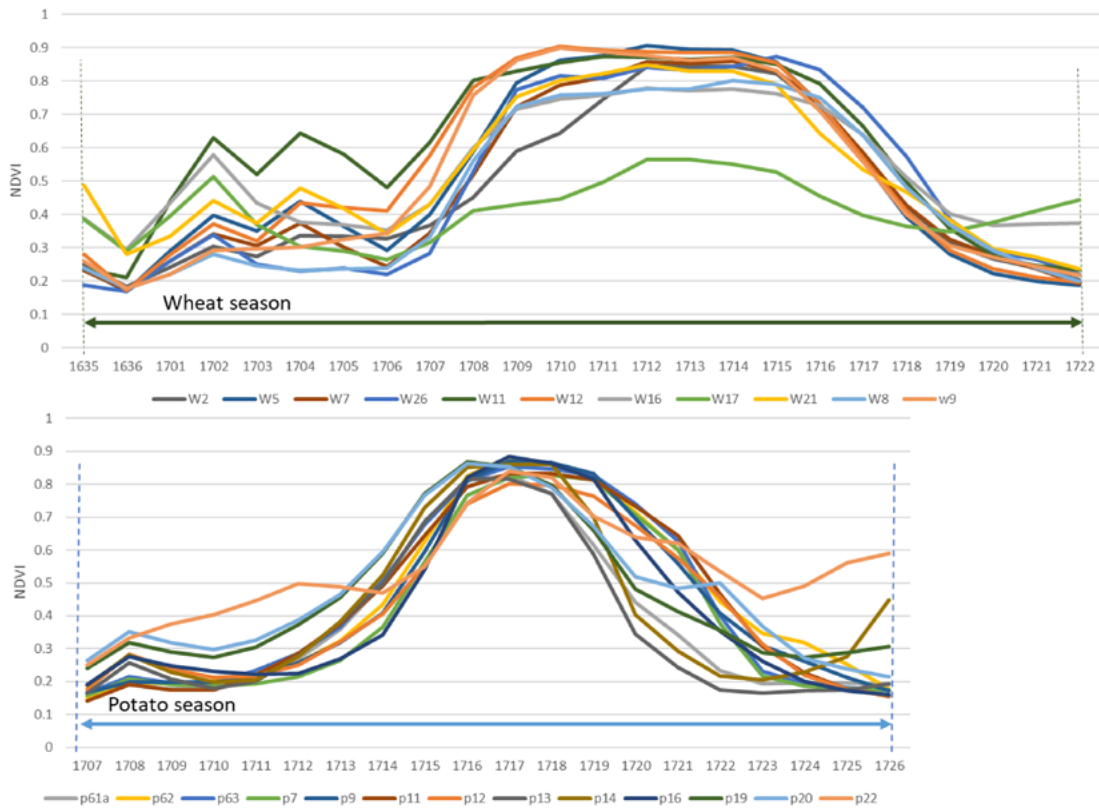
Figure B2. Dekadal NDVI for each plot for wheat potato. Trends shown are for the earliest plant date (SOS) of all farmer reported SOS to the last harvest date (EOS) of all EOS reported by farmers. Note that aggregation for yield was taken from the actual SOS and EOS per plot reported by farmer.

Appendix C. Eddy Covariance flux tower data views of Wankama-East, Niger – 2012

This annex contains the data used for the direct validation and comparison of ETI$_a$ - WaPOR with Eddy Covariance flux tower latent heat flux measurements at the Wankama-North site in Niger (NE-WAM). Flux tower data source © AMMA-CATCH (2018). Figure E1. shows a quick look of both the year 2012 measured 30-minute EC fluxes (17520 data points of the LE component in W.m^{-2}, with some gaps$^)$ and 2012 L1 ETI$_a$-WPR 10-day averages in mm.day^{-1} for the Wankama Nord site in the Sahel.
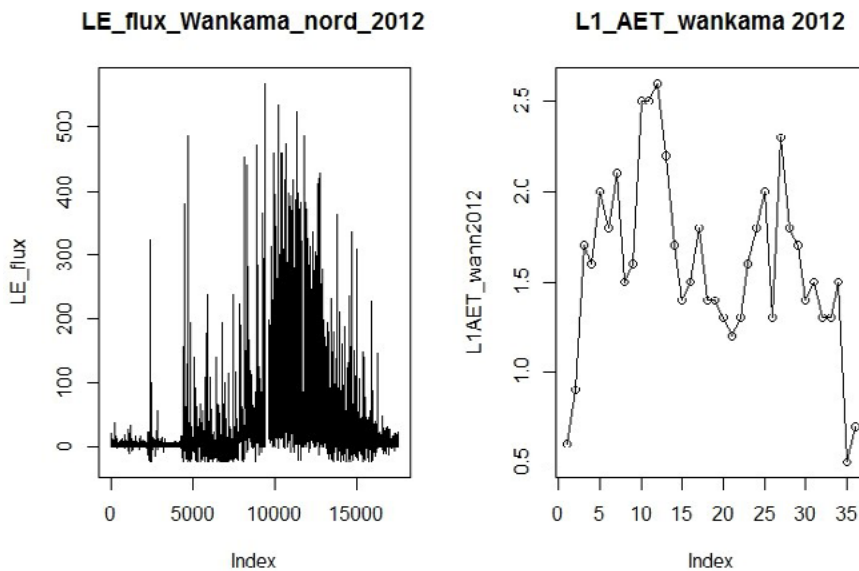
Figure E1. Raw LE flux data and ETI$_a$ - WPR (L1_AET in figure) time series for Wankama Nord site of 2012

Figure E.2 shows the daily ETI$_a$-EC time series derived from the flux tower LE fluxes versus the ETI$_a$-WPR ecadal. Note that the LE fluxes start to become important only after the first rains (see pictures below) when the ITCZ (Intertropical Convergence Zone) induces changing weather patterns in the region.
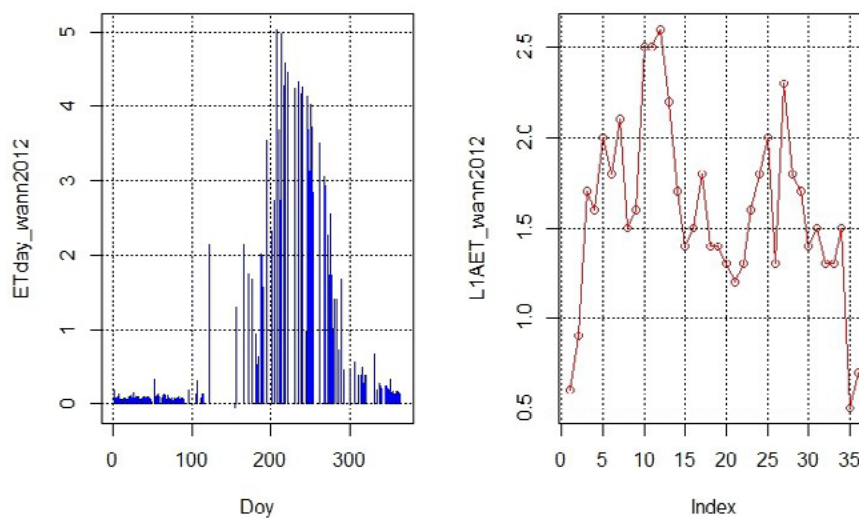
Figure E2. Daily tower ET$_a$-EC (left) in (mm/day) and L1 ETI$_a$-WPR 10-day average (mm/day) at Wankama-North 2012
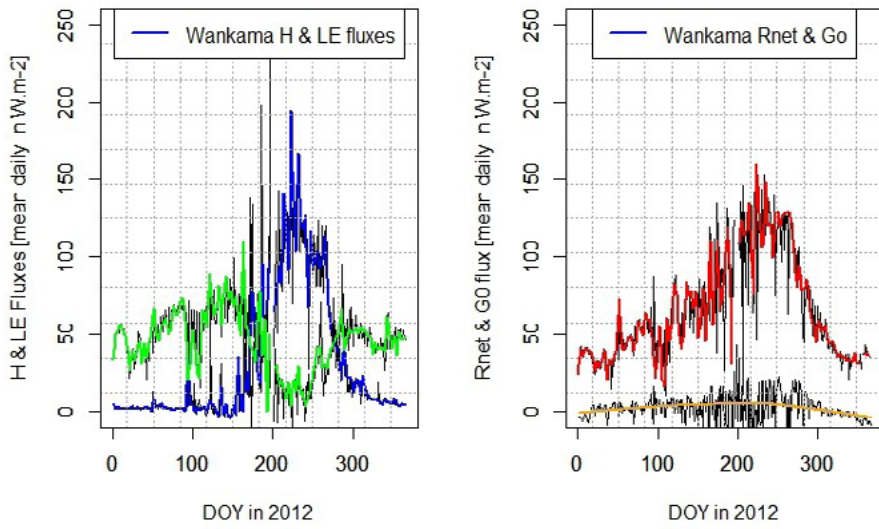
Figure E3. Time series of Daily mean turbulent fluxes (H+LE; left) and Net Radiation and Ground heat flux Wankama 2012 [Green: sensible heat H; Blue: Latent heat LE; Red: Rnet solar; Yellow: ground heat flux G0]
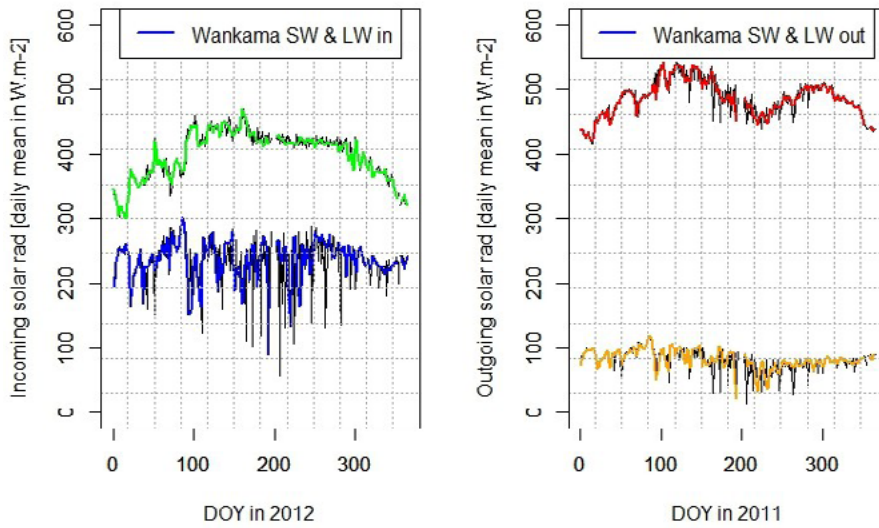
Figure E4. Solar (daily mean – 24-hour avg) incoming and outgoing radiation fluxes at Wankama during 2012 [Blue SW_in; Green LW_in; Red : LW_out; yellow SW_out]
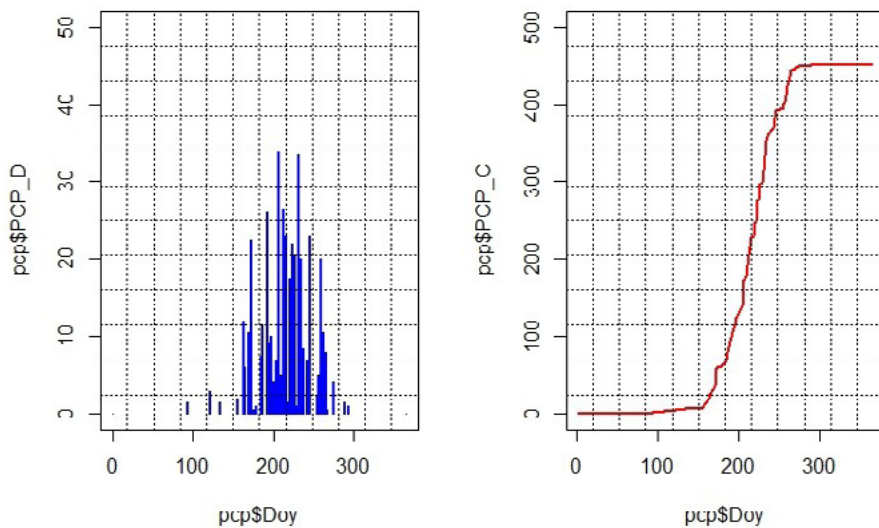
Figure E5. Daily (left) and cumulative rainfall at Wankama site in 2012 in [mm]

The daily rainfall amounts in [mm/day] and cumulative total (mm/year) for Wankama 2012 is shown in the Figure E5.
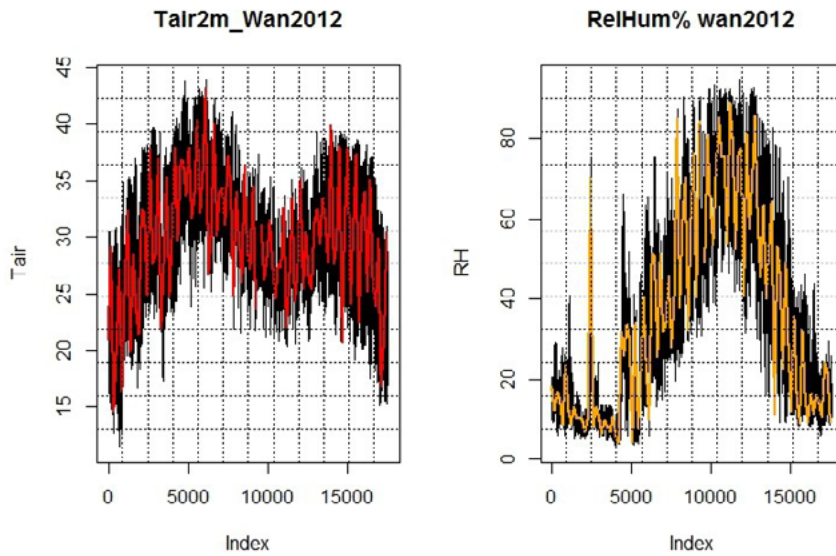
Figure E6. Meteorological and soil moisture and thermal data series at the Wankama site in 2012
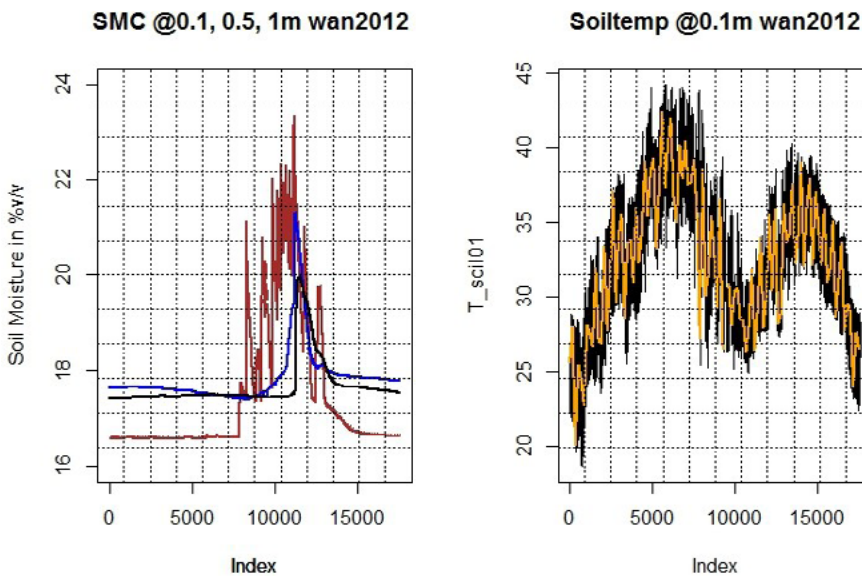
Figure E7. Time series of (raw) observation data on meteorological and soil moisture conditions at the Wankama flux tower site during 2012. (Index indicates observation number i.e. 17,520. 30-min per year and grid corresponds to months).

There is a clear correlation with the flux tower LE fluxes and derived ET values and the onset of the rainfall season and soil moisture availability. The L1 ETI_a - WPR data show a rather high correlation with the air temperature variations, and indicate that the ETlook-WaPOR algorithm is sensitive to this variable (ref. comparison of Tair with L1 ETI_a - WPR), and less to the prevailing moisture conditions and water available for evapotranspiration, in these climatic conditions and regions. Please note that ETI_a - WPR V1 data was used. The agreement between L1 ETI_a - WPR between V1 and V2 at this site is high – r=0.99, R^2=0.98 and bias =+7%. Therefore, although V2 showed a general increase as compared to V1, the temporal trend remains the same and responses to PCP at this site are not being picked up in by WaPOR.

Appendix D. Metrics ETI_a, NPP and AGBP WP L1 and L2 level consistency

Metric	ETI_a (mm/day)					NPP (gC/m^2/day)					AGBP WP (kg/m^3)				
2008 - present	min	5	50	95	max	min	5	50	95	max	min	5	50	95	max
RMSE	0.01	0.01	0.03	0.05	0.11	0.10	0.11	0.22	0.33	0.90	0.07	0.08	0.15	0.40	0.57
Correlation	0.70	0.95	0.98	1.00	1.00	0.74	0.97	0.98	0.99	1.00	0.60	0.75	0.96	0.99	0.99
R2	0.49	0.90	0.96	1.00	1.00	0.54	0.94	0.96	0.99	0.99	0.36	0.51	0.81	0.92	0.98
Bias (%)	0.00	0.00	0.07	0.22	0.40	0.00	0.00	0.07	0.19	0.51	0.01	0.02	0.03	0.14	0.30
Bias	-0.02	-0.01	0.01	0.03	0.05	-0.51	-0.13	0.00	0.14	0.32	-0.41	-0.13	-0.02	-0.01	0.06
Mean L2	0.10	0.11	0.15	0.17	0.20	0.50	0.58	0.84	1.13	1.25	0.50	0.64	0.90	1.19	0.00
Mean L1	0.11	0.12	0.15	0.18	0.20	0.51	0.51	0.53	0.55	1.25	0.53	0.61	0.83	1.07	1.25
< 2013	min	5	50	95	max	min	5	50	95	max	min	5	50	95	max
RMSE	0.07	0.07	0.07	0.07	0.13	0.10	0.10	0.10	0.10	0.17	0.07	0.07	0.07	0.07	0.13
Correlation	0.97	0.97	0.97	0.97	0.99	0.97	0.97	0.98	0.98	1.00	0.97	0.97	0.97	0.97	0.99
R2	0.95	0.95	0.95	0.95	0.98	0.98	0.98	0.99	0.99	0.99	0.95	0.96	0.97	0.98	0.98
Bias (%)	0.01	0.01	0.01	0.01	0.30	0.00	0.00	0.07	0.18	0.36	0.01	0.02	0.02	0.02	0.30
Bias	-0.41	-0.41	-0.41	-0.41	-0.01	-0.51	-0.48	-0.21	-0.18	0.17	-0.41	-0.02	-0.02	-0.01	-0.01
Mean L2	0.56	0.56	0.56	0.56	1.39	0.54	0.54	0.55	0.55	1.40	0.56	0.62	0.87	1.20	1.39
Mean L1	0.55	0.53	0.53	0.53	1.25	0.54	0.54	0.55	0.55	1.25	0.55	0.60	0.86	1.16	1.25
> 2013	min	5	50	95	max	min	5	50	95	max	min	5	50	95	max
RMSE	0.09	0.09	0.09	0.09	0.57	0.11	0.11	0.11	0.11	0.90	0.09	0.09	0.09	0.09	0.57
Correlation	0.60	0.60	0.60	0.60	0.99	0.74	0.76	0.93	0.94	1.00	0.60	0.60	0.60	0.60	0.99
R2	0.36	0.36	0.36	0.36	0.97	0.54	0.58	0.88	0.91	0.99	0.36	0.51	0.81	0.92	0.97
Bias (%)	0.01	0.01	0.01	0.01	0.19	0.00	0.00	0.07	0.19	0.51	0.01	0.07	0.09	0.14	0.19
Bias	-0.26	-0.26	-0.26	-0.26	0.06	-0.16	-0.16	-0.16	-0.15	0.32	-0.26	-0.14	-0.09	-0.05	0.06
Mean L2	0.50	0.58	0.58	0.58	1.42	0.50	0.51	0.52	0.53	1.19	0.50	0.68	0.92	1.19	1.42
Mean L1	0.53	0.53	0.53	0.53	1.19	0.51	0.51	0.52	0.53	1.18	0.53	0.61	0.83	1.07	1.19

Appendix E. Metrics ETI_a, NPP and AGBP WP L1 and L2 level consistency

Metric	ETI_a					NPP				
AWA	min	5	50	95	max	min	5	50	95	max
RMSE	0.42	0.50	0.66	0.85	1.01	0.30	0.41	0.60	0.81	1.03
Correlation	0.63	0.73	0.84	0.89	0.92	0.54	0.70	0.83	0.88	0.92
R^2	0.40	0.53	0.71	0.79	0.85	0.30	0.48	0.70	0.77	0.84
Bias (percent)	0.00	0.01	0.11	0.35	1.09	0.00	0.02	0.19	0.59	1.76
Bias	-1.21	-0.56	0.04	0.78	1.36	-0.64	-0.16	0.22	0.85	1.89
Mean L3	1.10	1.46	2.10	3.93	4.68	0.40	0.64	1.18	2.70	3.70
Mean L1	1.01	1.43	2.11	3.97	4.99	0.58	0.75	1.40	3.26	4.48
KOGA	min	5	50	95	max	min	5	50	95	max
RMSE	0.26	0.31	0.42	0.56	0.71	0.07	0.13	0.47	1.20	1.52
Correlation	0.40	0.50	0.67	0.74	0.77	0.36	0.50	0.69	0.78	0.84
R^2	0.16	0.25	0.45	0.54	0.60	0.13	0.25	0.48	0.60	0.70
Bias (percent)	0.00	0.01	0.09	0.37	0.91	0.00	0.03	0.21	0.56	11.71
Bias	-0.99	-0.49	0.04	0.58	1.13	-0.39	-0.23	0.09	0.58	0.86
Mean L3	0.80	1.34	2.28	3.83	4.72	0.01	0.19	0.65	2.16	3.01
Mean L1	0.95	1.34	2.27	3.97	4.67	0.08	0.18	0.70	2.54	3.32
BKA	min	5	50	95	max	min	5	50	95	max
RMSE	0.10	0.18	0.63	1.04	1.22	0.96	1.81	6.34	10.41	12.21
Correlation	0.49	0.62	0.73	0.82	0.87	0.49	0.62	0.73	0.82	0.87
R^2	0.24	0.38	0.53	0.67	0.75	0.24	0.38	0.53	0.67	0.75
Bias (percent)	0.00	0.01	0.10	0.35	0.81	0.00	0.01	0.10	0.35	0.81
Bias	-0.62	-0.35	-0.02	0.35	0.57	-6.16	-3.52	-0.21	3.49	5.72
Mean L3	0.06	0.36	1.45	2.56	3.73	0.64	3.59	14.52	25.59	37.26
Mean L1	0.09	0.35	1.42	2.66	3.66	0.87	3.45	14.22	26.57	36.57
ZAN	min	5	50	95	max	min	5	50	95	max
RMSE	0.23	0.32	0.64	1.02	1.11	0.17	0.22	0.43	0.83	1.05
Correlation	0.51	0.57	0.71	0.78	0.80	0.35	0.48	0.67	0.75	0.78
R^2	0.26	0.32	0.51	0.61	0.64	0.12	0.23	0.44	0.57	0.60
Bias (percent)	0.00	0.01	0.09	0.30	1.14	0.00	0.02	0.12	0.41	1.52
Bias	-2.17	-0.61	0.18	0.92	1.69	-1.01	-0.27	0.16	0.61	1.13
Mean L3	1.29	1.68	3.15	6.03	6.76	0.36	0.70	1.65	3.55	4.42
Mean L1	1.27	1.85	3.32	6.67	7.22	0.59	0.82	1.71	4.01	5.05
ODN	min	5	50	95	max	min	5	50	95	max
RMSE	0.15	0.29	0.64	0.98	1.62	0.01	0.06	0.25	0.56	0.74
Correlation	0.38	0.56	0.80	0.97	0.99	0.11	0.48	0.76	0.99	1.00
R^2	0.15	0.31	0.63	0.94	0.98	0.01	0.23	0.57	0.98	0.99
Bias (percent)	0.00	0.01	0.12	0.50	1.31	0.00	0.01	0.15	0.59	1.12
Bias	-2.07	-1.25	-0.08	0.81	1.80	-0.68	-0.37	0.00	0.33	0.66
Mean L3	0.91	1.38	3.45	5.32	6.06	0.09	0.20	0.71	2.14	3.05
Mean L1	0.85	1.54	3.23	5.20	6.28	0.15	0.21	0.73	2.19	3.01

Appendix F: FAO WaPOR web portal numerical output cross validation

number dekad	Category dekad	days/ dekad	NPP from WAPOR	NPP from ITC_DB	scaled by 1000	TBP-day	TBP-dek	AGBP ratio=0.65	I mm/day	I mm/dek	E mm/day	E-ITC_DB Integer	E_ITC_DB Scaled	E mm/dek	T mm/day	T mm/dek	ETIa_day mm/day	ETIa_Dek mm/dek	T_Dek mm/dek	ETIa_Dek m3/ha	T_Dek m3/ha	GBWP_dek kg/m3	NBWP_dek kg/m3	Chirps-P mm/dek	SMC
1	10/01/2018	10	0.687	687	0.69	15.27	152.67	99.23	0	0	0.6	6	0.6	6	0.6	6	1.2	12	6	120	60	0.83	1.65	19	65.00
2	20/01/2018	10	0.797	797	0.80	17.71	177.11	115.12	0	0	0.7	7	0.7	7	0.7	7	1.4	14	7	140	70	0.82	1.64	15	68.00
3	31/01/2018	11	0.764	764	0.76	16.98	186.75	121.39	0	0	0.6	6	0.6	6.6	0.6	6.6	1.2	13.2	6.6	132	66	0.92	1.84	21	62.00
4	10/02/2018	10	0.586	586	0.59	13.02	130.22	84.64	0	0	0.4	4	0.4	4	0.3	3	0.7	7	3	70	30	1.21	2.82	14	54.00
5	20/02/2018	10	0.280	280	0.28	6.22	62.22	40.44	0	0	0	0	0	0	0.2	2	0.2	2	2	20	20	2.02	2.02	12	38.00
6	28/02/2018	8	0.474	474	0.47	10.53	84.27	54.77	0	0	0.4	4	0.4	3.2	0.4	3.2	0.8	6.4	3.2	64	32	0.86	1.71	9	52.00
7	10/03/2018	10	0.481	481	0.48	10.69	106.89	69.48	0.1	1	0.5	5	0.5	5	0.3	3	0.9	9	3	90	30	0.77	2.32	114	69.00
8	20/03/2018	10	0.619	619	0.62	13.76	137.55	89.41	0.1	1	0.7	7	0.7	7	0.5	5	1.3	13	5	130	50	0.69	1.79	119	73.00
9	31/03/2018	11	1.107	1107	1.11	24.60	270.60	175.89	0	0	0.4	4	0.4	4.4	0.7	7.7	1.1	12.1	7.7	121	77	1.45	2.28	16	71.00
10	10/04/2018	10	1.429	1429	1.43	31.76	317.55	206.41	0.1	1	0.5	5	0.5	5	1	10	1.6	16	10	160	100	1.29	2.06	70	71.00
11	20/04/2018	10	1.315	1315	1.32	29.22	292.22	189.94	0.2	2	0.5	5	0.5	5	1	10	1.7	17	10	170	100	1.12	1.90	124	77.00
12	30/04/2018	10	1.549	1549	1.55	34.42	344.22	223.74	0.1	1	0.5	5	0.5	5	1.1	11	1.7	17	11	170	110	1.32	2.03	139	77.00
13	10/05/2018	10	1.767	1767	1.77	39.27	392.66	255.23	0.1	1	0.4	4	0.4	4	1.1	11	1.6	16	11	160	110	1.60	2.32	70	76.00
14	20/05/2018	10	1.641	1641	1.64	36.47	364.66	237.03	0.1	1	0.5	5	0.5	5	1.1	11	1.7	17	11	170	110	1.39	2.15	167	83.00
15	31/05/2018	11	1.693	1693	1.69	37.62	413.84	269.00	0	0	0.4	4	0.4	4.4	1	11	1.4	15.4	11	154	110	1.75	2.45	39	76.00
16	10/06/2018	10	1.273	1273	1.27	28.29	282.89	183.88	0	0	0.3	3	0.3	3	0.8	8	1.1	11	8	110	80	1.67	2.30	51	74.00
17	20/06/2018	10	1.489	1489	1.49	33.09	330.89	215.08	0	0	0.4	4	0.4	4	0.8	8	1.2	12	8	120	80	1.79	2.69	27	70.00
18	30/06/2018	10	1.310	1310	1.31	29.11	291.11	189.22	0	0	0.4	4	0.4	4	0.7	7	1.1	11	7	110	70	1.72	2.70	14	70.00
19	10/07/2018	10	1.165	1165	1.17	25.89	258.89	168.28	0	0	0.3	3	0.3	3	0.6	6	0.9	9	6	90	60	1.87	2.80	8	66.00
20	20/07/2018	10	1.145	1145	1.15	25.44	254.44	165.39	0	0	0.4	4	0.4	4	0.7	7	1.1	11	7	110	70	1.50	2.36	6	65.00
21	31/07/2018	11	1.100	1100	1.10	24.44	268.89	174.78	0	0	0.3	3	0.3	3.3	0.6	6.6	0.9	9.9	6.6	99	66	1.77	2.65	12	61.00
22	10/08/2018	10	1.286	1286	1.29	28.58	285.77	185.75	0	0	0.4	4	0.4	4	0.8	8	1.2	12	8	120	80	1.55	2.32	4	66.00
23	20/08/2018	10	1.109	1109	1.11	24.64	246.44	160.19	0	0	0.3	3	0.3	3	0.5	5	0.8	8	5	80	50	2.00	3.20	4	60.00
24	31/08/2018	11	0.802	802	0.80	17.82	196.04	127.43	0	0	0.3	3	0.3	3.3	0.4	4.4	0.7	7.7	4.4	77	44	1.65	2.90	35	60.00
25	10/09/2018	10	0.959	959	0.96	21.31	213.11	138.52	0	0	0.4	4	0.4	4	0.5	5	0.9	9	5	90	50	1.54	2.77	10	66.00
26	20/09/2018	10	0.622	622	0.62	13.82	138.22	89.84	0	0	0.3	3	0.3	3	0.4	4	0.7	7	4	70	40	1.28	2.25	8	49.00
27	30/09/2018	10	0.578	578	0.58	12.84	128.44	83.49	0	0	0.3	3	0.3	3	0.3	3	0.6	6	3	60	30	1.39	2.78	13	49.00
28	10/10/2018	10	0.449	449	0.45	9.98	99.78	64.85	0	0	0.3	3	0.3	3	0.3	3	0.6	6	3	60	30	1.08	2.16	16	50.00
29	20/10/2018	10	0.564	564	0.56	12.53	125.33	81.47	0	0	0.5	5	0.5	5	0.4	4	0.9	9	4	90	40	0.91	2.04	9	61.00
30	31/10/2018	11	0.509	509	0.51	11.31	124.42	80.87	0	0	0.4	4	0.4	4.4	0.3	3.3	0.7	7.7	3.3	77	33	1.05	2.45	23	58.00
31	10/11/2018	10	0.626	626	0.63	13.91	139.11	90.42	0	0	0.3	3	0.3	3	0.3	3	0.6	6	3	60	30	1.51	3.01	21	52.00
32	20/11/2018	10	0.776	776	0.78	17.24	172.44	112.09	0	0	0.3	3	0.3	3	0.4	4	0.7	7	4	70	40	1.60	2.80	21	52.00
33	30/11/2018	10	1.081	1081	1.08	24.02	240.22	156.14	0	0	0.3	3	0.3	3	0.6	6	0.9	9	6	90	60	1.73	2.60	24	57.00
34	10/12/2018	10	0.782	782	0.78	17.38	173.78	112.95	0	0	0.2	2	0.2	2	0.5	5	0.7	7	5	70	50	1.61	2.26	38	48.00
35	20/12/2018	10	1.145	1145	1.15	25.44	254.44	165.39	0	0	0.6	6	0.6	6	0.8	8	1.4	14	8	140	80	1.18	2.07	69	70.00
36	31/12/2018	11	1.394	1394	1.39	30.98	340.75	221.49	0	0	0.5	5	0.5	5.5	0.9	9.9	1.4	15.4	9.9	154	99	1.44	2.24	17	69.00
		365	35.353		35.35		7998.83	5199.24		8	14.6		14.6	148.1		225.7		381.8	225.7	3818	2257	1.39	2.34	1378	63.47

Annual WP		ETIa		381.8	
from WAPOR portal V2.0		use TBP	use AGBP	AGBP-use mean for each dekad	
GBWP	2.095	2.09503	1.361771	1.3857	
NBWP	3.544	3.54401	2.303607	2.3433	

NPP and E retrieved from WAPOR (https://wapor.apps.fao.org/home/WAPOR_2/1) and
Data base from ITC-ILWIS Toolbox, using coordinate (lat,lon): 0°49'44.57"S, 36°28'55.27"E (= -0.8290472222, 36.4820194444)
Results comparing values from both are identical for NPP and Evaporation (when scaling factors are applied)
In WaPOR V2.0 TBP annual is used for Biomass instead of AGBP (used in WAPOR V1.)

Gross - Net Biomass Production, sample location south of lake Naivasha-Kenya
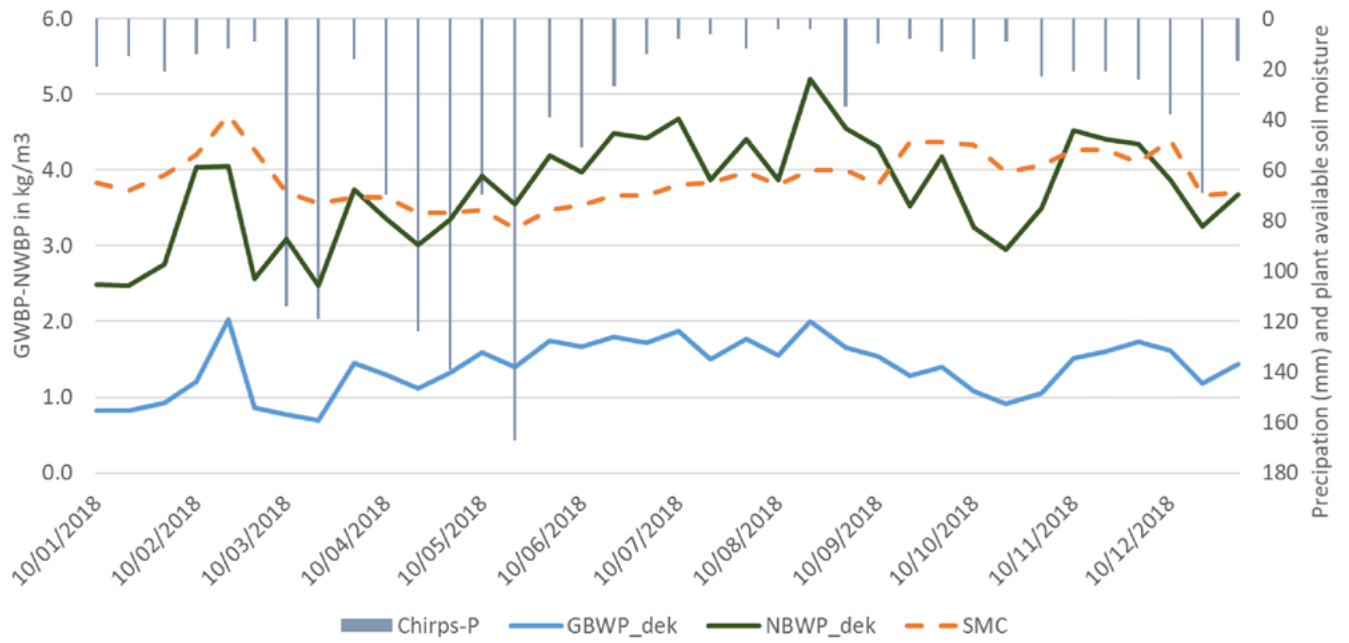
Legend: Chirps-P, GBWP_dek, NBWP_dek, SMC

WaPOR quality assessment

Technical report on the data quality of the WaPOR FAO database version 2

This report describes the quality assessment of the FAO's data portal to monitor Water Productivity through Open access of Remotely sensed derived data (WaPOR 2). The WaPOR 2 data portal has been prepared as a major output of the project: ´Using Remote Sensing in support of solutions to reduce agricultural water productivity gaps', funded by the Government of The Netherlands. The WaPOR database is a comprehensive database that provides information on biomass production (for food production) and evapotranspiration (for water consumption) for Africa and the Near East in near real time covering the period 1 January 2009 to date. This document presents the results of a validation of the version 2 of the WaPOR database, produced in collaboration with the FRAME consortium partners, eLEAF and VITO. The report summarises the work done by the validation partner (ITC-UTwente) to assess the quality of the new V2 core data components, using different validation methods.